



Carina Alexandra Rebelo Ramos
Licenciatura em Engenharia do Ambiente

Potential of CPV receivers integrating screen-printed solar cells

Dissertação para obtenção do Grau de Mestre em
Energias Renováveis – Conversão
Eléctrica e Utilização Sustentável

Orientador: Prof. Doutor Stanimir Valtchev
Co-orientador: Doutor Luís Pina

Júri:

Presidente: Prof. Doutor Adolfo Steiger Garção
Arguente(s): Prof. Doutor Jorge Pamies Teixeira
Vogal(ais): Prof. Doutor Stanimir Valtchev
Doutor Luís Pina



Carina Alexandra Rebelo Ramos

Licenciatura em Engenharia do Ambiente

Potential of CPV receivers integrating screen-printed solar cells

Dissertação para obtenção do Grau de Mestre em
Energias Renováveis – Conversão
Eléctrica e Utilização Sustentável

Orientador: Prof. Doutor Stanimir Valtchev
Co-orientador: Doutor Luís Pina

Júri:

Presidente: Prof. Doutor Adolfo Steiger Garção
Arguente(s): Prof. Doutor Jorge Pamies Teixeira
Vogal(ais): Prof. Doutor Stanimir Valtchev
Doutor Luís Pina

A presente dissertação intitulada “Potential of CPV receivers integrating screen-printed solar cells”, escrita por mim, Carina Alexandra Rebelo Ramos, tem o seguinte termo de COPYRIGHT:

“A Faculdade de Ciências e Tecnologia e a Universidade Nova de Lisboa tem o direito, perpétuo e sem limites geográficos, de arquivar e publicar esta dissertação através de exemplares impressos reproduzidos em papel ou de forma digital, ou por qualquer outro meio conhecido ou que venha a ser inventado, e de a divulgar através de repositórios científicos e de admitir a sua cópia e distribuição com objectivos educacionais ou de investigação, não comerciais, desde que seja dado crédito ao autor e editor.”

To my parents and brother, for believing in me.

To you David, for all patience and dedication.

I know that today they are very happy for me!

“The height of your accomplishments will equal the depth of
your convictions”

William F. Scolavino

Acknowledgements

Becomes essential, a word of thanks to all those who, directly or indirectly, enabled one more of the objectives of my life come truth.

I would like to thank...

... my supervisor Dr. Stanimir Valtchev for creating the conditions and the protocol that enabled me to develop this master thesis on the R&D Department of WS Energia, giving me the opportunity of doing research in a business environment, as I was looking forward to and for the support, interest and availability that always showed throughout the course of this work;

... my co-supervisor, Dr. Luis Pina, for all the support and guidance along this work, and for keeping my work focused on what really matters;

... MSc Filipa Reis for the supervision, advice, patience and also for helping me going through the hurdles of this work, without which there would have been impossible to perform the same;

... all the staff of WS Energia, for their time and warm welcome;

... all the FCUL team, for the unconditional help that always offered and by providing all the equipment that made possible the realization of the experimental part of this thesis.

... my family for the support during the thesis work and through all my master degree. In particular, my parents and brother, for all the patience and support not only during the writing stage of the thesis, but my entire life; to my cousin Vera Teles, for the help and support that always showed in the right moments;

... all my friends, for understanding my absences and for providing me great and extremely important relaxing times.

And finally, to David, for always being by my side over the years, even when we were apart; for the dedication, love, understanding and patient that always demonstrated. For this, I will always be grateful.

To all, my sincere thanks!

ABSTRACT

Photovoltaic systems present themselves as an excellent alternative for clean energy production. To reach large applications, obstructions as high silicon prices must be overcome. Solar concentration systems are a potential solution since silicon is replaced by cheaper material (like mirrors or lenses). Nevertheless, there are still many issues and challenges yet to overcome. One of these challenges is the economic cost of the solar cells, since the CPV systems need to integrate expensive high efficiency solar cells specially designed to operate at high levels of radiation. Thus, it is necessary to explore new approaches.

In this thesis presents a study of the potential of the screen-printed silicon solar cells to integrate the CPV systems, concretely the HSUN system. Two solar cells, conventional 1Sun and conventional 15Suns, were analyzed and integrated in the HSUN sub-receivers, in order to understand their behavior under several levels of concentration and when integrated in series in sub-receivers. After the first part of the experimental campaign (electrical characterization of solar cells) it was concluded that the conventional standard silicon solar cells are unsustainable for use in the HSUN system (which operates a 15 suns), since these solar cells only work properly up to a concentration of 5 suns. Regarding the Upgraded 1-sun silicon solar cells, the results were satisfactory regarding their behavior under concentration, until a concentration level of 20 suns.

In the second part of the experimental campaign, the Upgraded 1-sun solar cells were integrated in the HSUN sub-receivers and their behavior was analyzed. The results taking from this part of the experimental campaign prove the good performance of the Upgraded solar cells and that their performance is unaffected by their integration in the sub-receivers. Associated to this part of the experiments, was also performed the optimization of the mounting process of the sub-receivers. This optimization provided a faster process with a lower probability of damaging the solar cells. To a complete study of the potential of these solar cells, it is important to take into account the economic viability of the solar cells. Comparing the cost-efficiency of the standard conventional solar cells, the LGBC solar cells (cells used actually in the HSUN system) and the Upgraded 1-sun solar cells, it was concluded that the solar cells more viable up to a concentration level of 24 suns are the Upgraded 1-sun solar cells, being that from this concentration level the LGBC solar cells present themselves as the most viable.

Therefore, and taking into account all the work developed along this thesis, it was concluded that the most cost-efficient solar cells to integrate the HSUN system are the conventional solar cells with some characteristics optimized for the required concentration levels.

Keywords: Concentration Photovoltaic systems, Silicon solar cells, Screen- printing, Laser Grooved with Buried Contacts

RESUMO

Os sistemas fotovoltaicos apresentam-se como uma excelente alternativa para produção de energia limpa. Os concentradores solares mostram-se como uma potencial solução, uma vez que parte do silício é substituído por materiais menos dispendiosos (como espelhos e lentes). Contudo, existem ainda vários desafios associados a este tipo de sistemas que necessitam ser resolvidos. Um desses desafios prende-se com os custos económicos associados ao uso de células solares de alta eficiência muito caras, desenhadas para funcionarem a altos níveis de radiação. Assim, mostra-se necessário a exploração de novas ideias e tecnologias. Nesta tese é apresentado um estudo da potencialidade de células solares screen-printed de silício para integração em sistemas de CPV, concretamente no sistema HSUN.

Dois tipos de células solares, convencionais standards e células solares de silício optimizadas para uma concentração de 15 sóis, foram analisadas, com o objectivo de se perceber o seu comportamento e a sua performance sob vários níveis de concentração. No fim da primeira parte da campanha experimental desenvolvida (caracterização eléctrica das células solares), foi possível concluir que as células convencionais não são uma opção viável para integrar o sistema HSUN (que opera a uma concentração de 15 sóis), uma vez que as estas células apenas apresentam um correcto funcionamento até uma concentração de 5 sóis. No que respeita as células solares de silício optimizadas, os resultados foram satisfatórios, tendo em consideração o seu comportamento sob concentração até 20 sóis.

Na segunda parte da campanha experimental, as células solares optimizadas foram integradas em sub-receptores e o seu comportamento foi analisado. Os resultados obtidos provaram a boa performance, já demonstrada na sua caracterização eléctrica, e que o seu funcionamento não é afectado através da sua integração em sub-receptores. Associado a esta parte experimental, foi ainda realizada a optimização do processo de montagem dos sub-receptores. Esta optimização proporcionou um processo de montagem mais rápido e com menor probabilidade de danificação das células solares. Por fim, e comparando o custo vs. eficiência das células convencionais, das células solares optimizadas e das células solares de contacto enterrado (usadas actualmente no sistema HSUN), foi possível concluir que a célula solar mais viável até uma concentração de 24 sóis é a célula solar optimizada, sendo que a partir desse nível de concentração as células solares de contacto enterrado passam a ser as mais viáveis.

Assim, e tendo em conta todos os resultados obtidos ao longo do desenvolvimento desta tese, concluiu-se que as células solares mais viáveis para integrar o sistema HSUN são células solares convencionais com algumas características optimizadas para o nível de concentração requerido.

Palavras-chave: Sistemas de Concentração Fotovoltaica, Célula solar de silício, Tecnologia Screen-printing, Células LGBC

CONTENTS

Acknowledgements **xi**
ABSTRACT **xiii**
RESUMO **xv**
LIST OF TABLES **xxv**
List of Abbreviations..... **xxvii**

INTRODUCTION..... 1
1.1 Context 1
1.2 Scope and objectives 2
1.3. Structure of the thesis 3

Concentration Photovoltaic Systems 5
2.1. Photovoltaic Solar Energy 5
2.2. Concentration of photovoltaic 7
2.2.1. Why Concentration? 7
2.2.2. Fundamentals of CPV systems 8
2.2.1.1 Optics 9
2.2.1.2. Tracking systems..... 11
2.2.1.3.Receiver 11

Fundamentals of Solar Cells to CPV systems 13
3.1. Basic principles of photovoltaic solar cells 13
3.1.1. Equivalent electric circuit of the solar cell 13
3.2. Electrical parameters of a solar cell..... 19
3.2.1. Short-circuit current and open-circuit voltage..... 20
3.2.2. Maximum power point 20
3.2.3. Fill Factor 21

3.2.4. Conversion efficiency	22
3.3. Influence of temperature and radiation intensity on the characteristic curve	22
3.4. Overview of Solar Cells for CPV	23
3.4.1. Single-crystalline solar cells for CPV applications	25
3.4.1.1. Modified screen-printed solar cells	26
3.4.1.2. Laser Grooved Buried Contact (LGBC) solar cells	27
3.4.1.3. Back contact cells	29
3.4.1.3.1. Emitters wrap trough (EWT) solar cells	29
3.4.1.3.2. Metallization wrap trough (MWT) solar cells	30
Theoretical characterization of Solartec and KVAZAR solar cells	31
4.1. Physical characteristics of the KVAZAR and Solartec solar cells	31
4.1.1. KVAZAR solar cells	31
4.1.2. Solartec solar cell	36
4.2. Mathematical model to estimate the behavior of solar cells under concentration	39
4.3. Theoretical behavior of the Solartec and KVAZAR solar cells under concentration	43
Experimental characterization of the Solartec and KVAZAR solar cells	47
5.1. Electroluminescence of solar cells	47
5.1.1. Electroluminescence	47
5.1.2. Experimental procedure	49
5.1.3. Results	50
5.1.3.1. KVAZAR solar cells	50
5.1.3.2. Solartec solar cells	54
5.1.4. Main Conclusions	55
5.2. Measurement of electrical parameters of the solar cells	56
5.2.1. Electrical parameters	56
5.2.2. Experimental procedure	57
5.2.3. Results	59
5.2.3.1. KVAZAR solar cells	59
5.2.3.2. Solartec solar cells	64
5.2.4. Main conclusions	66
5.3. Measurement of the Series Resistance	68

5.3.1. I-V curves	68
5.3.1.1. Theoretical Introduction.....	68
5.3.1.2. Results	71
5.3.2. Suns Voc method.....	74
5.3.2.1. Theoretical Introduction.....	74
5.3.2.2. Results	75
5.3.3. Conclusions	75
5.4. Spectral Response and Quantum Efficiency	79
5.4.1. Theoretical Introduction	79
5.4.2. Experimental procedure.....	81
5.4.3. Results	82
5.5. Thermal coefficients of solar cells	86
5.5.1. Thermal coefficients concept.....	86
5.5.2. Experimental procedure.....	87
5.5.3. Results	88
5.5.4. Main conclusions.....	90
Integration of the solar cells in the HSUN sub-receivers.....	91
6.1. Integration of solar cells in the HSUN technology	91
6.2. Mounting process of the receiver and preliminary tests.....	92
6.2.1. Process.....	93
6.2.2. Tests.....	97
6.2.3. Optimization of the mounting process.....	116
6.2.3.1. Tests	118
6.3. Electrical performance	123
6.3.1 Experimental procedure.....	123
6.3.2. Results	124
6.3.2.1. Analysis of the results taking into account the incident radiation.....	127
6.3.2.2. Analysis of the results taking into account the radiation and cell temperature	129
6.3.2.2.1. Experimental procedure	129
6.3.2.2.2. Results.....	129
6.3.2.3. Adjust of the results obtained by the temperature estimated of the solar cells.....	131
6.3.3. Main conclusions	133

Cost-efficiency analysis of screen-printed solar cells to integrate CPV systems 135

CONCLUSIONS AND FUTURE WORK..... 139

 8.1. Conclusions 139

 8.2. Future Work 140

REFERENCES 143

ANNEXES 147

LIST OF FIGURES

Figure 2.1 - Adams and Days' Selenium glass tube	5
Figure 2.2 – Vanguard 1	6
Figure 2.3 - Annual Photovoltaic Installation from 2000 to 2010.....	7
Figure 2.4 – Concentration of the light in the solar cell.....	7
Figure 2.5 - Relative cost of the components of a PV systems as to its total cost for a conventional PV system and for a CPV system.	8
Figure 2.6 - Schematic of Linear-Focus Trough PV Concentrator	9
Figure 2.7 - Fresnel lens configurations.....	10
Figure 2.8 - Reflective concentrator configurations.....	10
Figure 2.9 – Types of Tracking systems: (a) 1 axis tracker and (b) 2 axis tracker.....	11
Figure 3.1 - Principle of operation of a solar cell.....	14
Figure 3.2 - I-V characteristic of a silicon diode.....	14
Figure 3.3 - Diagram of equivalent circuit;Characteristic curve of the cell in total darkness	16
Figure 3.4 - Diagram of equivalent circuit, Characteristic curve of the irradiated cell.....	17
Figure 3.5 - Representation of the electrical circuit of one real solar cell.....	17
Figure 3.6 - Effect of variation of series resistance in the I-V curve.....	18
Figure 3.7 - Effect of the variation of the parallel or shunt resistance in the I-V curve	18
Figure 3.8 - I-V and P-V characteristic curve of an silicon cell.....	19
Figure 3.9 - I-V curve and point of maximum power draw of the CIEMAT's simulator.	20
Figure 3.10 - Fill Factor of solar cells	21
Figure 3.11 - Effect of a) irradiance and b) temperature in the I-V curve.....	23
Figure 3.12 - Historic summary of champion cell efficiencies for various PV technologies.....	24
Figure 3.13 - (a) The structure of a MJ solar cell. (b) Graph of spectral irradiance G vs. Wavelength λ over the AM1.5 solar spectrum.	25
Figure 3.14 - Monocrystalline solar cells	26
Figure 3.15 - Normalized plot of Efficiency against the concentration ratio of the optimized and unoptimized grid solar cell.....	27
Figure 3.16 - Buried contact solar cells.....	28
Figure 3.17 - Buried contact in a silicon solar cell.....	28
Figure 3.18 - Emitters wrap trough (EWT) solar cells.....	29
Figure 3.19 - Metallization wrap trough (MWT) solar cells	30
Figure 4.1 - Front surface of the KVAZAR solar cell (main cell)	32
Figure 4.2 - Back surface of the KVAZAR solar cells (main cell)	32
Figure 4.3 - Drawing of the cut (and dimensions) performed in the solar cells	34

Figure 4.4 - Reference of the KVAZAR solar cells.....	34
Figure 4.5 – Number given to each cell according to its position at the conventional wafer.....	35
Figure 4.6 – KVAZAR solar cell	35
Figure 4.7 - Front surface of the Solartec solar cells.....	36
Figure 4.8 - Back surface of the Solartec solar cells	36
Figure 4.9 –Solartec solar cells with different front grid designs: a) one busbar; b) two busbars	37
Figure 4.10 – Reference of the Solartec solar cells	38
Figure 4.11 - Calculated values for Voc and Isc as function of concentration level in the a) KVAZAR solar cells and b)Solartec solar cells	43
Figure 4.12 - Estimated power loss (Ploss) and efficiency (ϵ) as a function of the concentration level of a) Solartec solar cells and b) KVAZAR solar cells	44
Figure 5.1 - Electroluminescence image of a) a monocrystalline and b) poly-crystalline silicon cell.	48
Figure 5.2 – Electroluminescence System.....	49
Figure 5.3 – Electroluminescence apparatus	50
Figure 5.4 - Power and characteristic curves of a solar cell	57
Figure 5.5 – Measurement of the FF from the I-V curve of a solar cell.....	57
Figure 5.6 – Solar Simulation located in the Laboratory of FCUL	58
Figure 5.7 – Detail of the solar cell placed on the sample holder in the solar simulator.....	58
Figure 5.8 – I-V curve of cell n° 6.2 with the I-V tracer	60
Figure 5.9 – I-V curve of cell n° 6.3 with the I-V tracer	60
Figure 5.10 – I-V curve of cell n° 6.4 with the I-V tracer	60
Figure 5.11 – I-V curve of cell n° 6.5 with the I-V tracer	60
Figure 5.12 – I-V curve of cell n° 6.6 with the I-V tracer	60
Figure 5.13 – I-V curve of cell n° 6.7 with the I-V tracer	60
Figure 5.14 – I-V curve of cell n° 6.8 with the I-V tracer	61
Figure 5.15 – Values of a) Voc and b) Isc measured from the I-V curves before and after the soldering process of the KVAZAR solar cells.....	61
Figure 5.16 – I-V curves traced with the four-point I-V measurement (green) and the I-V tracer (violet) of the a)solar cell n° 6.2, b) solar cell n° 6.4, c) solar cell n° 6.7 and d) solar cell n° 6.8	63
Figure 5.17 – I-V curve of cell n° 24.1 before and after the soldering process.....	64
Figure 5.18 – I-V curve of cell n° 24.2 before and after the soldering process.....	64
Figure 5.19 – I-V curve of cell n° 26.1 before and after the soldering process.....	65
Figure 5.20 – I-V curve of cell n° 26.2 before and after the soldering process.....	65
Figure 5.21 – I-V curve of cell n° 2BB.1 before and after the soldering process.....	65
Figure 5.22 – I-V curve of cell n° 2BB.2 before and after the soldering process.....	65
Figure 5.23 - Obtaining the series and shunt resistances from the I-V Curve.....	69

Figure 5.24 - Two I-V curves of the same solar cell under different illumination intensities.....	70
Figure 5.25 - I-V curve registered for the a) KVAZAR, b) Solartec and c) NaREC solar cells under 1, 2 and 10 suns. I-V curves are normalized to Isc and Voc.....	71
Figure 5.26 - Concentration Simulator placed in the FCUL laboratory.....	72
Figure 5.27 – Suns-Voc apparatus placed in the FCUL laboratory.....	74
Figure 5.28 - The spectral response of a silicon solar cell under glass	79
Figure 5.29 - Quantum Efficiency of a silicon solar cell.....	81
Figure 5.30 - System for measuring the spectral response and quantum efficiency	81
Figure 5.31 - Measurement of the SR in the solar cells: a) reference solar cell, b) KVAZAR or Solartec solar cell.....	82
Figure 5.32 - External quantum efficiency of a conventional solar cell (KVZ.40 – 6.8) measured in different positions on the cell.....	83
Figure 5.33 - External quantum efficiency of a conventional solar cell (KVZ.40 – 6.7) measured in different position.....	83
Figure 5.34 - External quantum efficiency of the Solartec solar cell a) class 24; b) class 26; c) with two busbar.....	84
Figure 5.35 - QE curves obtained for the KVAZAR and the Solartec solar cells.....	85
Figure 5.36 - Measured temperature coefficients for voltage for solar cell with uniform and nonuniform temperature during testing.....	86
Figure 5.37 – Solar Simulator located in the Laboratory of the WS Energia S.A.....	87
Figure 5.38 - Variation of the Voc and Isc as a function of the temperature of the: a) KVAZAR, b) SLT.C24, c) SLT.C26 and d) SLT.2BB solar cells.....	89
Figure 6.1 – HSUN module mounted on a 2-axes tracking system.....	92
Figure 6.2 – Components and characteristics of the PCB.....	93
Figure 6.3 – Sub-receiver. When three of these sub-receivers are connected, a receiver is obtained. .	93
Figure 6.4 –Specific position of the each component on the PCB.....	94
Figure 6.5 – Set of six PCBs that are the base for the HSUN sub-receivers.....	94
Figure 6.6 – Position where the thermal tape and the solder is placed on the PCB.....	95
Figure 6.7 – Mounting process of the sub-receivers	97
Figure 6.8 – Presence of spots in the solar cell of the sub-receiver n° 2.....	98
Figure 6.9 – Displacement of the ribbon from its specific position.....	98
Figure 6.10 – Unsoldered ribbon.....	99
Figure 6.11 – Diode displaced from its position on the PCB.....	99
Figure 6.12 – Percentage of sub-receivers that are within a certain range of Pmp.....	113
Figure 6.13 - Values of Pmp before (dark blue) and after (light blue) the re-soldering process.....	114
Figure 6.14 – Open-circuit voltage before and after the re-soldering process	114
Figure 6.15 – Short-circuit current before and after the re-soldering process.....	115

Figure 6.16 – Maximum power before and after the re-soldering process.....	116
Figure 6.17 – Short-circuit before and after the re-soldering process.....	116
Figure 6.18 – Open-circuit voltage before and after the re-soldering process	116
Figure 6.19 – Pressure Board	117
Figure 6.20 – Pen flux	118
Figure 6.21 – Presence of spot sand balls of soldering paste on the solar cell busbar.	119
Figure 6.22 – Percentage of sub-receivers that are within a certain range of Pmp.	120
Figure 6.23 – Maximum power point before and after the re-soldering process of sub-receivers.....	121
Figure 6.25 – Open circuit voltage before and after the re-soldering process.....	122
Figure 6.25 – Sub-receiver with the output ribbons soldered.....	123
Figure 6.27 – Experimental set to measure the I-V curves under outdoor conditions.	124
Figure 6.28 – Placement of the a) thermocouple at the rear surface of the sub-receiver and b) the radiation meter apparatus side-by-side with the sub-receiver.	124
Figure 6.29 – I-V curves measured to sub-receivers.....	125
Figure 6.30 – Measured values of Pmp of the sub-receiver and the average of the Pmp of the solar cells.	126
Figure 6.31 – Estimated values of FF of the sub-receiver.....	126
Figure 6.32 –Values of a) Isc and b) Voc of each solar cell (different red hue bars) and sub-receiver (blue bars) normalized at outdoor conditions.....	127
Figure 6.33 –Values of a) Isc and b) Voc of each solar cell (different red hue bars) and sub-receiver (blue bars) normalized at outdoor conditions.....	128
Figure 6.34 - Placement of the Thermocouple in the back rear surface of the solar cell	129
Figure 6.35 - I-V curves measured in the sunlight exposure from the a) SLT.C26-2 and b) SLT.C24-2 sub-receivers.	130
Figure 6.36 – Temperature of the rear surface of the cell and the temperature.....	131
Figure 6.37 – Temperatures of the sub-receivers estimated by two different methods.....	132
Figure 6.38 –Values of a) Isc and b) Voc of each solar cell and sub-receiver.	132
Figure 7.1 – Estimated cost-effectiveness and Pmp of solar cells.....	137

LIST OF TABLES

Table 2.1 - Description of Classes of CPV systems	9
Table 4.1 - Dimensions and materials of KVAZAR solar cells	33
Table 4.2 - Physical characteristics of solar cells	35
Table 4.3 – Dimensions and materials of Solartec solar cells	37
Table 4.4 - Calculated electrical parameters of Solartec and KVAZAR solar cells under different concentration levels	45
Table 5.1 - Photographs taken with the Electroluminescence method: before and after the cutting process of KVAZAR solar cells, and after the soldering process.....	53
Table 5.2 - Electroluminescent images taken to Solartec solar cells after the soldering process.....	54
Table 5.3 - Values of parameters of the solar cells tested before and after the soldering process.....	63
Table 5.4 – Electrical parameters estimated for KVAZAR solar cells at 1 sun.	64
Table 5.5 - Values of parameters of the solar cells tested before and after the soldering process.....	66
Table 5.6 - Values of electrical parameters of the Solartec and KVAZAR solar cells.....	66
Table 5.7 – Series Resistance estimated by the slope method.....	72
Table 5.8 – Series Resistance estimated by the multiple light intensities method.....	73
Table 5.9 - Series Resistance estimated by the Suns Voc setup	75
Table 5.10 – Series Resistance of the KVAZAR, Solartec and NaREC solar cells estimated by the different methods.	77
Table 5.11 – Thermal coefficients estimated for the Solartec and KVAZAR solar cells.....	89
Table 6.1 - Description of the soldering paste configuration used on each sub-receiver	101
Table 6.2 - Description of the soldering paste configuration used on each sub-receiver	102
Table 6.3 - Description of the soldering paste configuration used on each sub-receiver.	103
Table 6.4 - Description of the soldering paste configuration used on each sub-receiver	104
Table 6.5 - Description of the soldering paste configuration used on each sub-receiver	105
Table 6.6 - Description of the soldering paste configuration used on each sub-receiver	106
Table 6.7 - Description of the soldering paste configuration used on each sub-receiver.	107
Table 6.8 - Description of the soldering paste configuration used on each sub-receiver.	108
Table 6.9 – Method used in each of the sub-receiver	118
Table 7.1 – Technology and prices of the Solartec, NaREC and KVAZAR solar cells.....	136

List of Abbreviations

Acronyms

CPV – Concentrated photovoltaic

ECT – Equivalent Cell Temperature

EL – Electroluminescence

EWT – Emitters Wrap Trough

FCT-UNL – Faculdade de Ciências e Tecnologia – Universidade Nova de Lisboa

FCUL – Faculdade de Ciências da Universidade de Lisboa

HCPV – High Concentration Photovoltaic

I-V – Current-voltage

LCPV – Low Concentration Photovoltaic LGBC – Laser Grooved Buried Contact

MCPV – Medium Concentration Photovoltaic

MWT – Metallization Wrap Trough

QE – Quantum Efficiency

PCB – Printed Circuit Board

PV – Photovoltaic

RE – Renewable Energy

R&D – Research and Development

SR – Spectral Response

Variables

ε – Efficiency

λ – Wavelength

β – Thermal coefficient

E_g –Energy gap

FF – Fill Factor

I_0 - Reverse Saturation Current (or leakage current)

I_{MPP} – Current at Maximum Power Point

I_{sc} – Short-circuit current

k – Boltzmann constant

J_{sc} – Short-circuit current density P_{loss} – Power losses

P_{mp} – Maximum power point

q –Electron charge

R_s – Series resistance

R_{sh} – Shunt resistance

T – Temperature

V_{MPP} – Voltage at maximum power point

V_{oc} – Open circuit voltage

Chapter 1**INTRODUCTION****1.1 Context**

Since 1860, the average surface temperature increased 0.6 °C. Different future scenarios predict that by 2100, this temperature will increase between 1.5 and 6° C, if the energy choices and habits of current consumption remain unchanged [1].

The Renewable Energy whose conversion technologies have reached a maturity which allows commercial and technical perspective the application of economic significance, are forms of energy that regenerate cyclically in a reduced scale of time. That is, energies that are in constant renewal, are inexhaustible and can be continuously used [2]. Thus, the renewable energies are pointed out as one of the solutions to mitigate the energetic problems, as well as a sustainable alternative to fossil fuels [2]. Among them, solar energy has the biggest developing potential and has proven to be an efficient and cost-effective energy source for different applications.

The Sun is the most abundant power source and is estimated that the sunlight that reaches the Earth's surface is enough to provide more energy as it is currently used. On a global average, each square meter of land is exposed to enough sunlight to produce 1700 kWh of power every year [3].

Photovoltaic (PV) technology involves the generation of energy from the direct conversion of the sunlight into electricity. Since 2000, total PV production increased almost by two orders of magnitude, with annual growth rates between 40% and 90%. The most rapid growth in annual production over the last five years could be observed in Asia, where China and Taiwan together now account for almost 60% of world-wide production. However, the major barrier towards very large-scale use of PV systems has been the cost of electricity generation with this type of technology [4].

Concentrated photovoltaic (CPV), by concentrating the sunlight into the solar cells through the use of mirrors or lenses, decreases the silicon area necessary for the production of the same power, leading to a decrease of the price of electricity generated by the system. As so, the CPV technology is considered by some the technology with most potential to reach costs of electricity that can compete with fossil fuels [5].

The CPV configurations vary widely according to the concentration ratio, the type of optics (refractive or reflective) and the geometry, but also by the type of solar cells used. Since the CPV systems operate under concentration, it's necessary that the solar cells used in this kind of systems present several proprieties that lead to a good performance. Thus, the solar cell choice is decisive for a CPV system to achieve high performance and to be reliable over its entire lifetime [5].

1.2 Scope and objectives

This master thesis was developed within the framework of the HSUN project, a new CPV system that is being developed in a collaboration between the research and development (R&D) Wemans and Sorasio Laboratories of WS Energia, the *Departamento de Engenharia Electrotécnica from Faculdade de Ciências e Tecnologia – Universidade Nova de Lisboa* (FCT-UNL) and the *Faculdade de Ciências da Universidade de Lisboa* (FCUL) and intends to contribute to evolution of science and technology on photovoltaic systems, and thus increase the penetration of solar energy in the markets.

The objective of this research was to study the performance of various types of solar cells under solar concentration and thus, contributing for the development of the HSUN technology. Thus, taking into account the main objective, the thesis is divided in two distinct parts:

- Laboratorial characterization of the solar cells in study to validate the theoretical method that was used for predicting the behavior of solar cells under different concentration levels.
- Improvement of the mounting process of the HSUN receivers. Through the implementation of this process, the soldering of solar cells has become faster with a lower probability of damaging the solar cells. It was also performed an experimental campaign to understand the behavior of the solar cells when integrated into the HSUN sub-receivers.

The objectives were accomplished and are completely integrated in the project: the improved mounting process of the HSUN receivers is being used to the preparation of new prototypes and the solar cells studied are already being used in the new HSUN prototype. Some of parts of this work were presented in the European Photovoltaic Solar Energy Conference in Hamburg and the article and poster presented can be consulted in the Annex I.

1.3. Structure of the thesis

This thesis is organized in eight Chapters:

Chapter 1 sets the context, scope and main objectives of the thesis as the necessity of a correct choice of the solar cell that integrates the CPV system.

Chapter 2 presents the fundamental concepts and state of the art of concentrated photovoltaics systems

Chapter 3 presents the fundamental concepts of the solar cells and describes the state of the art of the solar cells that are suitable to integrate the CPV systems. Also in this chapter it is presented the physical characteristics of the solar cells under study in this thesis.

Chapter 4 covers the estimated behavior of the solar cells under different concentration levels. A mathematical model to estimate the behavior of solar cells under concentration is explained and the expected behavior of the solar cells under concentration is presented.

Chapter 5 describes the laboratorial characterization of the solar cells under study, with the presentation of a full experimental campaign where several experimental procedures were performed in order to test and analyze the electrical and physical parameters of the solar cells.

Chapter 6 describes the behavior of the solar cells tested integrated in the HSUN sub-receivers. Also in this chapter is explained the whole soldering process of solar cells developed in the context of this thesis.

Chapter 7 describes the cost-efficiency analysis of screen-printed solar cells to integrate CPV systems.

Chapter 8 presents the main conclusions of this work, as well as directions for future developments related to the solar cells in the HSUN project.

Concentration Photovoltaic Systems

This chapter introduces the fundamental concept and a brief history of Photovoltaic (PV) technology. Within this area, Concentration photovoltaic (CPV) systems are pointed out as an interesting technological option to significantly reduce the PV electricity costs. The main areas of CPV technology are then briefly described.

2.1. Photovoltaic Solar Energy

The photovoltaic (PV) effect consists on the direct conversion of sunlight into electricity. Such effect, involves the transfer of the photon energy of the incident radiation to the electrons of the atomic structure of the semiconductor material. This translates into the creation of free charges in the semiconductor, which are separated inside the device by the electric field of the junction, thus producing an electric current outside [6].

This effect was first observed in 1839 by Edmond Becquerel who found that metal plates, platinum or silver, dipped in an electrolyte, when exposed to light, produces a small potential difference. Later in 1877, two inventors from the U.S., W. G. Adams and R. E. Day, used the photoconductive properties of selenium, to develop the first solid state device for producing electricity when exposed to light (Fig. 2.1).

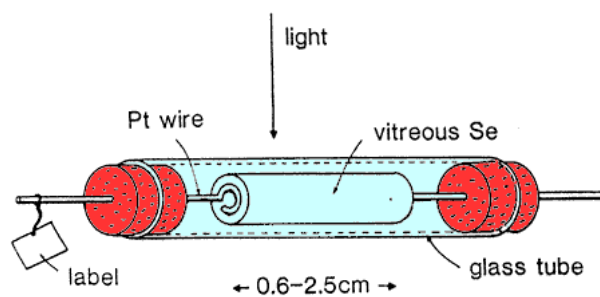


Figure 2.1 - Adams and Days' Selenium glass tube
Source: http://ihome21.kennesaw.edu/new/mods/solar_power.htm

This device consisted on a film of selenium, iron deposited on a substrate and a second film of gold, semi-transparent, which worked as a front contact. Despite the low conversion efficiency of the device (about 0.5%) in the late nineteenth century, the German engineer Werner Siemens (founder of the industrial empire with his name) marketed as selenium cell light meters for cameras [7]. With the advent of the space age, the photovoltaic technology has assumed a new importance, since the solar cells began to be used as backup to the chemical batteries used in satellites, in 1958 (Fig.2.2) [7].



Figure 2.2– Vanguard 1 was the fourth artificial satellite launched and the first to be solar power. It's the oldest satellite orbiting Earth, but there is no longer any communication with it.
Source: <http://nssdc.gsfc.nasa.gov/nmc/spacecraftDisplay.do?id=1958-002B>

The history of photovoltaic had expected its major scientific developments on the first half of the twentieth century, including the explanation of the photoelectric effect by Albert Einstein in 1905, the advent of quantum mechanics and in particular the theory of bands and the physics of semiconductor producers [7].

In the 80s, the PV has become an important source of electrical energy associated with electrical devices such as watches, calculators and radios and global photovoltaic production exceeded 9.3 MW [7]. Due to the growing demand for renewable energy sources, the manufacturing of solar cells and photovoltaic arrays has advanced considerably in recent years [6]. Driven by advances in technology and increases in manufacturing scale and sophistication, the cost of photovoltaic has declined steadily since the first solar cells were manufactured. Net metering and financial incentives, such as preferential for solar-generated electricity have supported solar PV installations in many countries [6]. In the last 11 years, the total PV production increased almost by two orders of magnitude, with annual growth rates between 40% and 90%. The most rapid growth in annual production over the last five years was observed in Asia, where China and Taiwan together now account for almost 60% of world-wide production (Fig. 2.3) [4].

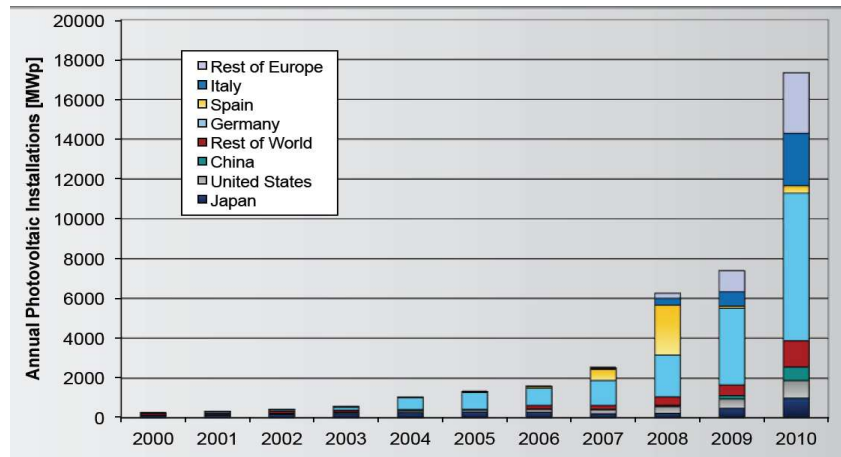


Figure 2.3 - Annual Photovoltaic Installation from 2000 to 2010
 Source: see reference [4]

2.2. Concentration of photovoltaic

2.2.1. Why Concentration?

Nowadays, the PV technology shows up as a very attractive option for clean energy generation. However, this technology have been limited in use due to the high cost associated to these systems [8] which was mainly associated to the solar cells price. One approach to reduce PV electricity cost lies in the development of concentration photovoltaic (CPV) systems which lead to a decrease in the amount of semiconductor material per watt of generated power by providing an increase of the radiation intensity per area (Fig. 2.4) [8].

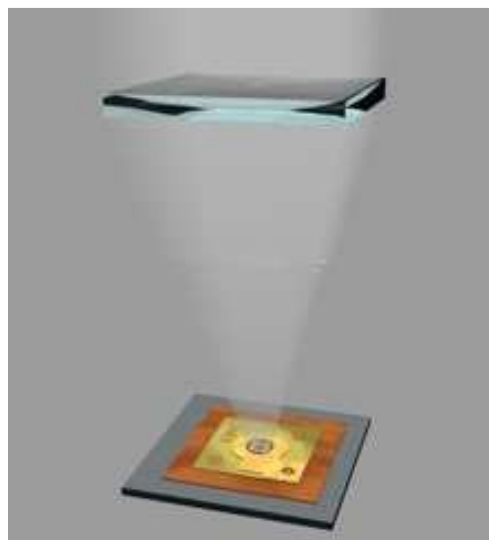


Figure 2.4 – Concentration of the light in the solar cell

Source: http://i00.i.aliimg.com/photo/v0/452739624/Dual_axis_solar_tracker_for_Concentrated_Photovoltaic.jpg

Such increase in the irradiation is provided by mirrors or lenses that concentrate solar radiation from a large area, into a smaller area [9]. Since the optical elements are cheaper than the solar cells, a further cost reduction on the PV electricity may be expected [9]. The CPV technology advantage is illustrated by Fig. 2.5 which shows the percentage of each PV system component cost as to the total cost of the system. The relative costs are presented for conventional silicon PV modules integrated in two different configurations: a fixed structure and a CPV system, the DoubleSun[®] technology which was developed by WS Energia S.A. As can be observed, in the case of CPV systems, the impact of semiconductor material (i.e. of the module), in the total cost of the system, decreases to almost a half.

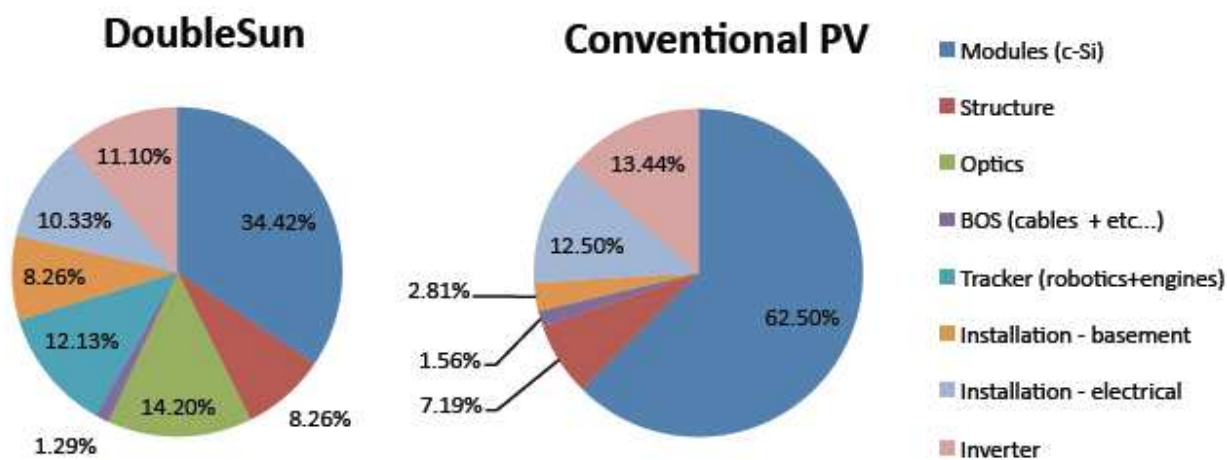


Figure 2.5 - Relative cost of the components of a PV systems as to its total cost for a conventional PV system (on the right-hand) and for a CPV system, the DoubleSun[®] technology (on the left-hand).

Source: Reis, Filipa, "LCoE analysis as a decision tool for design of concentrated photovoltaic system", 2011

2.2.2. Fundamentals of CPV systems

The CPV systems are usually classified taking into account its concentration level which can be quantified in terms of concentration intensity, or "suns". The "suns" concentration is defined as the ratio of the average intensity of the focused light on the cell active area divided by 1000W/m² (the standard peak solar irradiance)[10]. Thus, the CPV systems are divided in three classes: Low, Medium and High concentration systems (LCPV, MCPV and HCPV, respectively) as showed in Table 2.1.

Table 2.1 - Description of Classes of CPV systems

Source: S. Kurtz, "Opportunities and Challenges for Development of a Mature Concentrating Photovoltaic Power Industry", 2009

Class of CPV	Typical Concentration Ratio
High-concentration	>400 suns
Medium-concentration	10 suns – 100 suns
Low-concentration	2 suns -10suns

As showed in Fig. 2.6, a CPV system can be divided in 3 main components (optics, trackers and receiver) which are presented and brief described in the next sections.

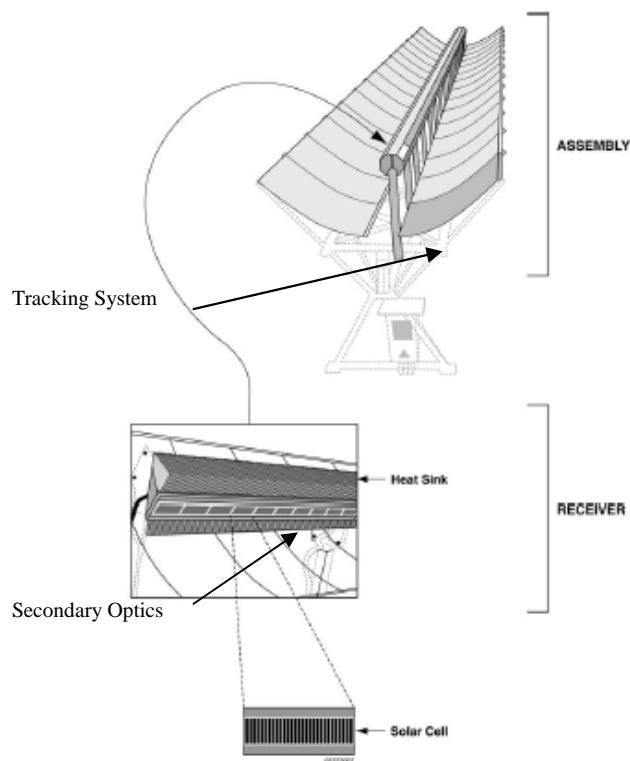


Figure 2.6 - Schematic of Linear-Focus Trough PV Concentrator
Source: IEC62108 Norm

2.2.2.1. Optics

The optics of a CPV system is the component that concentrates the sunlight into solar cells. It can be divided in two main groups: refractive optics and reflective optics. The refractive optics usually consists on Fresnel lenses and can have two distinct configurations: i) point-focus, where is

show a typical ray hitting the circular active area of the solar cell; or ii) linear focus, in which the sunlight is focused on a line of solar cells which are placed in a string (Fig. 2.7) [10].

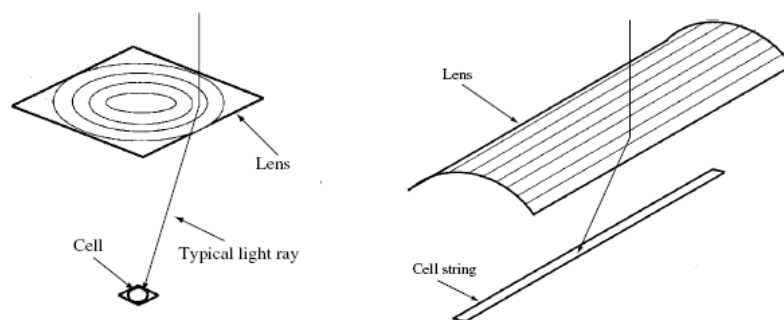


Figure 2.7 - Fresnel lens configurations: a point-focus Fresnel lens (on the left-hand) and a domed linear Fresnel (on the right-hand)
 Source: see reference [10].

Regarding the reflective optics, the most common solution is the use of mirrors. These components can have different configurations such as: i) linear (used for low concentration levels) and ii) parabolic shaped (used for medium and high concentration levels). As in the case of the Fresnel lenses, the parabolic shapes can be classified in two groups: parabolic with point focus, where parabolic dishes are used to focus the sunlight; and linear focus, where the light is focuses through the use of parabolic troughs (Fig. 2.8) [10].

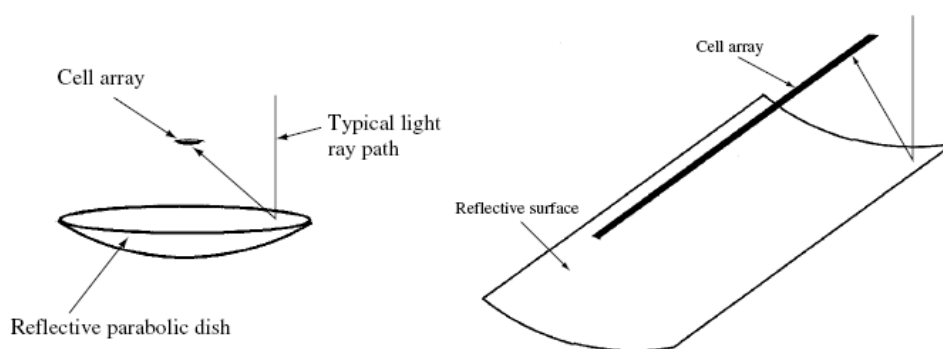


Figure 2.8 - Reflective concentrator configurations: a point-focus parabolic mirror concentrating (on the left-hand) and a linear parabolic (on the right-hand).
 Source: see reference [10].

As mentioned before, the mirrors or lenses described above are used in the CPV systems as the primary optics. However, many of the CPV configurations also use a secondary optics to raise the performance of the concentrator. Such improvement may lie on the increase of the acceptance angle

or even on a higher homogeneity of the radiation that falls on the cells. As the primary optics, there are several configurations for the secondary optics [10].

2.2.2.2. Tracking systems

To correctly concentrate the sunlight on the solar cells, the optics of the CPV systems have to be aligned with the sun rays, thus demanding for a tracking system which places the CPV system towards the sun from sunrise until sunset [8]. In general, the tracking systems, depending of the optics requirements, can track in 1 or 2 axes (Fig. 2.9). In the case of the point focus optics (that was mentioned above) usually requires the tracking in 2 axes while, in the case of the linear focus optics, the tracks in 1 vertical axis can be enough to guarantee a proper performance of the CPV system. Although in most cases the solar cells are the most expensive component that integrates the CPV system, in some of the cases, when a elevated tracking precision is required, the tracking system and its structure can become the most expensive component of a CPV system [10]. Thus, the higher the precision, the greater is the cost associated with this equipment.

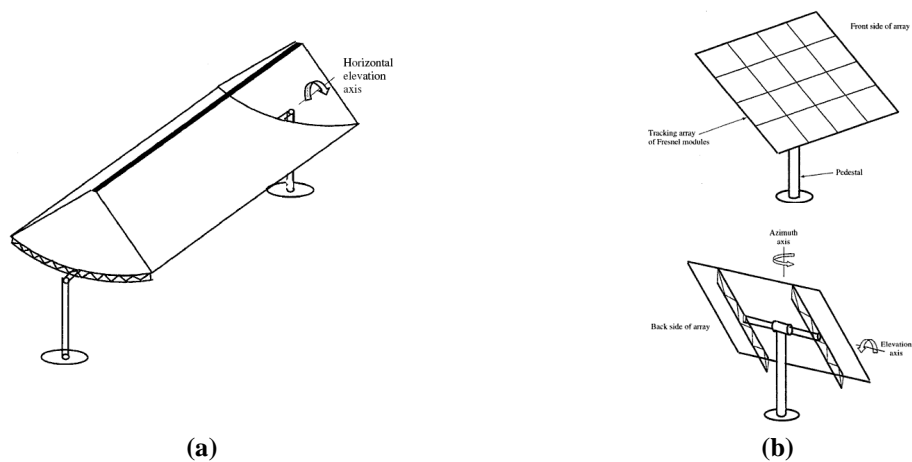


Figure 2.9 – Types of Tracking systems: (a) 1 axis tracker and (b) 2 axis tracker
Source : see reference [10].

2.2.2.2. Receiver

The concentrator receiver can be describe as the group of one or more solar cells and secondary optics (if present) that receives the concentrated sunlight and incorporates the means for thermal and electric energy transfer. A receiver could be made of several sub-receivers, where the sub-receiver can be classified as the elementary unit of the full-size receiver [11].

The concentration ratios that are reached in a CPV system leads to high temperatures, which affect the cells performance. Thus, a cooling system may be required. The cooling system can be classified in two strands: passive, where the cooling of the module is made through by aluminum fins; and active, where the cooling of the module is made with running water[11].

To a properly function in the CPV systems, the photovoltaic cells demand for specific requirements of the concentrated light and from the solar cell itself. This aspect will be addressed in detail in Chapter 3.

Fundamentals of Solar Cells to CPV systems

This Chapter covers the basic principles of PV solar cells by addressing: i) the equivalent electrical circuit; ii) the main electrical parameters that characterize a solar cell and iii) the influence of radiation and temperature on solar cells performance. This chapter ends with an overview of the solar cells that are suitable for CPV applications.

3.1. Basic principles of photovoltaic solar cells

3.1.1. Equivalent electric circuit of the solar cell

Photovoltaic cells are made of semiconductor material, i.e. material with intermediate characteristics between a conductor and an insulator. Silicon presents itself typically as sand. However, through the appropriate methods is obtained silicon in a pure form. The crystal of pure silicon has no free electrons and therefore is a poor electrical conductor [12].

Thus, in order to change this situation, percentages of other elements, as phosphorus and boron, are added to the silicon. This process is named doping. Through the doping of silicon with phosphorus, a material with free electrons or materials with negative charge carriers (n-type silicon) is obtained. By performing the same process, but now added boron instead of phosphorus, is obtained a material with the opposite characteristics, i.e. lack of electrons or a material with free positively charges (p-type silicon) [12].

Each solar cell is composed of a thin layer of n-type material and a thick layer of p-type material. Separately, both layers are electrically neutral. But together, in the p-n region, they form an electric field due to free electrons from the n-type silicon that occupy the gaps in the structure of the p-type silicon. So, by focusing light on the photovoltaic cell, the photons collide with other electrons present in the silicon structure, providing them energy and turning them into conductors. Due to the electric field generated by the p-n junction, electrons are guided and flow from the p-layer to the n-layer, converting part of the incident light into electrical energy direct current (Fig. 3.1)[12].

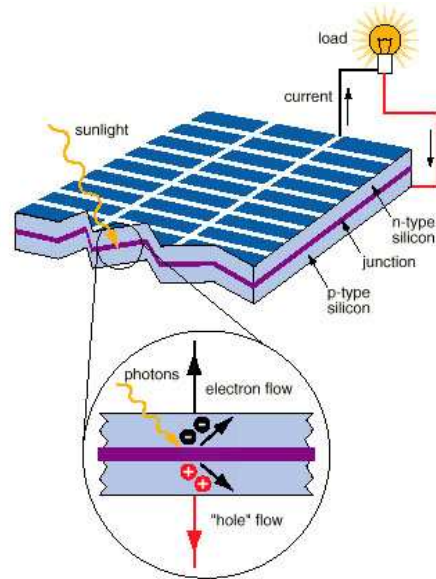


Figure 10- Principle of operation of a solar cell.
 Source: <http://www.esdalcollege.nl/eos/vakken/na/zonnecel.htm>

The junction works as a rectifier or diode because the application of a potential difference, with the positive potential applied to the p-type material, decreases the potential barrier and allows current to pass through the interface, while the application of a reverse potential difference increases the potential barrier and not allow the passage of current. Figure 3.2 illustrates the characteristic curve of a silicon diode [13].

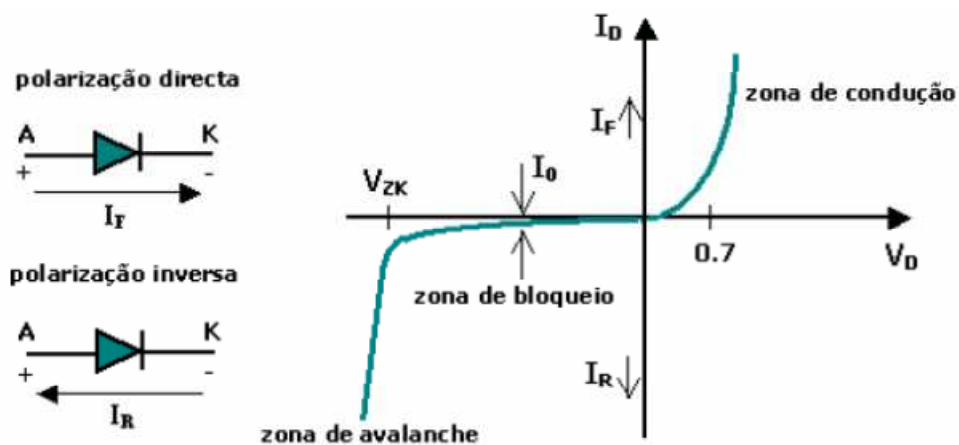


Figure 11 - I-V characteristic of a silicon diode
 Source: see reference [13]

When the diode is connected to a circuit so as that the potential is positive on the anode doped with impurities of type p, and negative on the cathode doped with impurities of type n, the diode is directly polarized. In this case its applied the first quadrant of characteristic curves, where, from a defined voltage (threshold driving voltage in this case is 0.7 V), the current will flow [13].

If the diode is reverse-biased, current is prevented to move in this direction and in this case, it applies to the third quadrant of the characteristic curve. The diode goes into avalanche or breakdown region when the reverse voltage exceeds a given threshold value (which may lead to its destruction), specific for each diode, called rupture strain. It is the "knee" strain of the I-V curve, and it is designated by V_{ZK} . In the region of rupture, the reverse current grows quickly, while the corresponding increase in voltage drop too low [13].

The expression that gives us the variation of intensity of the diode current (I_d) with a difference of potential on the terminals is the Shockley equation [13]:

$$I_d = I_0 \left(\exp\left(\frac{V}{mV_T}\right) - 1 \right) \quad (1)$$

where:

I_0 - Reverse Saturation Current (or leakage) that passes through the diode;

V - Difference of potential on the terminals of the diode;

m - Ideality factor of the diode (when $m = 1$, we have a ideal diode; when the $m > 1$, we have a real diode);

V_T - Thermal Potential that is given by the equation 2

$$V_T = \frac{kT}{q} \quad (2)$$

k - Boltzman Constant ($k = 1.38 \times 10^{-23} \text{ J/K}$);

T - Absolute temperature of the cell (in Kelvin);

q - Electron charge ($e = 1.60 \times 10^{-19} \text{ J/K}$).

The current I_d is void when $V = 0$, increases exponentially for positive values of qV and decreases when qV is negative for a value of saturation negative.

A solar cell that is not exposed to solar radiation is represented by the equivalent circuit of a diode and the respective I-V curve in Fig. 3.3 [13].

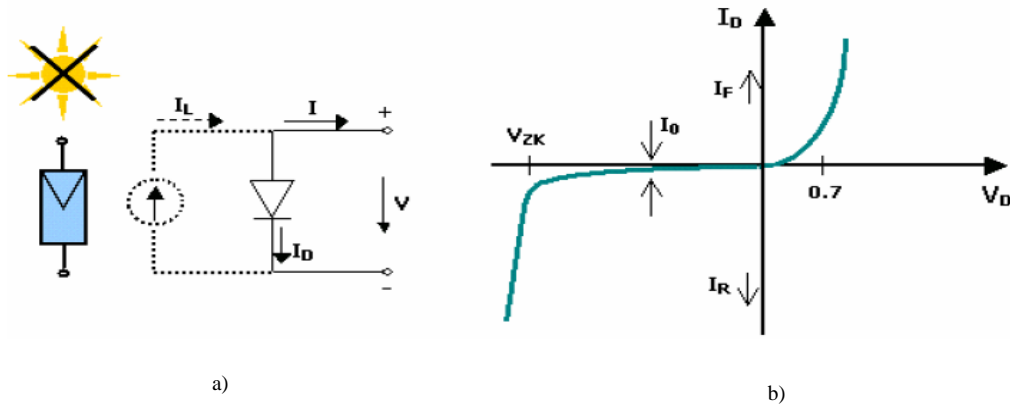


Figure 12 - a) Diagram of equivalent circuit; b) Characteristic curve of the cell in total darkness
Source: see reference [13]

The equation that expresses the variation of current vs. voltage for the ideal solar cell is given by [13]:

$$I = I_L - I_D \Leftrightarrow I = I_L - I_0 \left(\exp\left(\frac{V}{mV_T}\right) - 1 \right) \quad (3)$$

where I_L is the current generated due to exposure to light or solar radiation. Then, it proves that if does not exist solar radiation, the value of I_L is 0, and the equation (3) leads to the equation (1). In the presence of solar radiation, the characteristic curve of diode is deflected by the peak current I_L in the direction of reverse bias (fourth quadrant in the diagram of I-V curve) (Fig. 3.4) [13]. The current generated by the solar radiation can be electrically represented by a current source (Fig. 3.4).

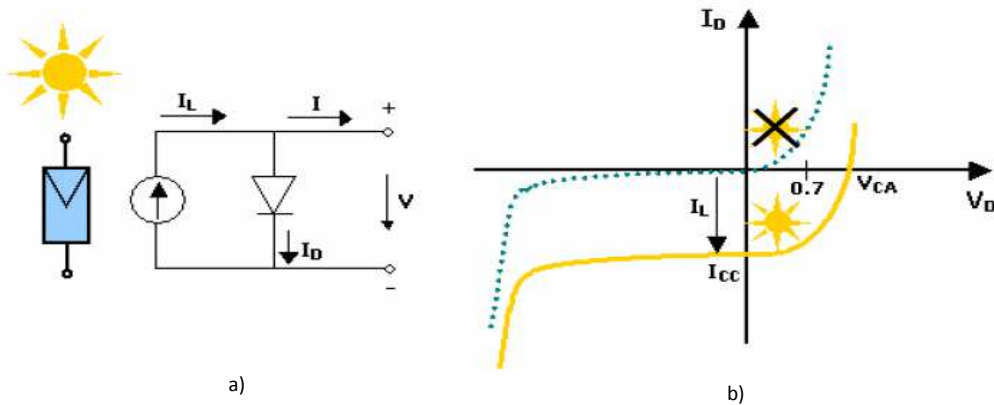


Figure 13 - a) Diagram of equivalent circuit b) Characteristic curve of the irradiated cell
Source: see reference [13]

However, contrary to what occurs in the ideal solar cell, in reality the PV cells have associated to their characteristic parasitic resistances that affect their performance. As such, the equivalent electric circuit should include two elements, the series (R_s) and shunt or parallel (R_{sh}) resistance [13]. Figure 3.5 shows the equivalent electric circuit that represents the operation of one real solar cell when connecting its terminals to one electrical charge (Z).

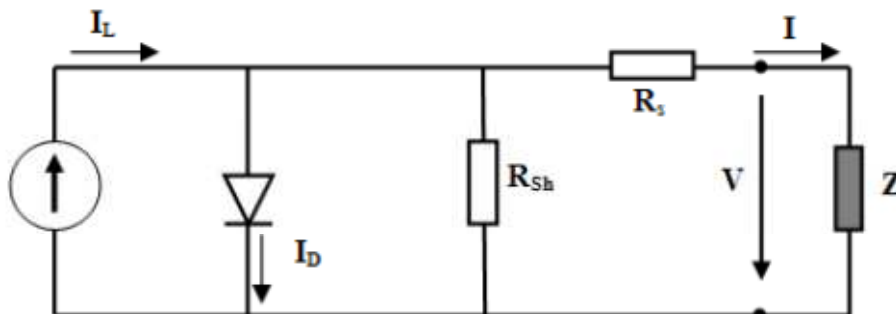


Figure 14 - Representation of the electrical circuit of one real solar cell
Source: http://www.newworldencyclopedia.org/entry/Solar_cell

The R_{sh} is arises from the defects present in the solar cells, while the R_s is formed by many individual resistances:

- Emitter sheet resistance;
- Bulk substrate;
- Resistance of the the busbar and fingers;
- Contact resistance between front gridlines and emitter;
- Resistance of the back busbar.

The main effect of R_s on the I-V curve is shown in Fig. 3.6 and consists on the reduction in the slope of the curve near the open circuit voltage (V_{oc}) region [6].

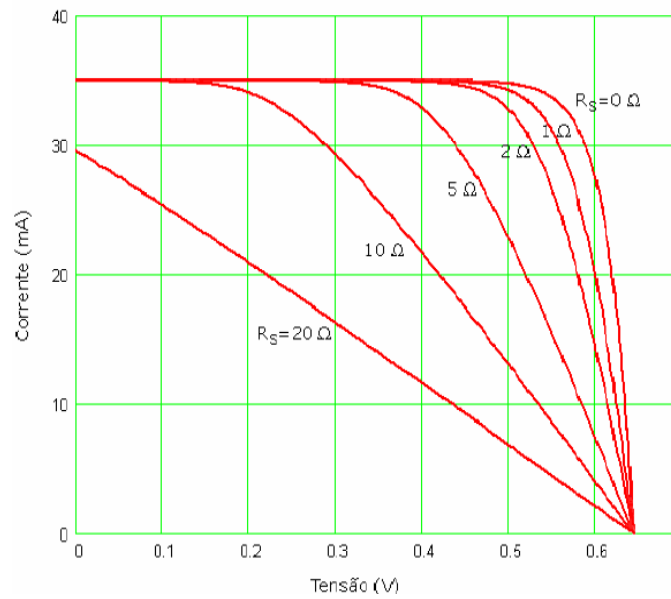


Figure 15 - Effect of variation of series resistance in the I-V curve
Source: see reference [14]

As mentioned above, the R_{sh} (shunt resistance) resistive component brings together the various factors which cause leakage current. Ideally R_{sh} is infinite and its effect on the characteristic curve is the reductions of the slope near the short-circuit current (I_{sc}) region, as shown in Fig. 3.7 [6].

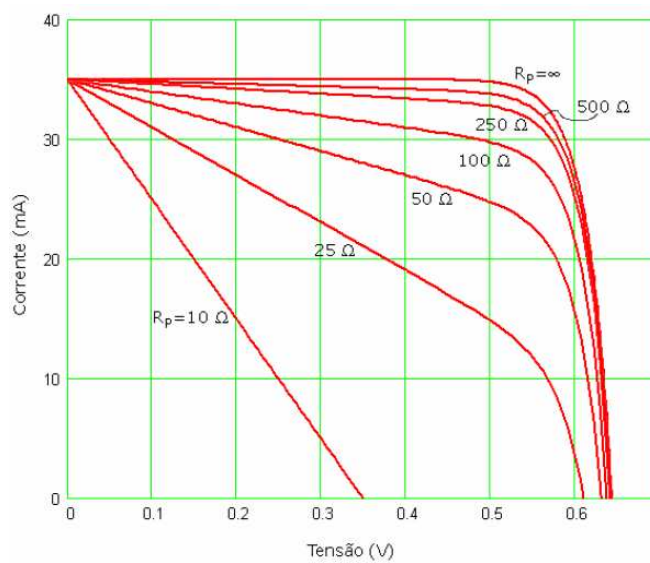


Figure 16 - Effect of the variation of the parallel or shunt resistance in the I-V curve
Source: see reference [14]

Both resistances influence the I-V curve by reducing the cell fill factor. Very high values of R_{sh} and very low values of R_s may cause the reduction in short circuit current and in the open circuit voltage, respectively. In the presence of these resistances, the general equation of the characteristic curve of the cell is given by [6, 15]:

$$I = I_L - I_0 \left(\exp \left(\frac{V + R_s \times I}{mV_T} \right) - 1 \right) - \frac{V + R_s \times I}{R_{sh}} \quad (4)$$

3.2. Electrical parameters of a solar cell

When through one variable resistance that varies the electrical charge on the terminals of a photovoltaic module or other photovoltaic device exposed to solar radiation, the photogenerated electrical current that runs through the resistance varies according to the voltage on the terminals. The graphical representation of current as a function of voltage is called the characteristic curve, also named I-V curve. Figure 3.8 represented a typical I-V curve and a P-V (Power-Voltage) curve for a solar module [13].

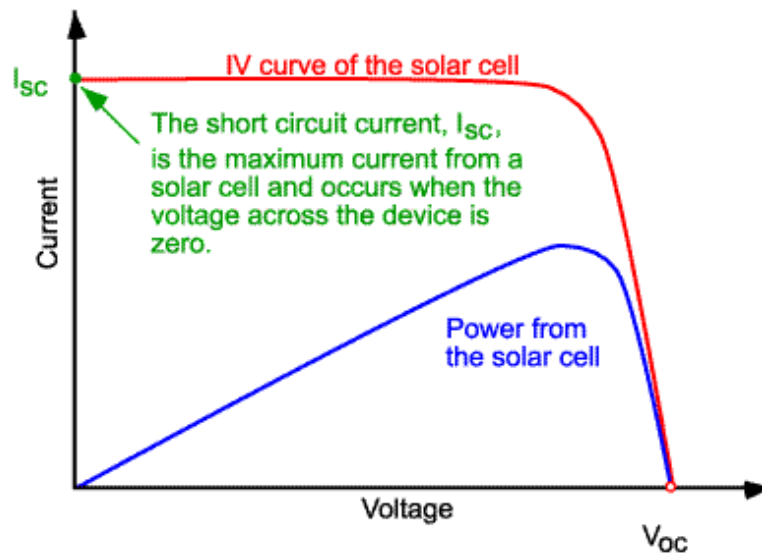


Figure 17 - I-V and P-V characteristic curve of an silicon cell
 Source: <http://www.cleanenergybrands.com/shoppingcart/products/HukseFlux-IV400.html>

Through the I-V curve of solar cell, it is therefore possible to find several parameters that allow the characterization of one solar cell.

3.2.1. Short-circuit current and open-circuit voltage

The two parameters obtained from the intercept of the I-V curve with the axis system for a given radiation and temperature, allow to characterize one solar cell of a given area.

This two parameters are the short-circuit current ($I_{sc} (V = 0)$) and the maximum voltage on the terminals of the cell by the open circuit voltage ($V_{oc} (I = 0)$) [16].

According to equation 5 and 6, the value of I_{sc} and the V_{oc} is given, respectively, by [16]:

$$I_{sc} = I_L \tag{5}$$

$$V_{oc} = m \times V_T \times \left(\frac{I_L}{I_0} + 1 \right) \tag{6}$$

3.2.2. Maximum power point

Another parameter that it can be seen through the I-V curve is the maximum power point (Pmp). The region of the characteristic curve between I_{sc} and V_{oc} that corresponds to cell functioning as a generator, for each point on the I-V curve, yielding a value of voltage and respective current, or a power ($P = V \times I$), which can be represented as shown in Fig. 3.9 [6].

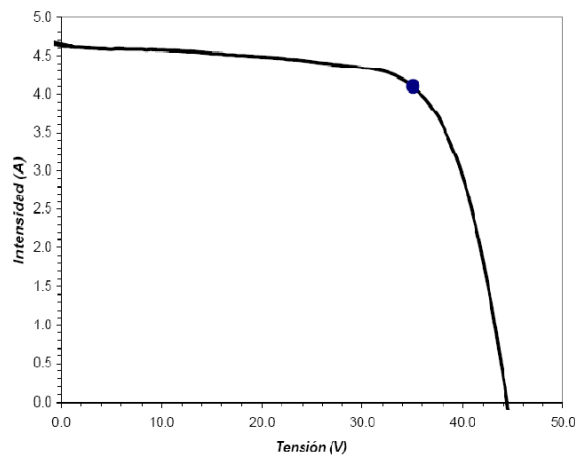


Figure 18 - I-V curve and point of maximum power draw of the CIEMAT's simulator.
Source: see reference [6].

The power delivered is given by the above product and there will be an operating point (I_{mpp} , V_{mpp}) at which maximum power is delivered - the point of maximum power.

In a short circuit or in an open circuit the power is zero. The maximum power that emerges from the cell (P_{mp}), occurs at the point of the characteristic curve where the product ($I \times V$) is maximum, ie $\frac{d(IV)}{d(V)} = \frac{d(P)}{d(V)} = 0$.

So, according to equation 7, the value of voltage at the maximum power point is given by [16]:

$$V_{mpp} = V_{OC} - m \times V_T \times \left(\frac{I_L}{I_0} + 1 \right) \quad (7)$$

And, according to the equation 8, the value of current at the maximum power is given by [16]:

$$I_{mpp} = I_0 - \frac{V_{mpp}}{V_T} \times \exp\left(\frac{V_{mpp}}{V_T}\right) \quad (8)$$

The value of maximum power is therefore calculated by the product of the maximum values of intensity and voltage of the solar cell at the Pmp, as can be seen in the equation 9 [14].

$$P_{mp} = V_{mpp} \times I(V_{mpp}) = V_{mpp} \times I_{mpp} \quad (9)$$

3.2.3. Fill Factor

The Fill Factor (FF) is a parameter which, in conjunction with V_{oc} and I_{sc} , determines the maximum power from a solar cell. The FF is defined as the ratio of the maximum power from the solar cell to the product of V_{oc} and I_{sc} and is represented in the following figure by the light blue area. It can be estimated by the equation 10 [14].

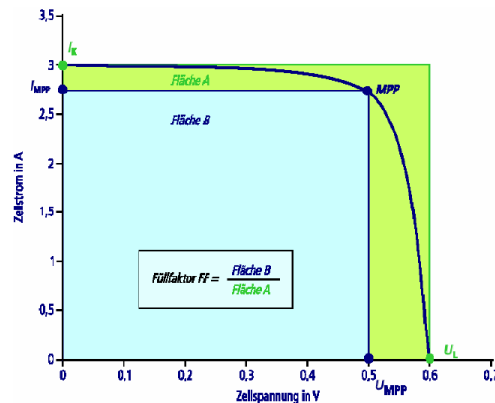


Figure 19 - Fill Factor of solar cells
Source: see reference [6].

$$FF = \frac{V_{mpp} \times I_{mpp}}{I_{sc} \times V_{oc}} \quad (10)$$

The FF is a parameter of great importance and of great practical use because it is the indicator of the quality of the cells[6].

Making use of the definition of FF, the Pmp delivered by a cell is given by equation 11 [6].

$$P_{mp} = FF \times I_{sc} \times V_{oc} \quad (11)$$

3.2.4. Conversion efficiency

The energy conversion efficiency of a solar cell is defined by the ratio between the Pmp and the power that falls on the solar cell, G [6].

$$\eta = \frac{P_{mp}}{G} \quad (12)$$

Naturally, this efficiency and maximum power is obtained only if the load resistance is adequate, given by V_{mpp} / I_{mpp} . For example, when one says that a commercial cell has an efficiency of 15% it means that if we had a cell surface of 1m² that is illuminated with 100W/m² of incident radiation, the maximum output power will be 15W [14].

3.3. Influence of temperature and radiation intensity on the characteristic curve

Factors such as the intensity of solar radiation and temperature directly influence the performance of a photovoltaic cell, which can easily be observed through its I-V curve, as showed in Fig. 3.11.

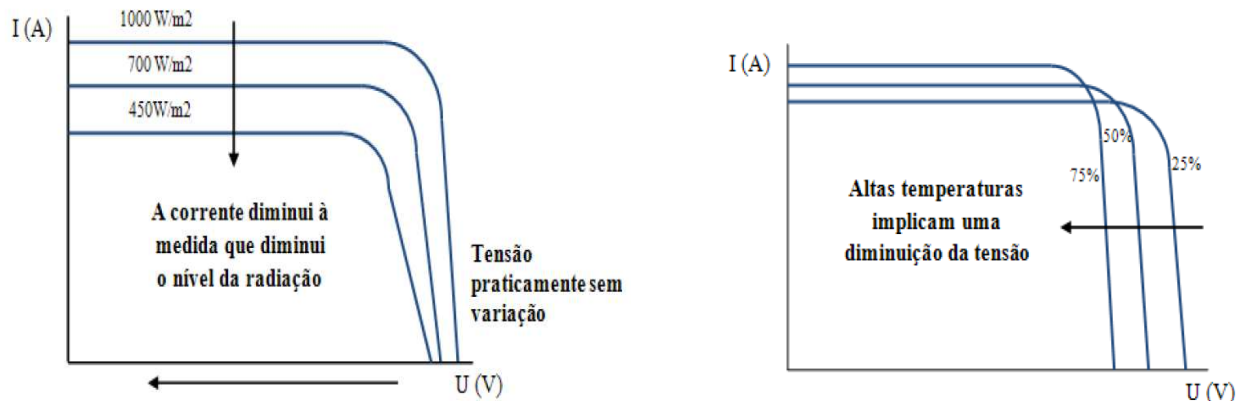


Figure 20 - Effect of a) irradiance and b) temperature in the I-V curve
Source: see reference [13]

As shown by Fig.3.11, the value of I_{sc} is increased with the raise of the incident radiation on the cell, but this variation is more important for lower values of incident radiation. When a PV cell is exposed to higher temperatures, the I_{sc} increases slightly, while the V_{oc} decreases more significantly. Thus, for a specified set of ambient conditions, higher temperatures result in a decrease of P_{mp} [13].

3.4. Overview of Solar Cells for CPV

Regarding terrestrial applications, the semiconductor devices used for the production of PV cells may be distinguished into several categories depending on the material structure and manufacturing process. Within the solar cells available on the market, the highest efficiencies are nowadays achieved by the crystalline and multijunction solar cells (Fig .3.12). These cells are also the most expensive; however, its cost is affordable for CPV applications in which the solar cell area is reduced [16].

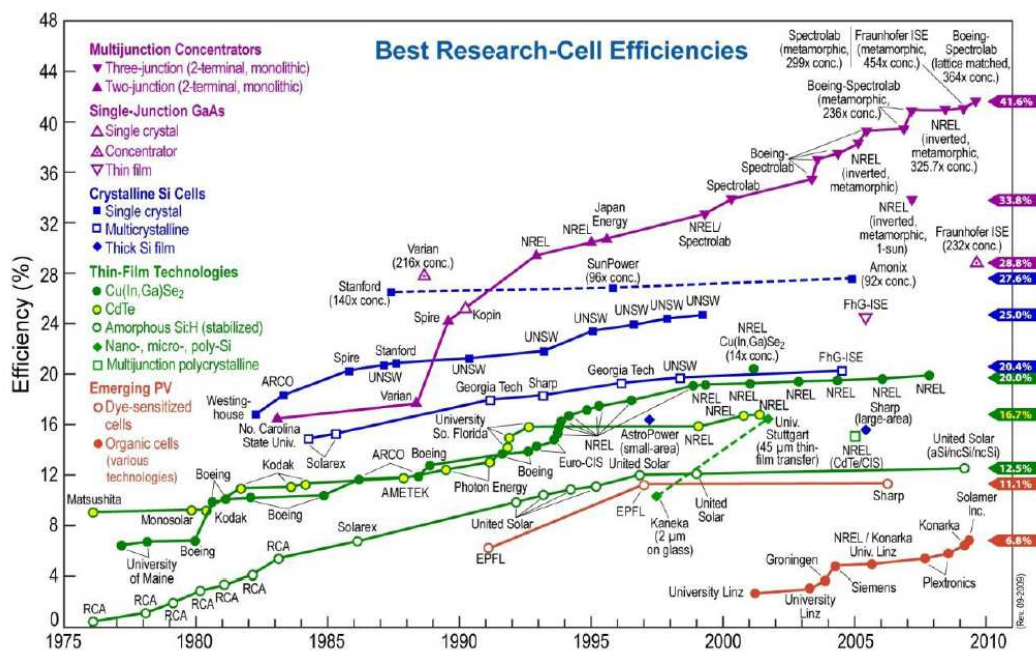


Figure 21 - Historic summary of champion cell efficiencies for various PV technologies. The highest efficiencies have been achieved for multijunction solar cells; these efficiencies are still increasing each year. Multijunction cell efficiencies have the potential to approach 50% in the coming years.
 Source: see reference [5]

Within the crystalline solar cells, the monocrystalline technology are historically the most widely used and marketed for converting solar energy into electricity and are made from a single silicon crystal. These cells are the most efficient of all silicon cells. The crystal is obtained from high purity fused silica ($\text{Si} = 99\%$ to 100%) in reactors under controlled atmosphere and with very slow speeds for the crystal growth (process known as Czochralski method). Finally, the cells are obtained by cutting the ingots into fine discs (0.4-0.5 mm thick). The efficiency of this solar cells to convert the sunlight into electricity is over 15% [17, 18].

Multijunction (MJ) cells consist of multiple semiconductors, each one capable of absorbing in a different region of electromagnetic spectrum. The semiconductors are carefully chosen to absorb nearly the entire solar spectrum, thus generating electricity from as much of the solar energy as possible (Fig. 3.13) [19]. This approach allows the cell to cover more of the light spectrum, but increases the complexity of cell design and manufacture. GaAs based multijunction devices are the most efficient solar cells to date. In October 2010, triple junction metamorphic cell reached a record high of 42.3%.

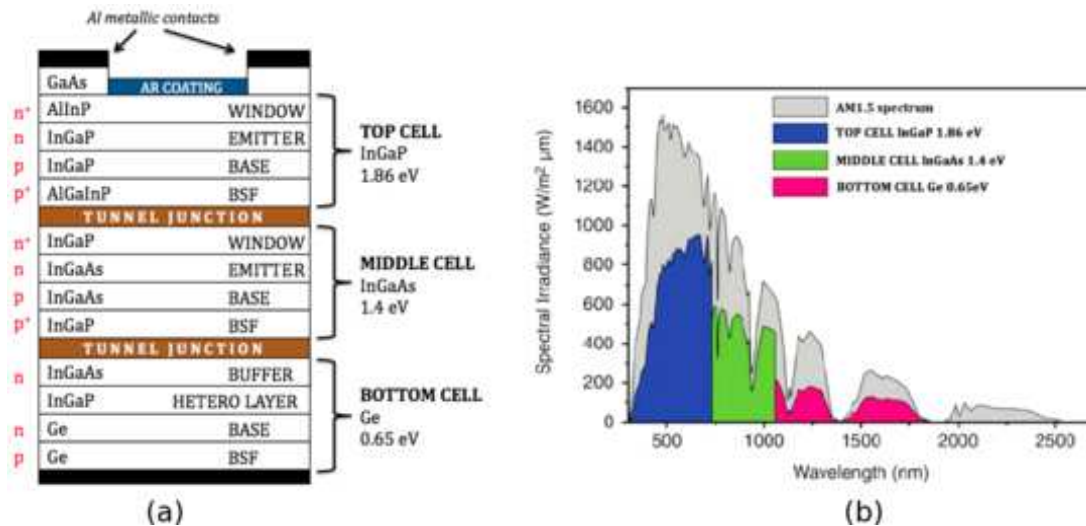


Figure 22 - (a) The structure of a MJ solar cell. There are six important types of layers: p-n junctions, back surface field (BSF) layers, window layers, tunnel junctions, anti-reflective coating and metallic contacts; **(b)** Graph of spectral irradiance G vs. Wavelength λ over the AM1.5 solar spectrum.

Source: http://en.wikipedia.org/wiki/Multi-junction_photovoltaic_cell

However, the MJ solar cells have a very high cost, which, in the short term, makes these solar cells unsuitable to integrate the low and medium concentration systems, such as the HSUN concept. As so, the silicon solar cells were pointed out as the most cost-effective solution to integrate the MCPV technology (as the HSUN system). The silicon solar cells have many years of on-field demonstration performance and a well standardized process for high volume production which makes this technology a very reliable technology benefitting from economies of scale [20].

3.4.1. Monocrystalline solar cells for CPV applications

The conventional standard monocrystalline solar cells (Fig. 3.14) are designed to work under 1000 W/m^2 (1 sun). When this type of solar cells are integrated in the CPV systems and exposed to higher amount of irradiation, the current that flows in the solar cells increases, as well as the Joule resistance losses, thus leading to a decrease of the FF and the efficiency of the solar cell) [21].

In order to guarantee an efficient operation of solar cells under concentration, highly efficiency solar cells must be fabricated specifically for concentration systems. In the following sections we describe several approaches that were taken to improve silicon solar cells efficiency under CPV applications.



Figure 23 - Monocrystalline solar cells

Source: <http://www.directindustry.com/prod/kpe-co-ltd/monocrystalline-photovoltaic-solar-cells-54445-358166.html>

3.4.1.1. Modified screen-printed solar cells

The modified conventional silicon solar cells shows up as the best choice for the existence of a compromise between high efficiency and low cost, since small changes on one-sun cell can lead to high efficiency cells with higher cost than the standard ones, but affordable when integrated in CPV systems and the industrial lines of standard silicon solar cells are easily adaptable to the new high efficiency silicon cells, thus benefiting from economies of scale [21].

The screen-printed method is an economical metallization technique used by most manufactures of conventional solar cells[22]. By printing additional metal on the solar cell front surface the resistive losses are reduced; however, additional metal causes additional shading of the top surface of the cell. Thus, the design of the front grid contact must result from a tradeoff between the shading and the resistive power loss [23]. With an optimized grid design, in accordance with conductivity and shadowing factor, we can maintain their efficiency up to a concentration level of 15 suns [24]. Through the optimized grid design we obtain a low-cost and low-level technological process which allows the use of conventional solar cells, with costs of production similar to the 1 sun conventional solar cells [24].

Shading losses can be improved through the use of prism covers, which refract light away from the metal fingers and hence cause the optical width of the fingers to be less than the geometrical width [19]. Figure 3.15 presents the efficiency variation of a silicon cell before and after electrolytic deposition to optimize the solar cells to 10 suns.

As can be seen, after the optimization of the front grid of the solar cell, the efficiency remains high until a concentration of 10 suns. Without the optimization of the front grid, the losses are significantly greater beyond 4 suns [24].

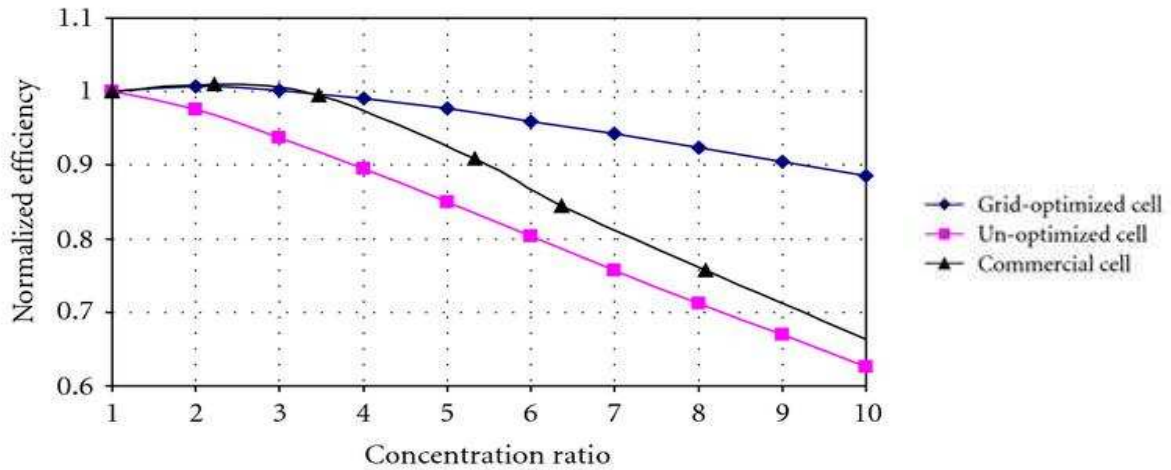


Figure 24 - Normalized plot of Efficiency against the concentration ratio of the optimized and unoptimized grid solar cell.
Source: see reference [24]

However, there are other approaches such as the Laser Grooved Buried Contact (LGBC) solar cells, the Emitters Wrap Trough (EWT) solar cells and the Metallization Wrap Trough (MWT) solar cells, among others. The main problem in using these technologies is that the production process of these new solar cells, such as occurred in multijunction solar cells, is still very recent and aren't yet completely solidified in the PV market. So, compared to Upgraded 1-sun solar cells, they are more expensive [20].

3.4.1.2. Laser Grooved Buried Contact (LGBC) solar cells

The buried contact solar cell is a high efficiency commercial solar cell technology based on a plated metal contact inside a laser-formed groove. The buried contact technology overcomes many of the disadvantages associated with screen-printed contacts and this allows that this type of solar cells presents a performance up to 25%. A schematic of a buried contact solar cell is shown in the Fig. 3.16 [22].

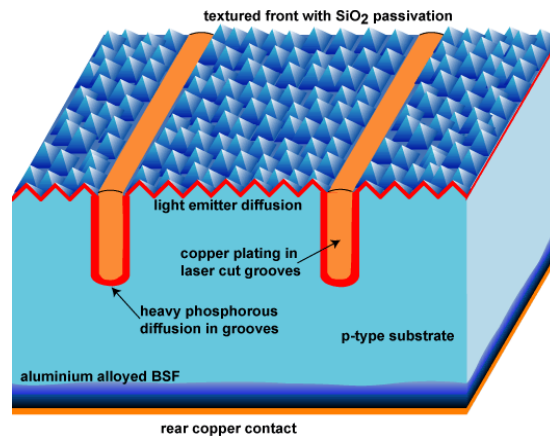


Figure 25 - Buried contact solar cells
 Source: <http://pvcfdrom.pveducation.org/MANUFACT/BCSC.HTM>

A key to the high efficiency feature of this type of technology is that, unlike in the screen-printed cells, the metal is buried in a laser-formed groove inside the solar cell. This type of contact allows for a large metal height-to-width ratio. So, by using this type of technology a large volume of metal is used in the contact finger, without having a wide strip of metal on the top surface (thus minimizing the shadow effect on the front of the solar cell) [20].

In addition to good reflection properties, the buried contact technology also allows low parasitic resistance losses due to its high metal ratio, its fine finger spacing and its plated metal for the contacts (Fig 3.17). The metal grid resistance is also low since the finger resistance is reduced by the large volume of metal in the grooves and by the use of copper, which has a lower resistivity than the metal paste used in screen printing.

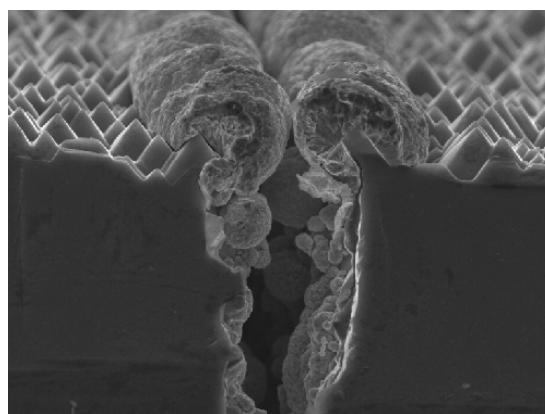


Figure 26 - Buried contact in a silicon solar cell
 Source: <http://pvcfdrom.pveducation.org/MANUFACT/BCSC.HTM>

Further, due to the inclusion of certain area-related costs as well as fixed costs in a PV system, a higher efficiency solar cell technology results in lower cost electricity. An additional advantage of

buried contact technology is that it can be used for concentrator systems [20] and, after the Upgraded 1-sun solar cells, it is the most viable technology to be used in the MCPV systems. The solar cells currently used in the HSUN system, manufactured by the NaREC company, are Laser Grooved Buried Contact (LGBC) solar cells and their specifications and electrical parameters are presented in the Annex II.

3.4.1.3. Back contact cells

3.4.1.3.1. Emitters wrap trough (EWT) solar cells

The "emitter-wrap-through" (EWT) solar cell is a back-contact cell that can use solar-grade silicon. "Emitter" refers to the current-collection junction that is commonly formed in silicon solar cells by diffusing phosphorus (an n-type dopant) into a p-type silicon substrate. The key enabling element for the EWT cell is the use of laser machining to make an array of holes in the silicon substrate (Fig. 3.18) [20].

These holes are diffused with phosphorus during the emitter diffusion, thereby wrapping the emitter from the front surface to the rear surface [20].

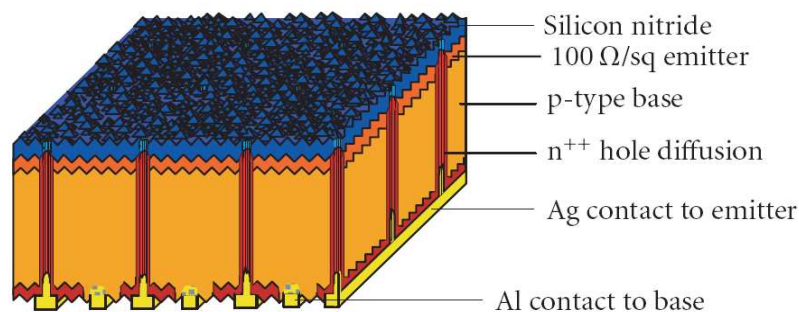


Figure 27 - Emitters wrap trough (EWT) solar cells
Source: see reference [20]

The EWT cell is particularly useful with low-quality solar-grade materials because there is an emitter on both the front and much of the rear surface over much of the cell. This effectively doubles the collection length of carriers in the bulk of the device. Early prototypes of the EWT cell at Sandia National Laboratories demonstrated efficiencies a little above 18% and 15%, using thin-film metallization and the more commercially relevant screen-printed metallization, respectively.

Theoretical calculations show that the cell structure is capable of efficiencies approaching 18% for a large-area cell using solar-grade materials and low-cost fabrication technologies like screen-printed metallization [25].

3.4.1.3.2. Metallization wrap trough (MWT) solar cells

The contact wrap-through or metallization wrap-through (MWT) back-contact cell is the concept that is most closely linked to the conventional cell structure. In these cells, the emitter is located near the front surface, but part of the front metallization grid is moved from the front to the rear surface (the busbar on the front surface of the solar cells are transferred to the rear side of the cell). In the schematic representation in Fig. 3.19, this is depicted as the busbar moving from one surface to the other, while the remaining front surface grid is connected to the interconnection pads on the rear surface by extending it through a number of openings in the wafer [20].

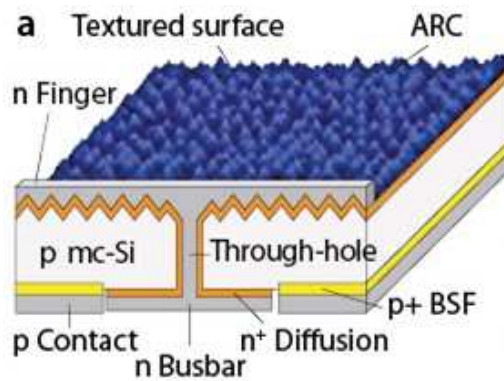


Figure 28 - Metallization wrap trough (MWT) solar cells
Source: see reference [20]

The MWT cells requires only a relatively small number of through-holes to direct photogenerated electrons to the back surface, through the metal electrodes and n-doped emitters, and produce higher collection photocurrents due to absence of a bus bar (main electrode) on the front surface (as in conventional cells). A high J_{sc} of 37.3 mA/cm^2 and an efficiency of 18.3% were reported for a recent MWT cell by Kyocera, and the module efficiency for MWT cell modules by ECN, 16.4%, is the highest reported to date [25].

To understand the real potential single crystalline silicon solar cells integrated in MCPV systems, different monocrystalline silicon solar cells were studied and the description of these solar cells are presented in the next chapters.

Theoretical characterization of Solartec and KVAZAR solar cells

This chapter covers the theoretical behavior of the Solartec and KVAZAR solar cells under concentration. In section 4.1, the physical characteristics of the Solartec and KVAZAR solar cells are presented; in section 4.2, a description of the mathematical model used for estimate the behavior of the solar cells is describe and in section 4.3, the theoretical results obtained and the consequents conclusions are presented.

4.1. Physical characteristics of the KVAZAR and Solartec solar cells

In this thesis two types of silicon solar cells were studied: i) the conventional solar cells, provided by the KVAZAR company and ii) Upgraded 1-sun screen printed silicon solar cells, provided by the Solartec company. In the next section, the physical characteristics of these solar cells are explained and the datasheets provided by the suppliers are presented in the Annex III.

4.1.1. KVAZAR solar cells

The KVAZAR conventional solar cells (Fig. 4.1), provided by the KVAZAR company, are made of monocrystalline silicon and the metallization method is the screen printing.

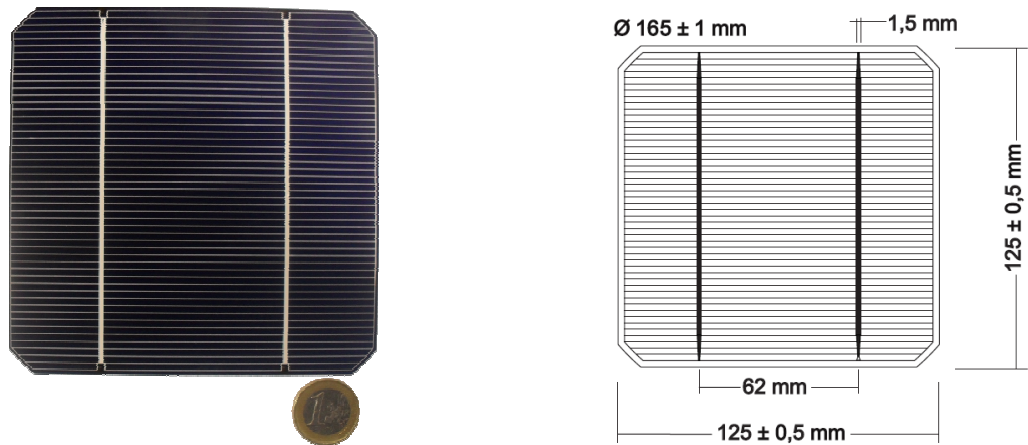


Figure 29 - Front surface of the KVAZAR solar cell (main cell)

The KVAZAR solar cells (Fig. 4.1) have a total area of 156.25 cm^2 and a thickness of $200 \mu\text{m}$, approximately. The active area of these conventional solar cells (i.e. total area less the area occupied by the contacts of the cell) is, approximately, 150 cm^2 .

The front of the solar cells is composed by a busbar and fingers (negative contact of the solar cell) with 1.5 mm and 0.04 mm of width, respectively. The back of the solar cells is composed by two soldering pads with 3mm of width and a back surface field (Fig. 4.2).

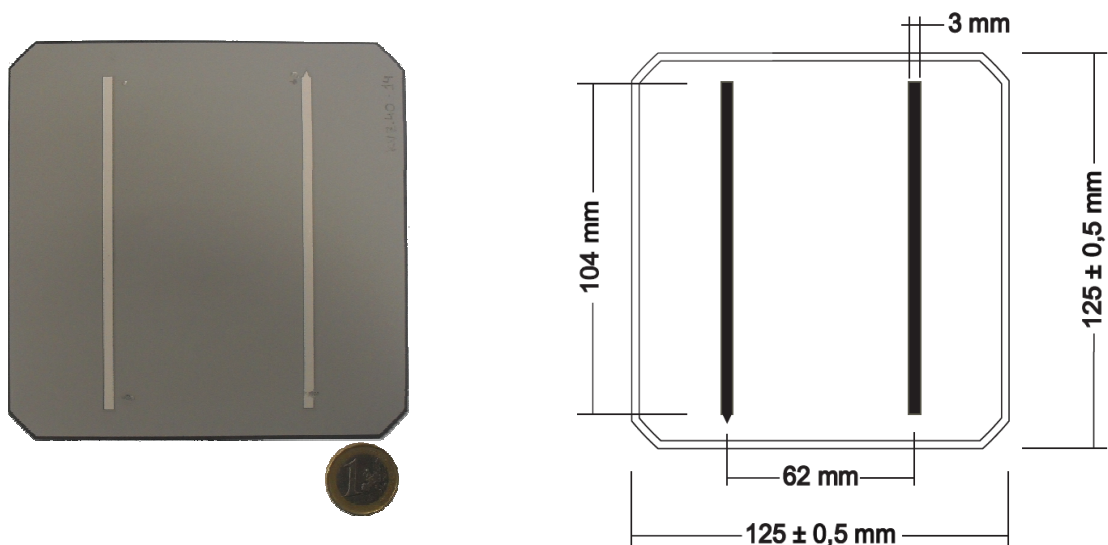


Figure 30 - Back surface of the KVAZAR solar cells (main cell)

Table 4.1 summarizes the main features (dimensions and materials) of the KVAZAR solar cells.

Table 4.1 - Dimensions and materials of KVAZAR solar cells

Dimensions		
Cell	Cell width (mm)	125
	Cell length (mm)	125
	Cell area (mm ²)	15625
	Thickness (mm)	0.20
	Active area (mm ²)	15000
Fingers	Number of fingers	50
	Finger width (mm)	0.04
	Finger length (mm)	125
	Distance between fingers (mm)	3
	Area occupied by the fingers (mm ²)	250
Busbar	Number of busbars	2
	Busbar width (mm)	1.50
	Busbar length (mm)	125
	Area occupied by the Busbar (mm ²)	375
Materials		
Waffer	Single crystalline silicon (sc-silicon)	
Front grid contacts	Cu + Ag	
Rear contact	AlSi alloy + Cu + Ag	

However, the cells used in the receivers that integrate the HSUN are smaller than the solar cells provided by KVAZAR. As such, we have cut the KVAZAR solar cells as sketched in Fig. 4.3.

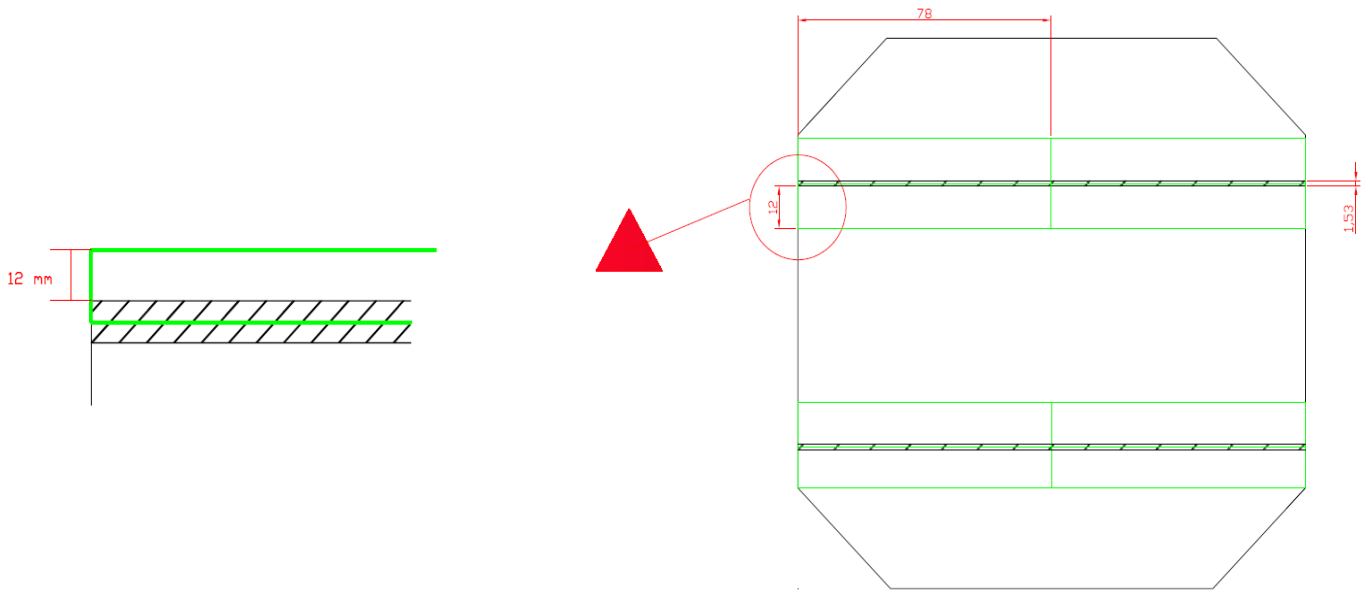


Figure 4.31 - Drawing of the cut (and dimensions) performed in the solar cells

Each cell was identified with a reference number as showed in Fig. 4.4. This reference number takes into account the position of the new cell in the “main cell” as showed in Fig. 4.5.

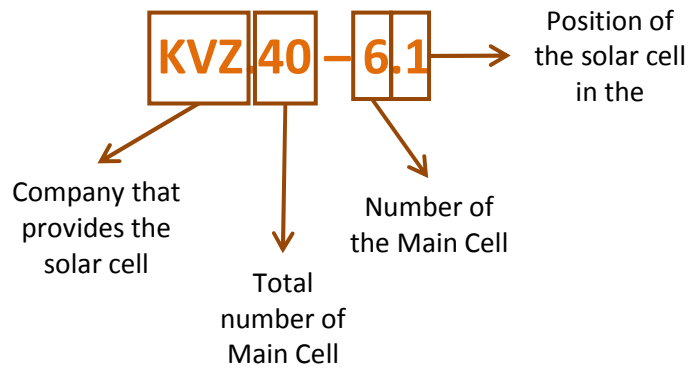


Figure 32 - Reference of the KVAZAR solar cells.

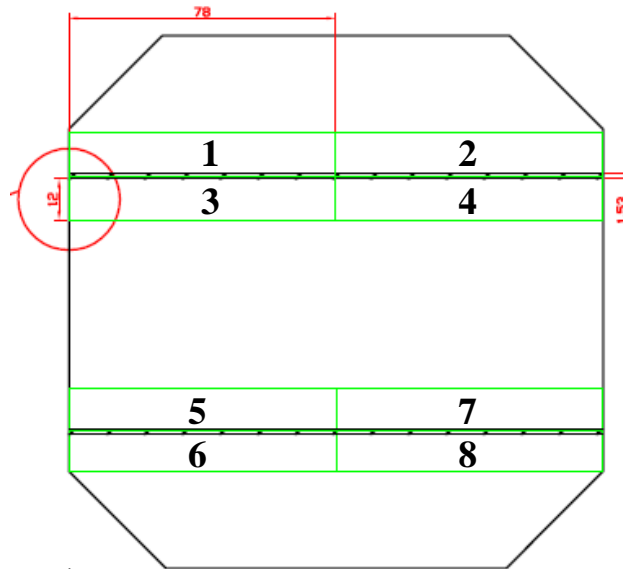


Figure 33 – Number given to each cell according to its position at the conventional wafer.

Table 4.2 presents the physical characteristics of the solar cells obtained after the cutting process.

Table 4.2 - Physical characteristics of solar cells

Dimensions		
Cell	Cell width (mm)	14
	Cell length (mm)	62.50
	Cell area (mm ²)	875
	Thickness (mm)	0.20
	Active area (mm ²)	814.13
Fingers	Number of fingers	25
	Finger width (mm)	0.04
	Finger length (mm)	14
	Distance between fingers (mm)	3
	Area occupied by the fingers (mm ²)	14
Busbar	Busbar width (mm)	0.75
	Busbar length (mm)	62.50
	Area occupied by the Busbar (mm ²)	46.88



Figure 34 – KVAZAR solar cell

4.1.2. Solartec solar cell

The Solartec solar cells (Fig. 4.7) are conventional solar cells that can be optimized taking into account the concentration level under which they are intended to operate. In this case, the cells were optimized for 15 suns which is the concentration level that is expected in the HSUN technology. These solar cells are made of monocrystalline silicon and the metallization method is the screen printing.



Figure 35 - Front surface of the Solartec solar cells

The Solartec solar cells (Fig. 4.7) have a total area of 8.78 cm^2 and a thickness of $180 \mu\text{m}$. The active area of these solar cells (i.e. total area less the area occupied by the contacts of the cell) is about 4.75 cm^2 .

As in the case of KVAZAR solar cells, the Solartec solar cells presents a front surface of the solar cells is composed by a busbar and fingers (negative contact of the solar cell) with 1.5 mm and 0.02 mm of width, respectively. However, in these solar cells, the back of the solar cells is composed by an oval soldering pad with 3 mm of diameter and a back surface field (Fig. 4.8).

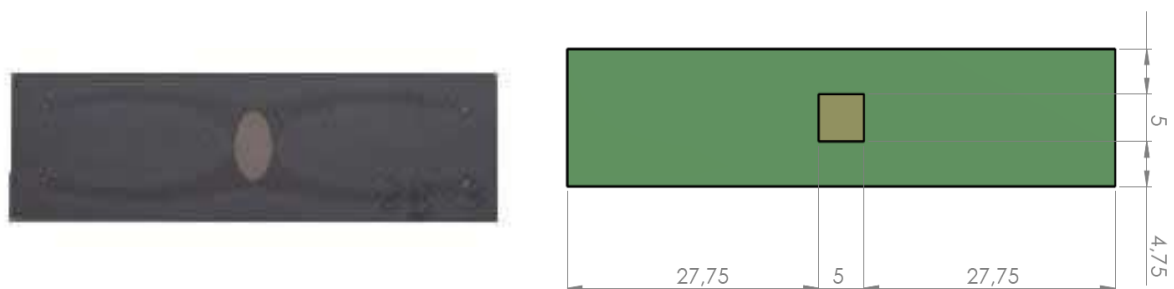


Figure 36 - Back surface of the Solartec solar cells

All the cells provided by Solartec have the same dimensions and thickness; however they may differ in the front grid design and class:

- **Front grid design:** the cells can have one or two busbar in the front surface (Fig. 4.9).
- **Classes:** there are five different classes 23, 24, 25, 26 and 27. This classification is provided by Solartec according to the electrical performance of each solar cell. However, in this thesis only the classes 24 and 26 were analyzed.

Table 4.3 summarizes the main features (dimensions and the materials) of the Solartec solar cells and the Fig. 4.9 presents the front grid designs of the Solartec solar cells.

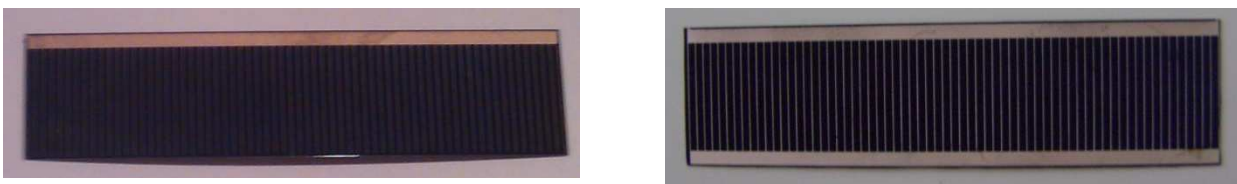


Figure 37 –Solartec solar cells with different front grid designs: a) one busbar; b) two busbars

Table 4.3 – Dimensions and materials of Solartec solar cells

Dimensions		Classes	2BB
Cell	Cell width (mm)	14.50	16
	Cell length (mm)	60	60
	Cell area (mm ²)	870	960
	Thickness (mm)	0.18	0.18
	Active area (mm ²)	760.11	759.36
Fingers	Number of fingers	66	66
	Finger width (mm)	0.02	0.02
	Finger length (mm)	14.50	14.50
	Distance between fingers (mm)	0.50	0.50
	Area occupied by the fingers (mm ²)	19.14	19.14
Busbar	Number of busbars	1	2
	Busbar width (mm)	1.50	1.50
	Busbar length (mm)	60.50	60.50
	Area occupied by the Busbar (mm ²)	90.75	181.50
Materials			
Waffer	Single crystalline silicon (sc-silicon)		
Front grid contacts	Cu + Ag		
Rear contact	AlSi alloy + Cu + Ag		

Although these solar cells find themselves organized on a variety of electrical classes, the present research focuses on the solar cells classified with the class 24 and class 26. As in the KVAZAR solar cells, the Solartec cells were also identified with a reference number (Fig. 4.10).

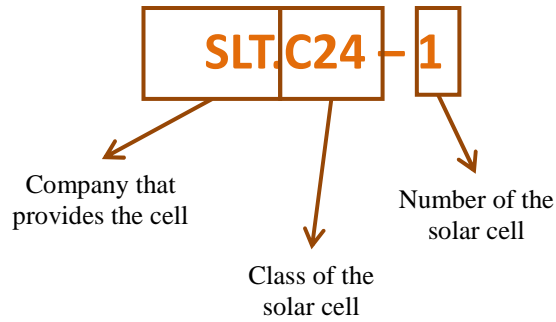


Figure 38 – Reference of the Solartec solar cells

4.2. Mathematical model to estimate the behavior of solar cells under concentration

The availability of effective modeling techniques to accurately estimate the device behavior is quite important to know the viability of solar cells in the different situations to which they are exposed [26].

In the case of solar cells, through the knowledge of their electrical parameters measured and estimated when the solar cells operate at 1 sun, it is possible to estimate the electrical parameters for different concentration levels [21].

Since the short-circuit density, J_{sc} , is proportional to the irradiance of the cell (eq. (13)), thus the current density under concentration can be described by:

$$J_{sc} (@ X \text{ suns}) = X J_{sc} (@ 1 \text{ suns}) \quad (13)$$

where X is the concentration level that falls on the solar cell.

The open circuit voltage, V_{oc} , increases like the logarithm of intensity. So, the value of this parameter under concentration is given by [21]:

$$V_{oc} (@ X \text{ suns}) = \frac{m k_B T}{q} \ln \left(\frac{X J_{sc}}{J_0} + 1 \right) \approx V_{oc} (@ 1 \text{ suns}) + \frac{m k_B T}{q} \ln(X) \quad (14)$$

where q is the electron charge, T is the cell temperature and k_B is the Boltzmann constant.

If the cell Fill Factor (FF) remained constant then the power delivered by the cell should increase by a factor [21]:

$$Factor = X \left(1 + \frac{m k_B T}{q V_{oc} (@ 1 \text{ suns})} \right) \ln(X) \quad (15)$$

And the efficiency (\mathcal{E}) by a factor [21]:

$$Factor = \left(1 + \frac{m k_B T}{q V_{OC}(@ 1 \text{ suns})}\right) \ln(X) \quad (16)$$

However, as discussed in the previous sections, a solar cell has a series resistance (R_s) where the power is dissipated as heat (P_{loss}) [21]. Thus,

$$P_{loss} = I^2 \times R_s \quad (17)$$

where I is the current flowing from the cell. Since this current is proportional to the concentration, based on eq. (13) and eq. (17), the power wasted is given by the following equation:

$$P_{loss} (@ X \text{ suns}) \cong X^2 \times I_{SC} (@ 1 \text{ sun})^2 \times R_s \quad (18)$$

Generally FF increases as V_{oc} increases, mostly because of reduced diode current. However, FF is most dependent on parasitic factors, such as shunt resistance and, most importantly at high illumination levels, series resistance [26]. Thus, when considering the series resistance, the FF will be no longer a constant value, and can be estimate by the following approximation:

$$P'_{mp} (@ X \text{ suns}) \cong V_{mpp} (@ X \text{ suns}) \times I_{MPP} (@ X \text{ suns}) - I_{mpp}^2 (@ X \text{ suns}) R_s \quad (19)$$

$$P'_{mp} (@ X \text{ suns}) \cong V_{mpp} (@ X \text{ suns}) \times I_{mpp} (@ X \text{ suns}) \times \left(1 - \frac{I_{mpp} (@ X \text{ suns})}{V_{mpp} (@ X \text{ suns})} R_s\right) \quad (20)$$

$$P'_{mp} (@ X \text{ suns}) \cong P_{mp} (@ X \text{ suns}) \times \left(1 - \frac{I_{sc} (@ X \text{ suns})}{V_{oc} (@ X \text{ suns})} R_s\right) \quad (21)$$

$$P'_{mp(@ X suns)} \cong P_{mp(@ X suns)} \times \left(1 - \frac{R_S}{R_{CH(@ X suns)}} \right) \quad (22)$$

where R_{CH} is the characteristic resistance of the cell. Through the definition of a normalized series resistance (R_s), it comes:

$$r_{s(@ X suns)} = \frac{R_S}{R_{CH(@ X suns)}} \quad (23)$$

Thus, by replacing the eq. (22) in the eq. (23) we have:

$$P'_{mp(@ X suns)} \cong P_{mp(@ X suns)} \times (1 - r_s) \quad (24)$$

Assuming that the V_{oc} and I_{sc} are not affected by the series resistance allows the impact of series resistance on FF to be determined by:

$$\begin{aligned} V'_{OC(@ X suns)} \times I'_{SC(@ X suns)} \times P'_{mp(@ X suns)} & \quad (25) \\ \cong V_{OC(@ X suns)} \times I_{SC(@ X suns)} \times P_{mp(@ X suns)} \times (1 - r_{S(@ X suns)}) & \end{aligned}$$

$$FF'_{(@ X suns)} \cong FF_0 \times (1 - r_{S(@ X suns)}) \quad (26)$$

where FF_0 is the fill factor without taking into account the series resistance and FF' is the fill factor including the losses due to the series resistance. Thus, the efficiency must be calculated by:

$$\varepsilon'_{(@ X suns)} = \frac{V_{OC(@ X suns)} \times I_{SC(@ X suns)} \times FF'_{(@ X suns)}}{P_{in(@ X suns)}} \quad (27)$$

where $P_{in(@ X suns)}$ is the input power, which is defined as:

$$P_{in(@ X suns)} = X P_{in(@ 1 sun)} \quad (28)$$

where $P_{in(@ 1 sun)}$ is 1000W/m^2 .

At last, by replacing equations (13), (14), (26) and (28) in equation (27), we obtain to the following equation [26]:

$$\varepsilon_{(@ X suns)} = \frac{I_{SC(@ 1 sun)} \times FF_0}{P_{in(@ 1 sun)}} \left[V_{OC(@ 1 sun)} + \frac{kT}{q} \ln(X) - R_s X I_{SC(@ 1 sun)} \right] \quad (29)$$

It can also be calculated the maximum efficiency of the solar cell that will be reached for a certain concentration X (i.e. $\frac{d\varepsilon}{dX} = 0$). Thus, the optimum concentration level of a solar cell can be estimated by equation (30).

$$X = \frac{kT}{q} \left(\frac{1}{R_s \times I_{SC(@ 1 sun)}} \right) \quad (30)$$

4.3. Theoretical behavior of the Solartec and KVAZAR solar cells under concentration

As previously explained, the HSUN system operates a concentration of 15 suns. As such, it is important to understand the behavior and the viability of the tested solar cells under different concentration levels. Considering the equations (1) and (2), described in section 4.2, Fig.4.11 shows the expected values for Isc and Voc as a function of concentration for both Solartec and KVAZAR solar cells.

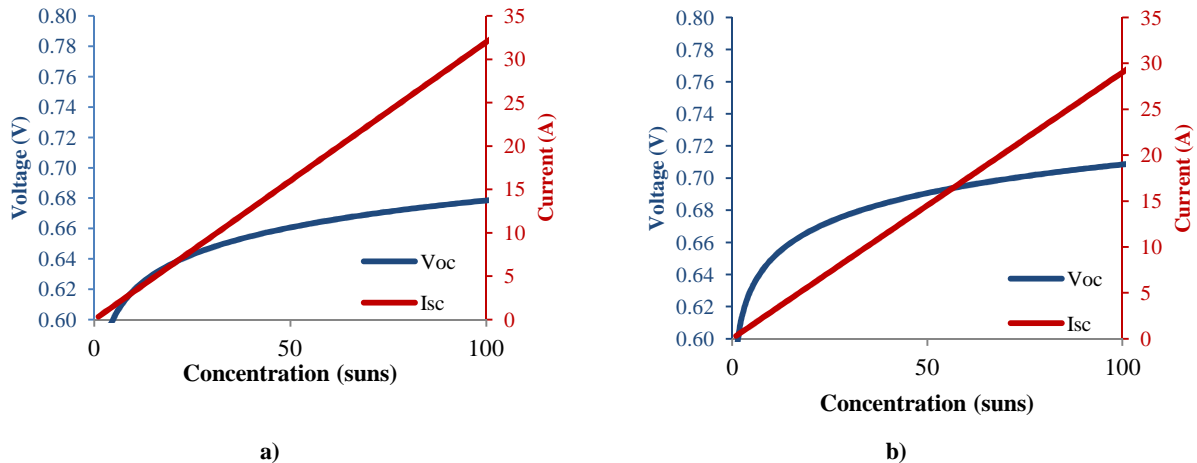


Figure 39 - Calculated values for Voc and Isc as function of concentration level in the a) KVAZAR solar cells and b) Solartec solar cells

As expected, the value of Isc increases linearly with increasing concentration, while the value of Voc increases with the logarithm of concentration. At a concentration level of 15 suns, the values of Isc and Voc in the Solartec and KVAZAR solar cells were estimated to be 4.35 A and 0.66 V and 4.8 A and 0.63 V, respectively. As can be observed the Voc values achieved by the Solartec solar cells are higher than the values reached by the solar cells provided by KVAZAR. However, as mentioned before, the efficiency of a solar cell depends on many factors. Although the relative increase in efficiency of the ideal cell is proportional to the natural logarithm of the concentration ratio, in the practical devices the efficiency cannot increase indefinitely.

As already mentioned, a real solar cell has a finite series resistance (R_s) that leads to power dissipated as heat. Resistance directly influences both voltage and current, and an increasing resistance will cause the voltage-current curve of the solar cell to move away from the so-called maximum power point. So, when the solar cells are exposed to a higher concentration of sunlight, the current flowing from the solar cell also raises, leading to a rapidly grows of the power wasted. Due to this situation, it is important that the solar cells used in CPV systems can maintain a low value of R_s . Through the use of the value of R_s measured to 1 sun of Solartec and KVAZAR solar cells (0.09 Ω and 0.06 Ω , respectively), the power loss (due to the Joule effect) and efficiency of the cells were also estimated (Fig. 4.12) and the results showed an exponential increase of the

power losses and decrease of the efficiency. As can be seen in Fig. 4.12, the KVAZAR conventional cells presented an higher increase of power losses from a concentration of 5 suns, while the Solartec cells presented an higher power losses only from the 12 suns, where at a concentration level of 15 suns, the power losses on the Solartec and KVAZAR solar cell were estimated to be 2.02 W and 2.074 W, respectively. The values obtained by the KVAZAR solar cells already were expected, since the conventional cells are designed to work under 1 sun conditions. The efficiency of the solar cells also suffers a great drop. In this case, the Solartec and KVAZAR solar cells, at 15 suns, reached a value of efficiency of 10.3 % and 4.2%, respectively.

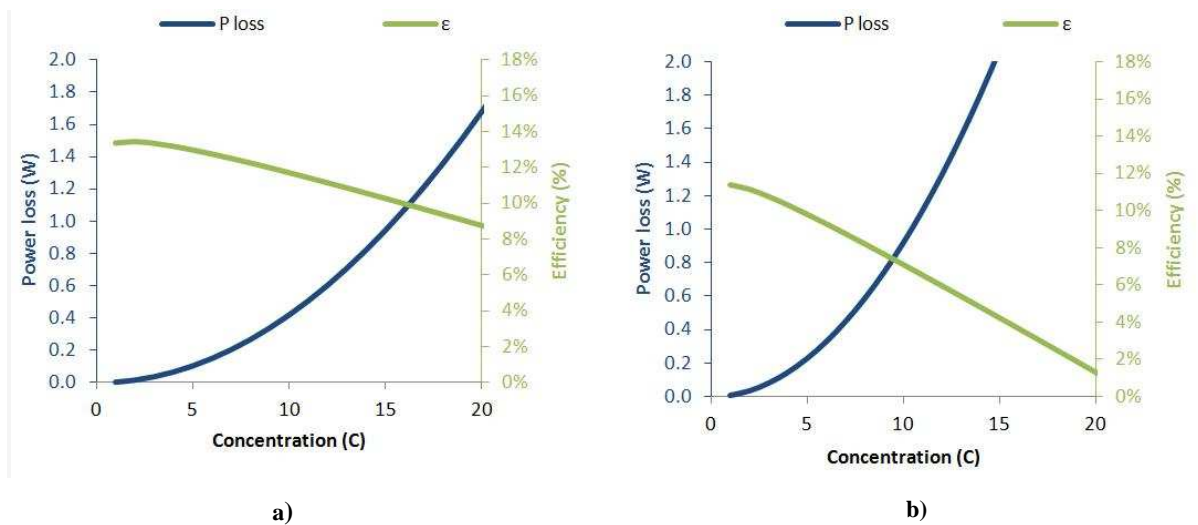


Figure 40 - Estimated power loss (P_{loss}) and efficiency (ϵ) as a function of the concentration level of a) Solartec solar cells and b) KVAZAR solar cells

The expected electrical parameters for the Solartec and KVAZAR solar cells under different concentration levels are summarized in Table 4.4. As can be seen in Table 4.4, the values of efficiency of the Solartec solar cell decrease until they reach a concentration of 20 suns (8.7%), while the FF values remain high until a concentration of 15 suns (54%). Contrary to what happened in the case of Solartec cells, the values of efficiency and FF estimated for the KVAZAR solar cells presents a high decrease from the 5 suns. As so, the KVAZAR solar cells seem not to be the most suitable type of solar cell to integrate a CPV system, as the HSUN technology.

Table 4.4- Calculated electrical parameters of Solartec and KVAZAR solar cells under different concentration levels

	C (suns)	Isc (A)	Voc (V)	Pmp (W)	FF (%)	E (%)
Solartec	5	1.45	0.63	0.64	71	13
	10	2.9	0.65	1.32	62	11.7
	15	4.35	0.66	2.02	54	10.3
	20	5.8	0.67	2.70	45	8.7
	30	8.7	0.68	4.15	29	5.6
KVAZAR	5	1.60	0.60	0.64	52	9.8
	10	3.20	0.62	1.32	37	7.1
	15	4.80	0.63	2.02	22	4.2
	20	6.40	0.64	2.70	7	1.3
	30	8	0.643	-0.412	-8	0

However, in order to validate the data obtained analytically, a characterization of these solar cells was performed and is described in the next chapter of this thesis.

Experimental characterization of the Solartec and KVAZAR solar cells

This chapter covers the electrical characterization of the Solartec and KVAZAR solar cells under concentration, where several experiments were performed as the electroluminescence of the solar cells (section 5.1), the measurement of the electrical parameters (section 5.2), the measurement of the series resistance (section 5.3), the spectral response (section 5.4) and the measurement of the thermal coefficients of the solar cells (section 5.6).

5.1. Electroluminescence of solar cells

In order to find out if the soldering and the cutting process damaged the solar cells, the electroluminescence was performed in the KVAZAR and Solartec solar cells.

In this chapter it is performed a brief review of the main concept about the electroluminescence process, followed by the description of the experimental process and discussion of the results.

5.1.1. Electroluminescence

The determination of electroluminescence (EL) in solar cells is an important characterization tool. It can provide spatially resolved information about defects which may limit the efficiency and lifetime of the solar cell. Thus, the EL techniques are very important to manufacturers not only in research and development, but also in solar cell production [27, 28].

Electroluminescence imaging takes advantages of the inter-band recombination of excited charge carriers in solar cells. For electroluminescence investigation, the solar cell is supplied, via

their metal contacts, with a certain external excitation current which is provided by a power source. Thus, the solar cell is operated as a light emitting diode and the emitted radiation, due to recombination effects, is detected with a sensitive camera. [27, 29]. Since EL is a low light source, a dark environment is required in order to decrease the background noise during the measure. The images provided by this technique show the damaged areas of a solar cell as dark spots or less bright than the good areas [30]. The EL technique provide images with very high resolution that enable to resolve details that should be hardly perceptible to the eye (Fig. 5.1), such as [30, 31]:

- Micro cracks;
- Bad finger contacts;
- Electrical shunts;
- Broken contacts;
- Fragments in broken cells;
- Electrically separated cell areas;
- Grain boundaries;
- Crystallization faults in cell material.

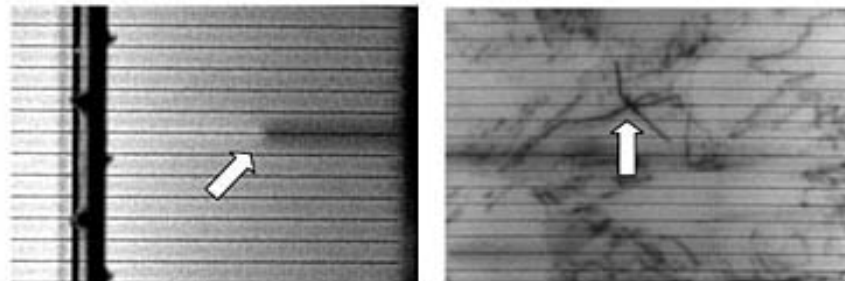


Figure 41 - Electroluminescence image of a) a monocrystalline and b) poly-crystalline silicon cell. The intensity of the light given off is proportional to the voltage, so poorly contacted and inactive regions show up as dark areas. The micro crack and printing problem are not detectable with visual inspection.

Source: <http://www.cepsolar.com/electroluminescence-imaging>

In a typical EL system configuration (Fig. 5.2)., the solar cell is placed in the camera's field of view, and the contact to the anode and cathode leads of the solar cell is performed. A constant current sources connected to the contacts of the solar cell [27]. In order to keep out ambient light and protect the operator to be exposed to the current on the solar cell, the whole system is inside a box properly designed. The camera collects an image while the current is on, and then sends it to a computer for analysis. The computer displays the EL image and gives information on the solar cell such as dark defects or black spots [32].

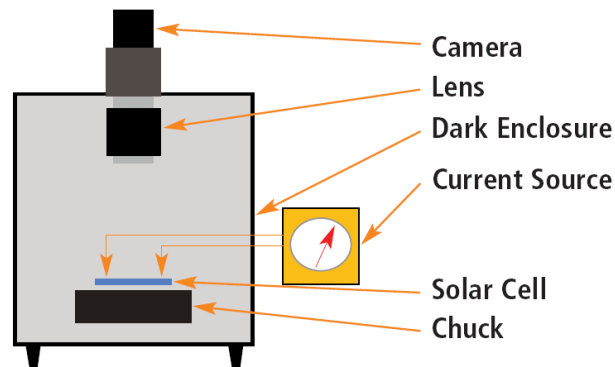


Figure 42 – Electroluminescence System.

Source: True, Bruce, Photoluminescence and Electroluminescence for Silicon Solar Cell Inspection, APPLICATIONS SCIENTIST, INTEVAC, INC., website "http://www.laser2000.de/fileadmin/kataloge/INTEVAC_SolarCellWhitePaper_BruceTrue.pdf

5.1.2. Experimental procedure

In this thesis, the electroluminescence technique was used in order to understand if the cutting method (in case of KVAZAR solar cells) and the soldering process damages the solar cells in analysis.

In the case of KVAZAR solar cells, the EL technique was performed in three different steps: i) in the main cell before it was sliced; ii) in the solar cells obtained after the cutting process and; iii) in the solar cells after the soldering process. For the Solartec solar cells, only step iii) was carried out, since the solar cells provided by Solartec company had already suitable dimensions to integrate HSUN.

The experiment was performed in the EL apparatus presented in Figure 435.3. The current injected into the solar cell was 1 A and the images took 60 seconds to be captured. The values used in voltage source were:

- Voltage = 1,405 V
- Limiting value of voltage (Voltage Compliance.) = 2,1 V



Figure 43 – Electroluminescence apparatus, located in the laboratory of the Faculty of Science, University of Lisbon (FCUL)

5.1.3. Results

5.1.3.1. KVAZAR solar cells

Table 5.1 presents the photographs that were taken to the KVAZAR solar cells with the EL method for the steps i) to iii) referred in section 5.1.2. The photos taken before the cutting process, i.e. to main cell, presents a thin black line which is due to the needle required for the negative contact of the primary cell. It can still be seen in this photo, small black spots (marked in red). This spots highlights the existence of small defects in the main solar cell surface, which may have occurred during the deposition of the front contacts paste.








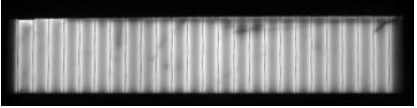
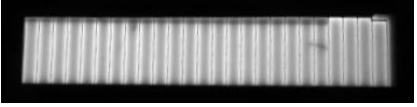
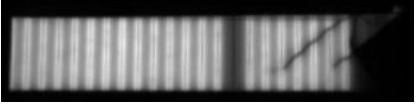
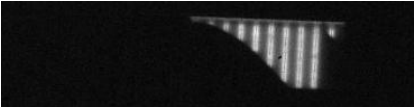
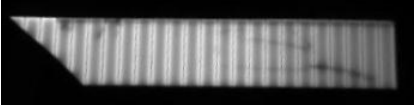
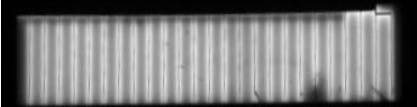
Regarding the photographs obtained after the cutting process of the main solar cell, no difference was observed as to the photographs taken before the cutting process and after the soldering process. This situation proves that the solar cells were physically unaffected by the cutting and soldering process.

However, in Table 5.1 it can also be observed that the KVZ.40-6.5 and KVZ.40 -6.6 show dark spots and cracks. In these cases, the damages are not inherent to the soldering process, but due

to their handling during the experimental process. The solar cells n° 6.5 and 6.7 have broken during the electrical characterization of the solar cells.

It also must be noticed that the photos taken before the soldering process shows a brightest area near the point where the needle is injecting the current into the cell and some of the cells are brighter than others. This effect occurs due the method used to inject the current into the cell and to the quality of the contacts. This situation can be proved through the observation of the photos taken after the soldering process. In this case, the contacts are soldered (providing them a better quality), causing in the solar cells a more homogeneous brightness in the illuminated area.

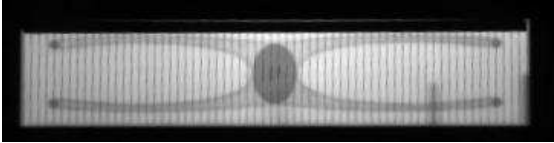
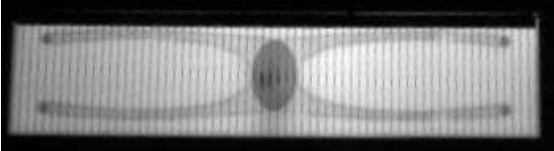
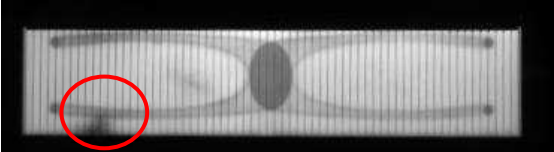
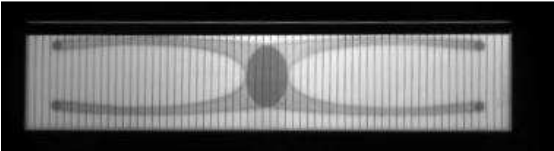
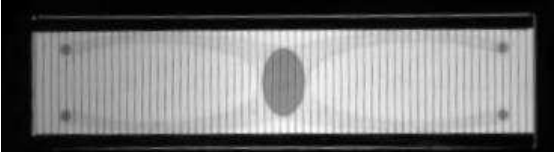
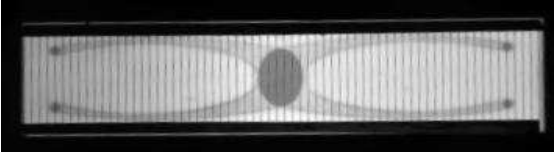
Table 5.1 - Photographs taken with the Electroluminescence method: before and after the cutting process of KVAZAR solar cells, and after the soldering process.

Main Cell before the Cutting process	Solar cells obtain from the cutting process	Solar cells after the soldering process
<p data-bbox="116 491 235 517">KVZ.40-6</p> 	<p data-bbox="943 347 1099 373">KVZ.40 – 6.2</p>  <p data-bbox="943 517 1099 542">KVZ.40 – 6.4</p>  <p data-bbox="943 692 1099 718">KVZ.40 – 6.5</p>  <p data-bbox="943 868 1099 893">KVZ.40 – 6.6</p>  <p data-bbox="943 1027 1099 1053">KVZ.40 – 6.7</p>  <p data-bbox="943 1187 1099 1212">KVZ.40 – 6.8</p> 	     

5.1.3.2. Solartec solar cells

Table 5.2 presents the electroluminescence images that were taken to the Solartec solar cells after the soldering process.

Table 5.1- Electroluminescent images taken to Solartec solar cells after the soldering process.

Classification of the solar cell	After the soldering process
CLASS 24.1	
CLASS 24.2	
CLASS 26.1	
CLASS 26.2	
2BB.1	
2BB.2	

The image taken to the cell SLT.C26 -1 (Table 5.2), shows a small black spot (marked in red). This spot highlights the existence of a small defect in the solar cell surface, probably occurred during the deposition of the front contacts metallization. The absence of black spots/lines near the busbar of the cells showed in Table 5.2, leads to the conclusion that the soldering process is harmless

to the cells. This means that the Solartec solar cells, as in the case of KVAZAR solar cells, were physically unaffected by the soldering process.

5.1.4. Main Conclusions

The main conclusions are:

- a) The process used to cut the solar cells was proved to be harmless to the solar cells.
- b) In both cell types (KVAZAR and Solartec), the EL photographs taken before and after the soldering process proved that the solar cells were unaffected by the soldering process, i.e. the appearance of new black spots after the soldering process was undetectable.

5.2. Measurement of electrical parameters of the solar cells

The electrical behavior of the cells should be well known. As such, it was carried out a study of the behavior of KVAZAR and Solartec solar cells under uniform light, to be known the electrical parameters of the solar cells. The electrical characteristics of cells tested were previously estimated for different levels of concentration.

Thus, in this chapter it is performed a brief review of the main concept about the electrical parameters of the solar cells and the measured process, followed by the description of the experimental process and discussion of the results.

5.2.1. Electrical parameters

According to S. Madougou *et al.*, there are several techniques in the literature to determine the electrical and recombination parameters of solar cells [33]. In this thesis, the electrical parameters of the cells were obtained only by the method based on the I-V curve [34]. As mentioned in the Chapter 3, through the cell characteristic I-V curve we can obtain the main electrical parameters for the characterization of solar cells under study, such as the I_{sc} , the V_{oc} , FF and P_{mp} . To correctly measure an I-V curve, some parameters, such as the incident irradiance and its spectrum and the cell temperature should be controlled [35]. Usually the I-V curve is measured under standard test conditions (STC), which are: [3]:

- Incident Irradiance: 1000 W/m²
- Spectrum of incident irradiance: AM1.5 G
- Temperature of the solar cell: 25⁰C.

As can be seen in Fig. 5.4, the value of V_{oc} and I_{sc} corresponds to the value where the current and voltage are zero in the I-V curve, respectively [36]. It can also be observed that the maximum power point (P_{mp}) of the I-V curve corresponds to the point at which the maximum value of voltage and current is reached (Fig. 5.4) [33, 37].

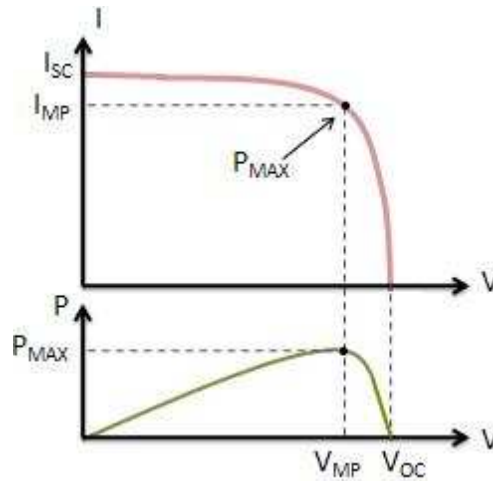


Figure 44 - Power and characteristic curves of a solar cell
 Source: <http://zone.ni.com/devzone/cda/tut/p/id/7230>

Another electrical parameter that can be calculated from the I-V curve is the Fill Factor (FF). This parameter is calculated by comparing the maximum power (P_{mpp}) reached by the solar cell with the theoretical ideal power (P_T) that would be calculated from the multiplication of the value of open circuit voltage and the value of short circuit current [31]: The FF can also be interpreted graphically as the ratio of the rectangular areas as shown in Fig. 5.5 (ideal and real area) [6].

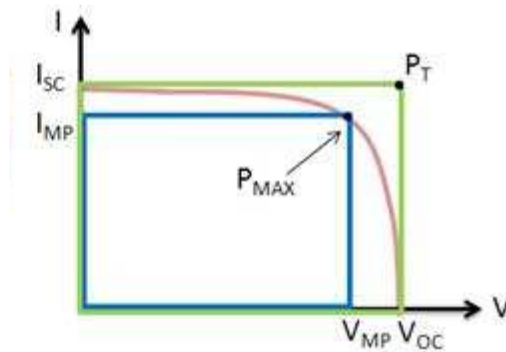


Figure 45 – Measurement of the FF from the I-V curve of a solar cell
 Source: <http://zone.ni.com/devzone/cda/tut/p/id/7230>

5.2.2. Experimental procedure

In order to estimate the electrical parameters of solar cells under study (KVAZAR and Solartec), the I-V curves were measured for each cell, in a calibrated solar simulator with a light intensity of one sun ($1000W/m^2$) (Fig. 5.6). The temperature of the cell is maintained constant by a cooling system that consists on a water flux passing through the sample holder. It must be noticed that the cell length is slightly higher than the sample holder, which could lead to a slight increase of

the cell temperature; however the temperature of the cell has remained constant as it will be seen. All the cells were measured at the same position (Fig. 5.7).

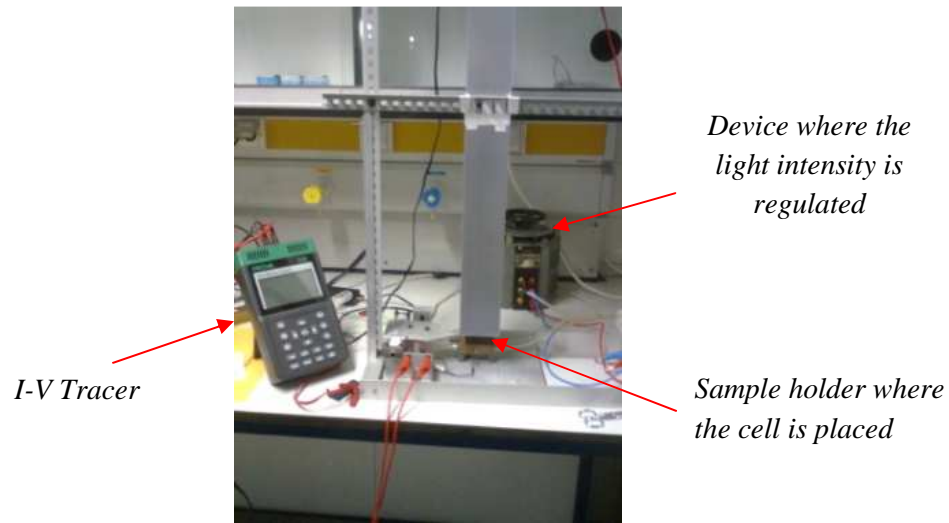


Figure 46 – Solar Simulation located in the Laboratory of FCUL

The I-V curves of solar cells that are being studied were measured before and after the soldering process. Thus, it becomes possible to determine what effect the soldering process causes in the electrical behavior of the solar cells (Fig. 5.7).

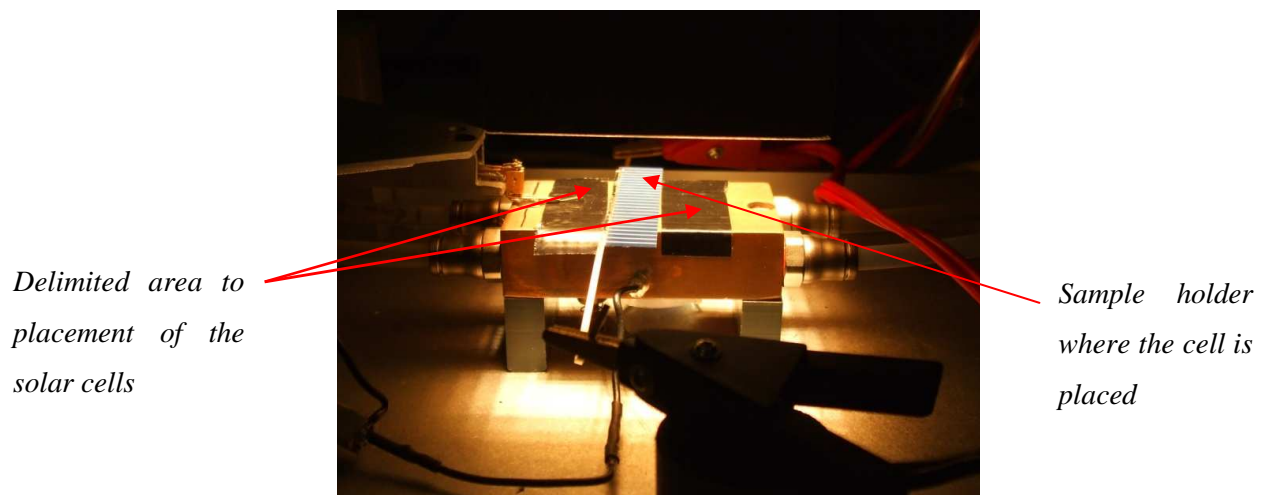


Figure 47 – Detail of the solar cell placed on the sample holder in the solar simulator.

To validate the data obtained we have performed the I-V curve measurements using two different acquisition methods: the I-V Tracer apparatus and the direct acquisition method (Four-point I-V measurement).

In this last method, the I-V curves are measured automatically through a computer program, where the cell is stepped through several voltage limiting levels, measuring the current values corresponding to these points. In the end, through the voltage-current points found, the I-V curve of the solar cell is traced. Unlike in the I-V Tracer apparatus, which uses only two points of the cell to measure the I-V curve (crocodiles that are connected to positive and negative contacts of the cell), in the direct acquisition method are used four points (two points in the positive contact (table where the cell is placed and the needle that comes in contact with the back of the cell) and two contact points on the negative (two needles which come into contact with the busbar) of the solar cell) [38].

5.2.3. Results

5.2.3.1. KVAZAR solar cells

As mentioned before, during the experiment, I-V curves at 1 sun were traced for each solar cell by using two different methods: 1) the I-V Tracer apparatus and 2) the direct acquisition method.

1. I-V Tracer

The I-V curves measured with the I-V tracer apparatus shows that:

- In all the cells, the I-V curve measured after the soldering process has a lower series resistance (slope near the V_{oc}) than the ones that were measured before the soldering process.
- Fig. 5.9 and 5.12 shows a decrease of the I_{sc} after the soldering process. This decrease should be to the fact that the solar cell has been damaged during the soldering process and the part that was broken is not electrically connected to the rest of the cell.

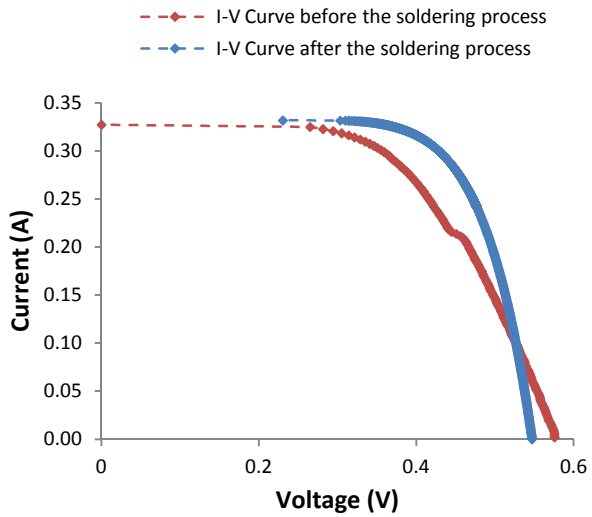


Figure 48 – I-V curve of cell n° 6.2 with the I-V tracer

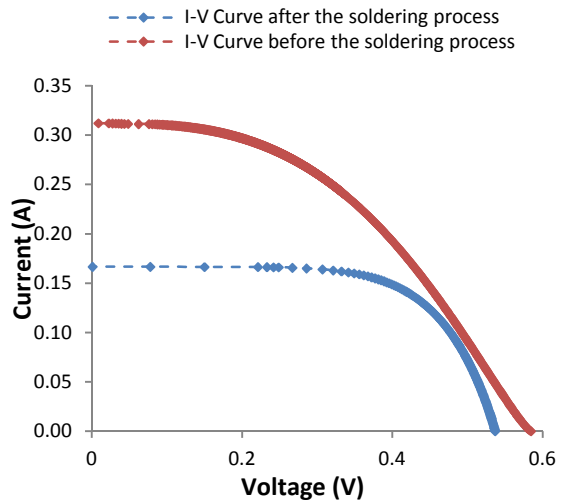


Figure 49 – I-V curve of cell n° 6.3 with the I-V tracer

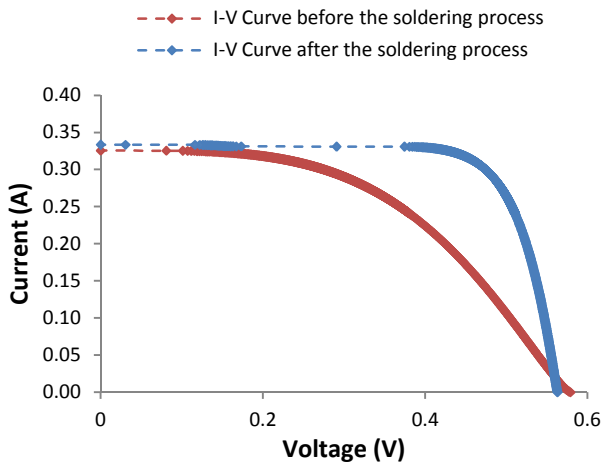


Figure 50 – I-V curve of cell n° 6.4 with the I-V tracer

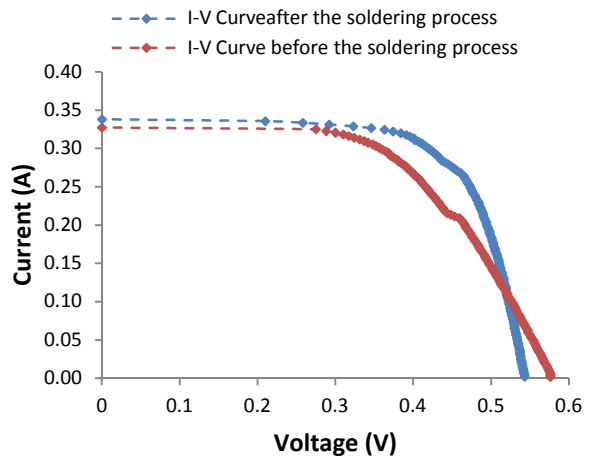


Figure 51 – I-V curve of cell n° 6.5 with the I-V tracer

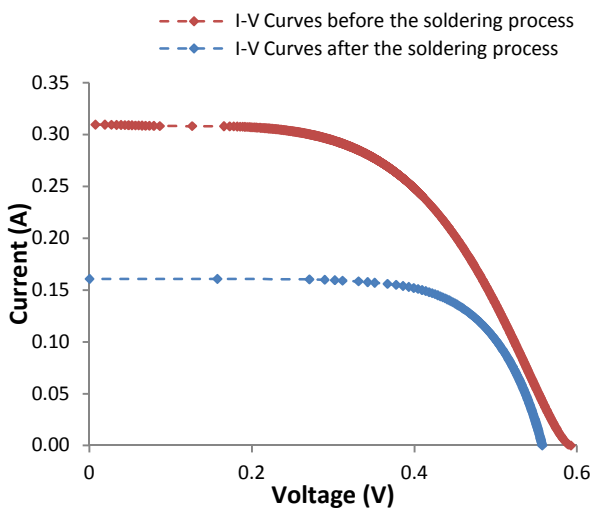


Figure 52 – I-V curve of cell n° 6.6 with the I-V tracer

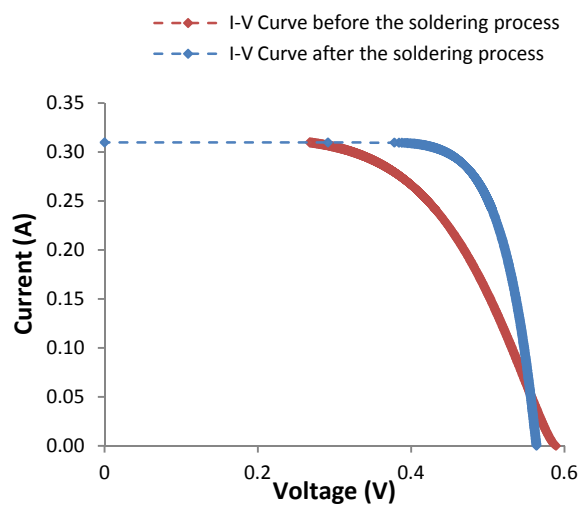


Figure 53 – I-V curve of cell n° 6.7 with the I-V tracer

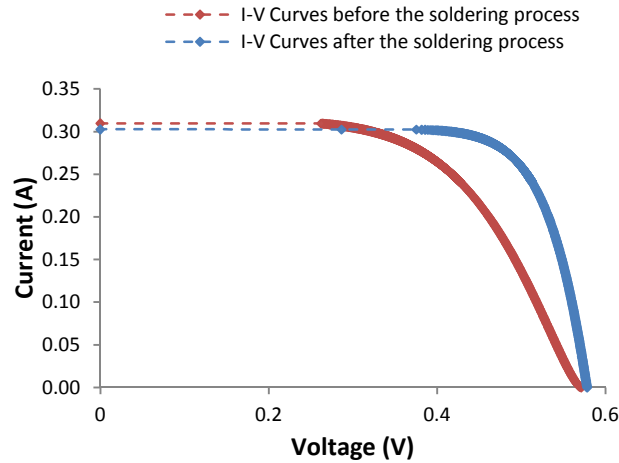


Figure 54 – I-V curve of cell n° 6.8 with the I-V tracer

Table 5.3 shows the electrical parameters (V_{oc} ; I_{sc} ; V_{mpp} ; I_{mpp} and P_{mp}) that were taken from the I-V curves of each solar cell before and after the soldering process.

As expected, the value of I_{sc} remains almost constant through all the experience. However, in the case of the KVZ.40-6.3 and KVZ.40-6.6 solar cells, the value of I_{sc} decreases after the soldering process (decrease between 0.05 and 0.17 A). This situation is due to the fact that these solar cells were broken during the measurements (Fig. 5.9 and 5.13). In the case of the value of V_{oc} before and after the soldering process, the values decrease between 0.004V and 0.03V. However, in the case of KVZ.40-6.8 solar cell, the value of V_{oc} increased after the soldering process (increase between 0.004 and 0.008V) (Fig.5.15). Based in Table 5.3, it is also possible to observe that the electrical values of the solar cells have presented only small variations (variations between 0.01A and 0.04 A and .001 V and 0.02 V).

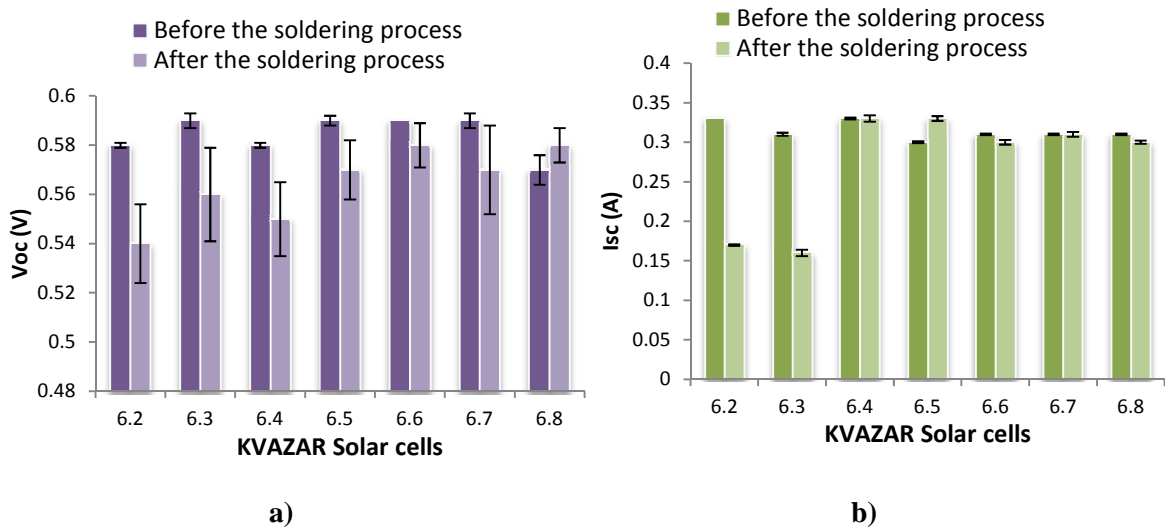


Figure 55 – Values of a) V_{oc} and b) I_{sc} measured from the I-V curves before and after the soldering process of the KVAZAR solar cells

Table 5.2 - Values of parameters of the solar cells tested before and after the soldering process.

Cell N°	Before the soldering process					After the soldering process					
	Voc (V)	Isc (A)	Vmpp (V)	Impp (A)	Pmp (W)	Voc (V)	Isc (A)	Vmpp (V)	Impp (A)	Pmp (W)	
KVAZAR solar cell	6.2	0.58 ± 0.001	0.33 ± 0.000	0.38 ± 0.008	0.29 ± 0.007	0.11 ± 0.001	0.54 ± 0.016	0.17 ± 0.001	0.42 ± 0.004	0.14 ± 0.001	0.06 ± 0.000
	6.3	0.59 ± 0.003	0.31 ± 0.002	0.33 ± 0.003	0.26 ± 0.001	0.08 ± 0.001	0.56 ± 0.019	0.16 ± 0.004	0.46 ± 0.006	0.13 ± 0.001	0.06 ± 0.001
	6.4	0.58 ± 0.001	0.33 ± 0.001	0.34 ± 0.004	0.27 ± 0.002	0.09 ± 0.002	0.55 ± 0.015	0.33 ± 0.004	0.42 ± 0.003	0.30 ± 0.002	0.13 ± 0.002
	6.5	0.59 ± 0.002	0.30 ± 0.001	0.40 ± 0.004	0.27 ± 0.003	0.11 ± 0.000	0.57 ± 0.012	0.33 ± 0.003	0.47 ± 0.002	0.31 ± 0.003	0.14 ± 0.001
	6.6	0.59 ± 0.000	0.31 ± 0.001	0.38 ± 0.023	0.27 ± 0.003	0.10 ± 0.007	0.58 ± 0.009	0.30 ± 0.003	0.46 ± 0.001	0.26 ± 0.001	0.12 ± 0.001
	6.7	0.59 ± 0.003	0.31 ± 0.001	0.39 ± 0.002	0.27 ± 0.002	0.10 ± 0.001	0.57 ± 0.018	0.31 ± 0.003	0.47 ± 0.002	0.29 ± 0.002	0.13 ± 0.001
	6.8	0.57 ± 0.006	0.31 ± 0.001	0.39 ± 0.004	0.27 ± 0.002	0.10 ± 0.001	0.58 ± 0.007	0.30 ± 0.002	0.48 ± 0.003	0.28 ± 0.002	0.13 ± 0.001

2. Direct acquisition method (Four-point I-V measurement)

As it can be seen in the Fig. 5.16, the I-V curves obtained by the Four-point I-V measurement (violet curves) presented a lower value of series resistance as to the I-V curves obtained with the I-V Tracer (green curves). This situation is due to the fact that with the use of four point measurement method, the resistance associated to the contacts and to cables is inexistent.

However, when we compare the values of Voc and Isc obtained by the two methods, can be conclude that are similar (variations between 0.03 A and 0.05 A, and 0.01 V and 0.03 V).

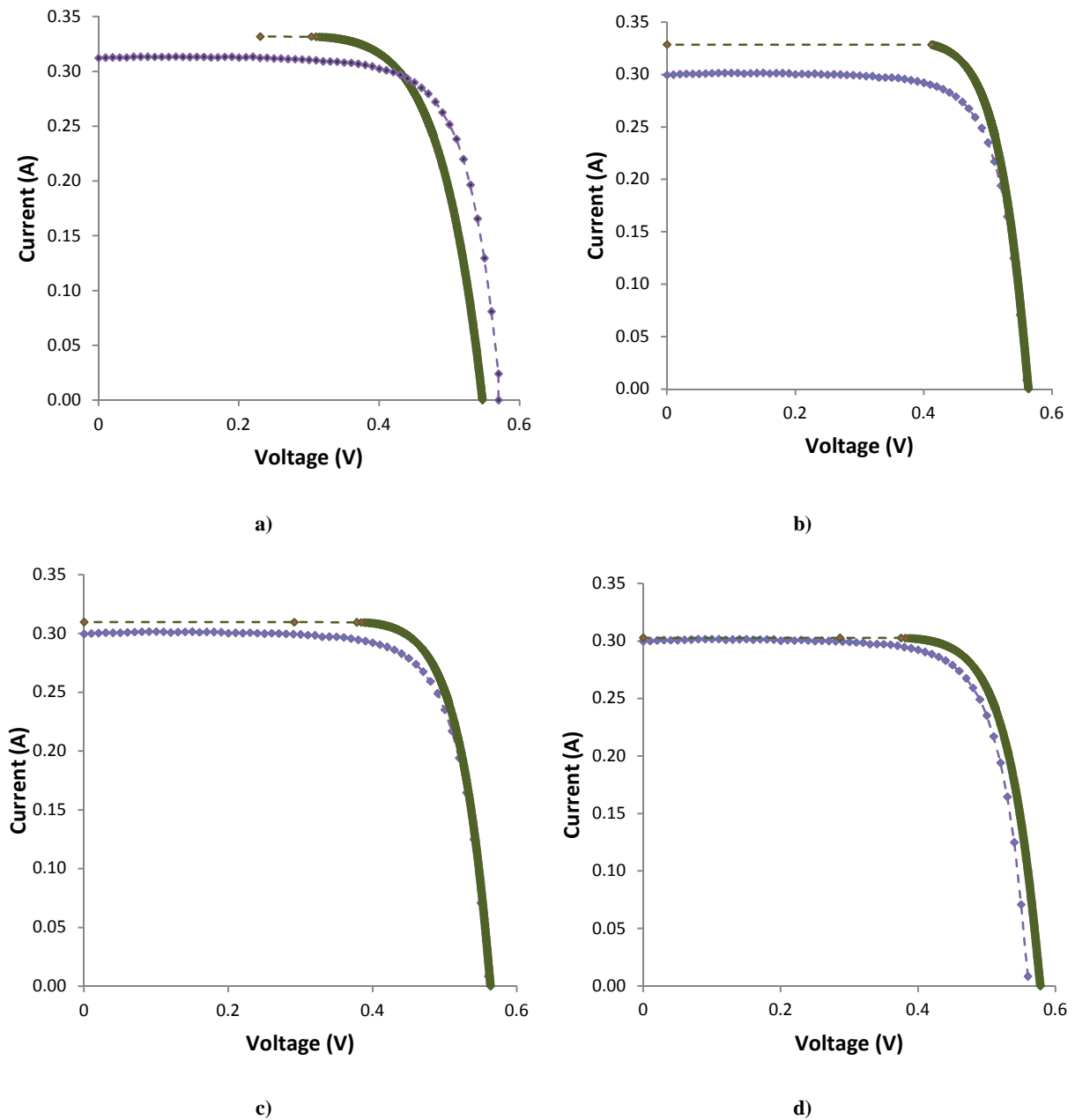


Figure 56 – I-V curves traced with the four-point I-V measurement (green) and the I-V tracer (violet) of the a) solar cell n° 6.2, b) solar cell n° 6.4, c) solar cell n° 6.7 and d) solar cell n° 6.8

Table 5.4 presents the electrical parameters measured for the KVAZAR solar cells at 1 sun using the four point I-V curve measurement.

Table 5.3 – Electrical parameters estimated for KVAZAR solar cells at 1 sun.

Electrical parameters	
Concentration	@ 1 sun (1000W/m ²)
Isc (A)	0.32±0.003
Voc (V)	0.56±0.001
Pmp (W)	0.12±0.002
Impp (A)	0.28±0.003
Vmpp (V)	0.43±0.001
Efficiency	0.15±0.003
Fillfactor	0.67±0.002

5.2.3.2. Solartec solar cells

As it was observed in the method of acquisition of the I-V curve through the I-V Tracer apparatus, the resistances associated to the cables were higher. Thus in the case of Solartec solar cells the I-V curves were only acquired through the direct acquisition method.

As can be seen in the Fig. 5.17 to 5.22, the I-V curve measured after the soldering process has a lower value of Voc than the ones that were measured before the soldering process. This situation can result from a slight increase in temperature of the solar cells.

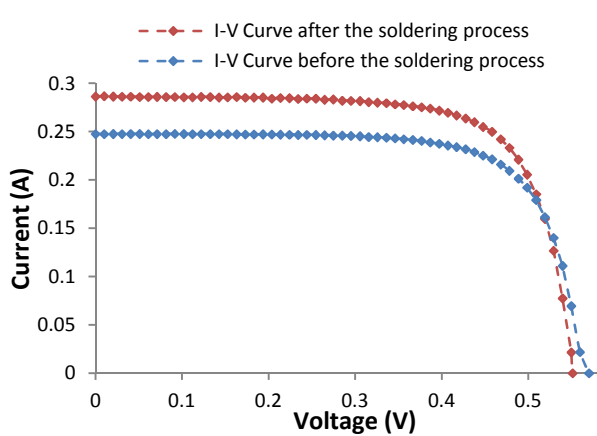


Figure 57 – I-V curve of cell n° 24.1 before and after the soldering process

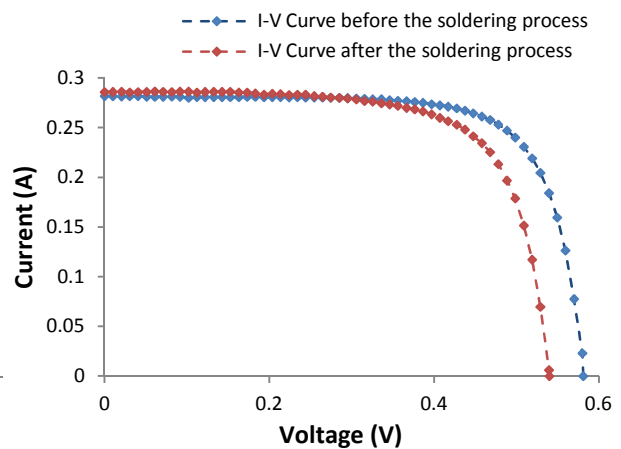


Figure 58 – I-V curve of cell n° 24.2 before and after the soldering process

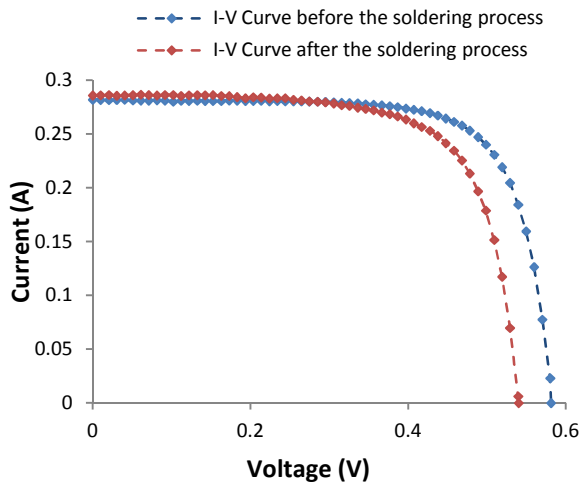


Figure 59 – I-V curve of cell n° 26.1 before and after the soldering process

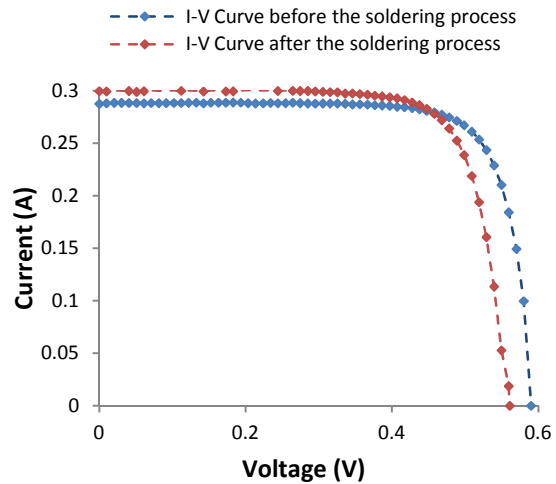


Figure 60 – I-V curve of cell n° 26.2 before and after the soldering process

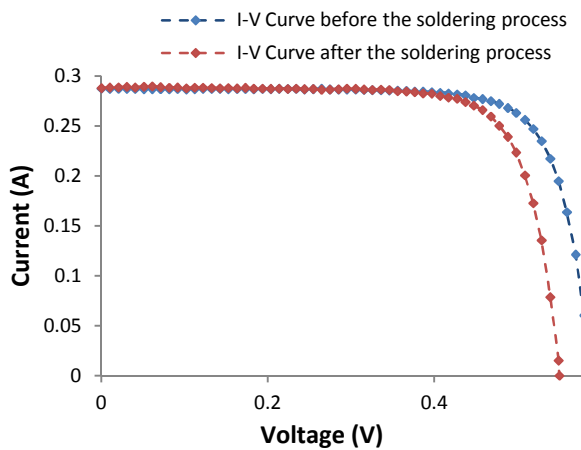


Figure 61 – I-V curve of cell n° 2BB.1 before and after the soldering process

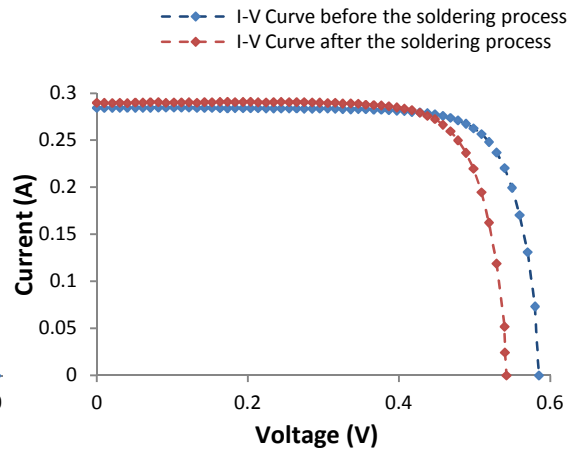


Figure 62 – I-V curve of cell n° 2BB.2 before and after the soldering process

Table 5.5 shows the electrical parameters that were taken from the I-V curves of each solar cell before and after the soldering process. Analyzing the results presented in Table 5.5 it can be observed that in the case of cell SLT.C24, the value of P_{mp} is higher after the soldering process, while in other tested cells, after the soldering process, the value of P_{mp} has decreased or remained equal. As expected, the value of I_{sc} remains almost constant through all the experience (variation between 0.02 and 0.06A).

In the case of the value of V_{oc} before and after the soldering process, the values decrease between 0.04V and 0.03V. However, in the case of SLT.C24 solar cell, the value of V_{oc} remains equal after the soldering process.

Based in Table 5.5, it is also possible to observe that the electrical values of the solar cells present only slight variations (the Voc presents variations between 0 V and 0.01V, the Isc presents variations between 0.01 A and 0.04 A and the Pmp presents variations between 0.01 W and 0.03 W).

However, it is also possible to observe that the SLT.C24 solar cells have lower electric values (as the Isc and FF) when compared with SLT.C26 solar cells.

Another observation visible through the Table 5.5 is that the value of Isc is relatively lower than the value of Isc achieved in the KVAZAR solar cells. This situation can be justified due to the fact that Solartec cells have an increased number of fingers (because they are conventional solar cells optimized for concentration), and consequently less active area due to higher shadowing on the front surface.

Table 5.4 - Values of parameters of the solar cells tested before and after the soldering process.

Electrical parameters at 1 sun (1000 W/m ²)						
CELL	Before the soldering process			After the soldering process		
	Class 24	Class 26	2BB	Class 24	Class 26	2BB
Isc (A)	0.25	0.28	0.29	0.29	0.29	0.29
Voc (V)	0.58	0.58	0.59	0.58	0.54	0.55
Pmp (W)	0.10	0.12	0.13	0.11	0.12	0.12
Imp (A)	0.21	0.25	0.25	0.24	0.26	0.24
Vmpp (V)	0.48	0.49	0.51	0.47	0.48	0.49
Fillfactor (%)	70	75	75	67	80	74

5.2.4. Main conclusions

In Table 5.6 are presented the values of electrical parameters obtained for the Solartec and KVAZAR solar cells.

Table 5.5 - Values of electrical parameters of the Solartec and KVAZAR solar cells.

Electrical parameters of solar cells @ 1 sun (1000W/m ²)				
	KVAZAR	Class 24	Class 26	2BB
Isc (A)	0.32	0.25	0.28	0.29
Voc (V)	0.56	0.58	0.58	0.59
Pmp (W)	0.12	0.10	0.12	0.13
Imp (A)	0.28	0.21	0.25	0.25
Vmpp (V)	0.43	0.48	0.49	0.51
Fillfactor	0.67	0.70	0.75	0.75

Through the values presented, it can be concluded that, when compared, the Solartec solar cells show lower values of I_{sc} at one sun, while the value of V_{oc} is very similar in all solar cells, and the value of FF and P_{mpp} is higher in the Solartec solar cells.

On the contrary as occurred with the direct acquisition method, the I-V Tracer apparatus shows associated values of resistance of cables, since in this method the contacts are made through long and thin wires and only two points make contact with the solar cell. So, it can be concluded that the direct acquisition method is more suitable to measure the I-V curves of the solar cells.

After the soldering process, the I-V curves obtained have lower series resistance (slope near the V_{oc}) than the ones that were measured before the soldering process, since after the soldering process the contacts presents a better quality.

5.3. Measurement of the Series Resistance

For high current devices, such as solar cells, minimization of the ohmic series resistance losses is crucial. The analysis of the series resistance (R_s) requires an accurate determined value and should also give a conclusive proof of its correctness [35]. There are many techniques to measure/estimate the series resistance of solar cells. In this chapter we present the R_s estimated for the KVAZAR and Solartec solar cells by using two different methods: i) I-V curve measurement and ii) Suns-Voc. The concept behind each of the previous methods as well as the experimental procedure and results are described in the following lines.

5.3.1. I-V curves

5.3.1.1. Theoretical Introduction

A current-voltage (I-V) curve is usually described as the possible combinations of current and voltage output of a photovoltaic (PV) device. However, to represent a real behavior of the device, it should be taken into account the presence of parasitic series resistance and shunt conductance as an integral part of the system [35].

Through the I-V curves, the series resistance can be estimated by two methods: **i) The Slope method at constant light intensity** and **ii) Multiple light intensity method.**

i) Slope method at constant light intensity

As mentioned in the previous chapters, the maximum voltage value is achieved at open circuit conditions thus being known as the open circuit voltage (V_{oc}). At this point, the series resistance is infinitely high and there is no current [39].

Thus, in this method, series resistance is estimated by the inverse of the slope of the I-V curve near the V_{oc} (equation (31)). The R_s parameter is one of the parameters that mainly influence the I-V curve of a solar cell. As can be seen in Figure 5.23, how much higher is the value of R_s , greater is the slope of the IV curve near the point $I = 0$ [32].[40]

$$R_s = \frac{-1}{\text{Slope of the } I - V \text{ curve near the } V_{oc}} \quad (31)$$

This is the method to calculate the series resistance most commonly used, since it is only necessary to know the I-V curve of the solar cell under study (Fig. 5.23).

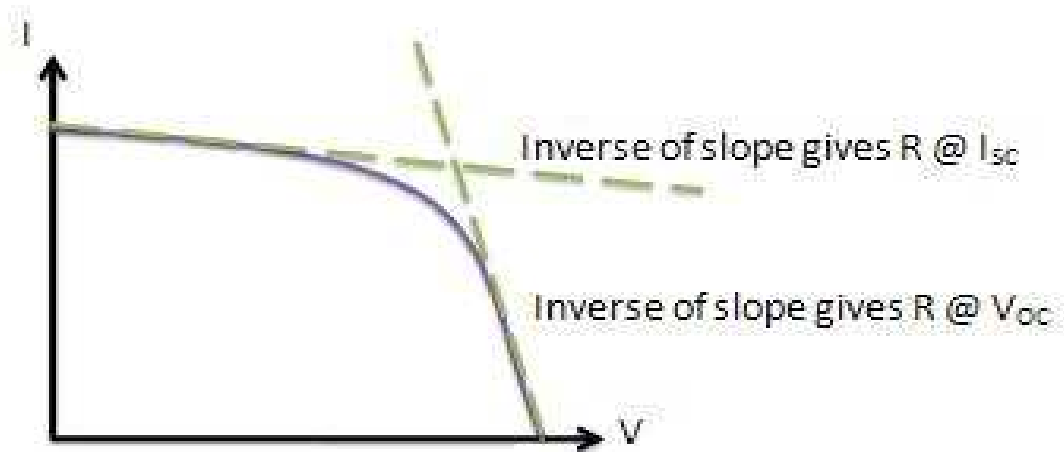


Figure 63 - Obtaining the series and shunt resistances from the I-V Curve.

ii) Multiple light intensity method

In this method the series resistance is calculated through the use of two I-V curves measured at different light intensities. Such curves have also two different values of Isc (Isc₁ and Isc₂, respectively). Then, a value of current below the Isc is picked (δI) and is subtracted from the value of Isc on both curves (eq. (32) and eq. (33)), originating two new points equally spaced from the point where $V = 0$ (Fig. 5.24) [33][34].

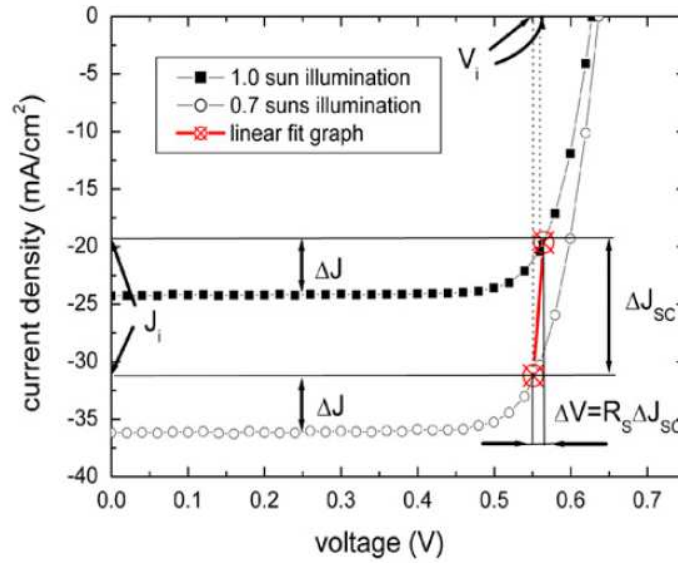


Figure 64 - Two I-V curves of the same solar cell under different illumination intensities.
Source: See reference [33]

$$I_1 = I_{SC1} - \delta I \quad (32)$$

$$I_2 = I_{SC2} - \delta I \quad (33)$$

The values of current obtained from the new points, corresponds the voltage values (V_1 and V_2 , respectively) to calculate the series resistance [33]. So can be said that the series resistance is calculated by:

$$R_s = \frac{V_1 - V_2}{I_1 - I_2} \quad (34)$$

Thus, replacing the equations (32) and (33) in the equation (34),

$$R_s = \frac{V_1 - V_2}{I_{sc1} - I_{sc2}} \quad (35)$$

where V_1 and V_2 are the voltage that corresponds to I_1 and I_2 , respectively.

5.3.1.2. Results

In order to estimate the series resistance by using the two methods explained in section 5.3.1.1. we have exposed to different light intensities (1, 2 and 10 suns) all the solar cells under analysis and the I-V curve was measured. Figure 5.25 shows the I-V curves registered for the KVAZAR, Solartec and NaREC solar cells, normalized to the Isc and Voc of each curve.

From these I-V curves it must be noticed that, as the concentration level increases, the KVAZAR solar cell shows higher resistive losses (lower FF) than the Solartec and NaREC solar cell.

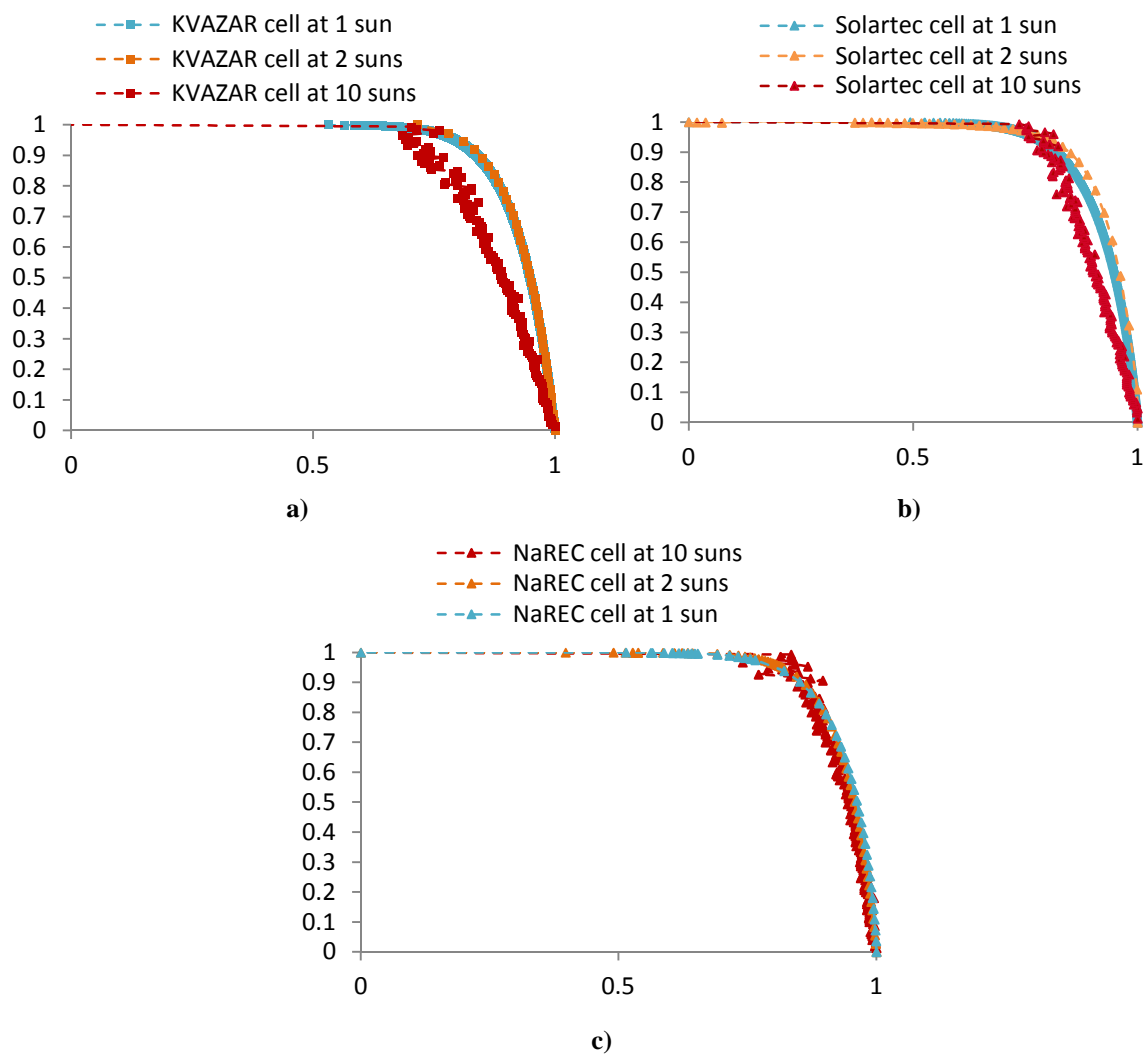


Figure 65 - I-V curve registered for the a) KVAZAR, b) Solartec and c) NaREC solar cells under 1, 2 and 10 suns. I-V curves are normalized to Isc and Voc.

It is also important to refer that the oscillation of the I-V curves under 10 suns is due to the oscillation of the lamp in the concentration simulator (Fig. 5.26).



Figure 66 - Concentration Simulator placed in the FCUL laboratory

Through the I-V curves obtained for each solar cell we have calculated the series resistance values by: i) the slope method at constant light intensity and ii) the multiple light intensity method.

Table 5.7 presents the results obtained by the slope method at constant light intensity.

Table 5.6 – Series Resistance estimated by the slope method

C	1 sun (1000W/m ²)	2 suns (2000W/m ²)	10 suns (10000W/m ²)	
KVAZAR	0.16 ± 0.03 Ω	0.14 ± 0.01 Ω	0.20 ± 0.14 Ω	
Class 24	0.065 ± 0.02 Ω	0.19 ± 0.11 Ω	0.20 ± 0.007 Ω	
Solartec	Class 26	0.045 ± 0.007 Ω	0.165 ± 0.02 Ω	0.12 ± 0.007 Ω
	2BB	0.045 ± 0.007 Ω	0.125 ± 0.02 Ω	0.13 ± 0.01 Ω
NaREC	0.15 ± 0.03Ω	0.16± 0.03 Ω	0.11± 0.03 Ω	

From this table it must be noticed that the series resistance (Rs) estimated for the KVAZAR solar cells are higher than the one estimated for the NaREC solar cells at 1 sun. However, at 2 suns, the Rs estimated are higher in the NaREC solar cells. On the other hand, the series resistance (Rs) estimated for the Solartec solar cells are higher than the one estimated for the NaREC solar cells at 2 and 10 suns. However, at 1 sun, the Rs estimated are higher in the NaREC solar cells.

Although the Rs obtained for the Solartec solar cells, at 10 suns, is higher than the value of the value obtain to the NaREC solar cells, it can be noticed that the difference is relatively small. The same situation do not occur in the Rs values obtained for the KVAZAR solar cells at 10 suns, since

this values are more higher when comparing with two other cells. This situation can be explained by the technology of the solar cells. In the case of Solartec and NaREC solar cells, their production technology were designed to operate under concentration, while the KVAZAR solar cells are conventional silicon solar cells (which means that they are not prepared to be exposed to high levels of radiation).

It can also be observe that in the same group of solar cells (i.e. the Solartec solar cells) were obtained different values of Rs. When the three classes of Solartec cells are compared, it is observed that the higher values of Rs obtained was in the Solartec solar cells with the class 24 and the lowest values in the class of two busbars.

The values obtained in class 24 can be justified due to electrical classes in which these solar cells are classified. As mentioned in section 4.1(Physical Characteristics of the KVAZAR and Solartec solar cells) of this thesis, the Solartec solar cells, despite having the same physical characteristics, are grouped into different electrical classes (Class 24 and Class 26).

In the case of solar cells with two busbars, the Rs values are lower than the obtained in other solar cells, due to their design. As mentioned before, the series resistance depends of the movement of current through the emitter and base of the solar cell, the contact resistance between the metal contact and the silicon, and finally the resistance of the top and rear metal contacts. As these solar cells have two busbars, the current generated in the cell will not be subject to go "one way" so long, since the current generated will be distributed homogeneously by the two busbars. Through this simple division of output current between the two busbars, the resistance associated to the contacts of the solar cell is relatively reduced.

In the case of multiple light intensity method, it were used the I-V curve obtained under 1 and 10 suns to estimate the series resistance. The results obtained are presented in the following table.

Table 5.7 – Series Resistance estimated by the multiple light intensities method

Cell		Rs (Ω)
	KVAZAR	0.046 \mp 0.03
	Class 24	0.06 \mp 0.02
Solartec	Class 26	0.035 \mp 0.02
	2BB	0.059 \mp 0.02
	NaREC	0.075 \mp 0.02

As it can be seen in the Table 5.8, and as in the slope method, the values of Rs estimated for the KVAZAR solar cells are relatively higher when compared to the values of Rs estimated for the NaREC solar cells, while the values of Rs obtained for the Solartec solar cells are lower when compared with two other cells.

5.3.2. Suns-Voc method

5.3.2.1. Theoretical Introduction

The Suns-Voc method directly measures the Voc parameter as a function of the light intensity [40]. Since it is a direct electrical measurement with an electrical contact, and assuming that the spectrum of the lamp is similar and the cell temperature is constant, the Voc measured at one sun should match with the value from a I -V curve obtained in the solar simulator [41]. This method can provide a large range of information that can be used in a large number of ways; the most important for this dissertation is the calculation of series resistance of the solar cells [40].

The Suns-Voc setup (Fig. 5.27) includes a light source whose intensity decreases linearly with time, at a rate that allows for quasi-stationary measurement but fast enough to avoid an increase in the temperature of the solar cell. The intensity of the light source is constantly monitored by a calibrated sensor and the Voc is measured directly from the contacts of the solar cell. The Suns-V_{OC} measurement provides the I-V curve of the diode without the effects of series resistance and the concentration level at the samples is exposing [40, 41].

By fitting to the Suns-Voc curve this setup provides estimation for the R_s.

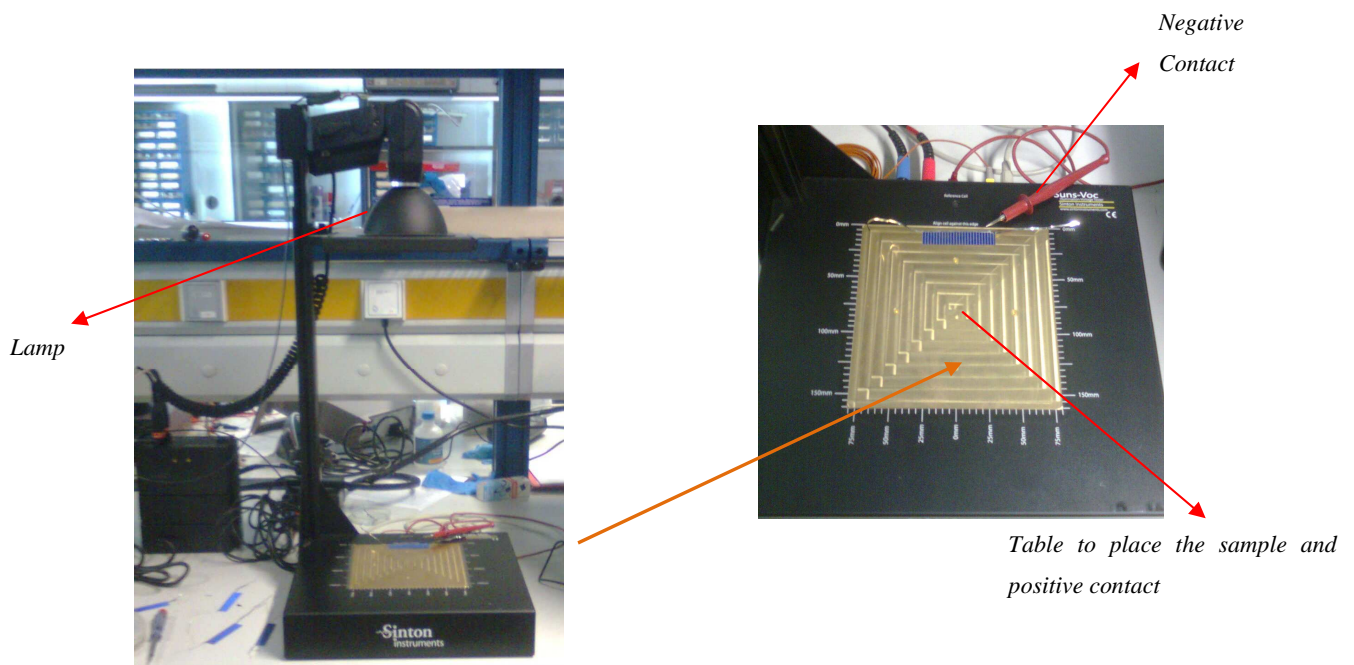


Figure 67 – Suns-Voc apparatus placed in the FCUL laboratory.

5.3.2.2. Results

Table 5.9 presents the results of R_s obtained by the Sun-Voc method for the KVAZAR, Solartec and NaREC solar cells.

Table 5.8 - Series Resistance estimated by the Suns Voc setup

Cell		Before the soldering process R_s (Ω)	After the soldering process R_s (Ω)
KVAZAR		0.096 ± 0.002	0.095 ± 0.002
Solartec	Class 24	0.120 ± 0.001	0.112 ± 0.002
	Class 26	0.102 ± 0.0002	0.098 ± 0.0004
	2BB	0.105 ± 0.003	0.096 ± 0.002
NaREC		0.098 ± 0.0006	0.098 ± 0.0006

As the values obtained by the slope method, the results presented in Table 5.9 shows that the series resistance (R_s) estimated for the KVAZAR and Solartec solar cell is very close the R_s values of the NaREC solar cell. It can also be observe that the values of R_s obtained in the Solartec solar cells before the soldering process was higher that the values obtained after the soldering process. This situation occurs due the fact that after the soldering process, the quality of the contacts of solar cells improved leading to lower resistivity losses.

5.3.3. Conclusions

Table 5.10 shows the values obtained for the series resistance of the KVAZAR, Solartec and NaREC solar cells using the four methods presented in this thesis.

Table 5.9 – Series Resistance of the KVAZAR, Solartec and NaREC solar cells estimated by the different methods.

Cell	KVAZAR	Solartec	NaREC		
		Class 24	Class 26	2BB	
I-V curve					
Slope near Voc					
C = 1 sun	0.16 Ω \mp 0.03	0.065 Ω \mp 0.02	0.045 Ω \mp 0.007	0.045 Ω \mp 0.007	0.15 Ω \mp 0.04
C = 2 suns	0.14 Ω \mp 0.01	0.19 Ω \mp 0.11	0.165 Ω \mp 0.02	0.125 Ω \mp 0.02	0.16 Ω \mp 0.03
C = 10 suns	0.20 Ω \mp 0.14	0.195 Ω \mp 0.007	0.12 Ω \mp 0.007	0.13 Ω \mp 0.01	0.11 Ω \mp 0.03
Multiple light intensity					
	0.046 \mp 0.03 Ω	0.06 \mp 0.02 Ω	0.035 \mp 0.02 Ω	0.059 \mp 0.02 Ω	0.075 Ω \mp 0.01
Suns Voc					
	0.095 Ω \mp 0.002	0.112 Ω \mp 0.002	0.098 Ω \mp 0.0004	0.096 Ω \mp 0.002	0.098 Ω \mp 0.0006

The main conclusions are:

a. When expose to 1 or 2 suns, the standard commercial silicon solar cell from KVAZAR features a series resistance similar to the NaREC solar cell, while the Solartec solar cells features a series resistance lower to the NaREC solar cell;

b. This difference becomes higher when the solar cells are exposed under concentrated radiation; while the R_s values of KVAZAR solar cells raise under 10 suns, the R_s values of NaREC solar cells remain low. However, in the case of the Solartec solar cell, although the R_s values raises under 10 suns, when compared with the values obtained by the NaREC solar cells, the values are very similar;

c. When compared the several groups of Solartec cells, the cells classified with the class 24 are the cells that show higher values of R_s and the solar cells with two busbars shows the lowers R_s values.

5.4. Spectral Response and Quantum Efficiency

For a full characterization of the solar cells, a spectral response (SR) experiment was carried out in order to determine the quantum efficiency of the KVAZAR and Solartec solar cells.

This chapter starts with a brief description of the Spectral Response concept, which is followed by the experimental procedure and results obtained.

5.4.1. Theoretical Introduction

The concept of spectral response (SR) shows itself very similar to the concept of quantum efficiency (QE). The spectral response (Fig. 5.28) is the ratio between the current generated by the solar cell and the power incident on the solar cell, while the quantum efficiency (QE) can be describe as the ratio between the number of output electrons and the number of photons incident on the solar cell [42].

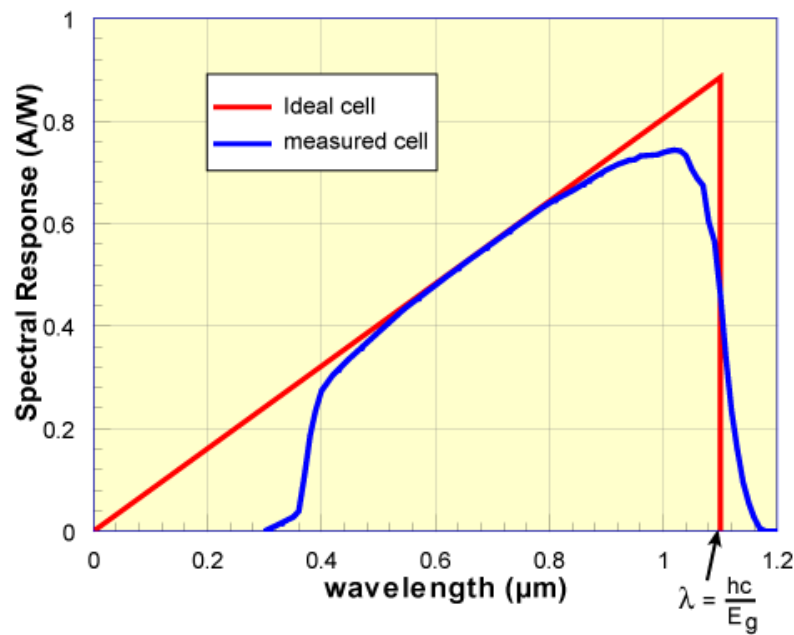


Figure 68 - The spectral response of a silicon solar cell under glass. As can be observed, at short wavelengths (below the 400 nm) the glass absorbs most of the light, leading to a very low response of the solar cell. In the intermediate wavelengths, the solar cell approaches the ideal (line marked in red). However, in the long wavelengths (under 1100 nm) the solar cell response falls back to zero.

Source: See Reference [37]

The spectral response (SR) of the tested cell (under short-circuit) is obtained using the relationship shown in equation (36) [42],

$$SR_{ext}(\lambda) = SR_{ext}^{ref}(\lambda) \frac{a(\lambda)}{a_{ref}(\lambda)} \quad (36)$$

where $a(\lambda)$ is the amplitude of the signal in the cell that we intend to test, $a_{ref}(\lambda)$ is the amplitude measured in the reference cell and $SR_{ext}^{ref}(\lambda)$ is the spectral response of the reference solar cell.

In the case of an ideal solar cell, the SR and the QE curves are limited in the higher wavelengths, due the inability of the semiconductor (as in the case of a solar cell) to absorb photons with energies below the band gap. However, when we observe the SR curve it is possible to see that, unlike the square shape that QE curves presents along the entire spectrum, the SR curve decreases in the small photon wavelengths. This situation occurs due the fact that in these kinds of wavelengths, the photon has a higher energy which consequently leads to a reduced ratio of photons and power. [42].

The SR is an important parameter since it is the SR that is measured from a solar cell, and from this the quantum efficiency is calculated. The QE can be determined through the SR by replacing the power of the light at a particular wavelength with the photon flux for the same wavelength [43]. So, the QE can be calculated by [44],

$$QE = \frac{hc}{q\lambda} SR \quad (37)$$

Where c and h are respectively the speed of light and Planck's constant, λ the wavelength and q represents the electron charge.

Figure 5.29 presents the quantum efficiency of an ideal and a real silicon solar cell [37]. As can be seen in Fig. 5.29, the QE for photons with energy below the band gap is zero. It can also be seen that while QE of an ideally solar cell, as mentioned before, has a square shape, the QE for most of the real solar cells is reduced due to recombination effects, reflections and low diffusion length.

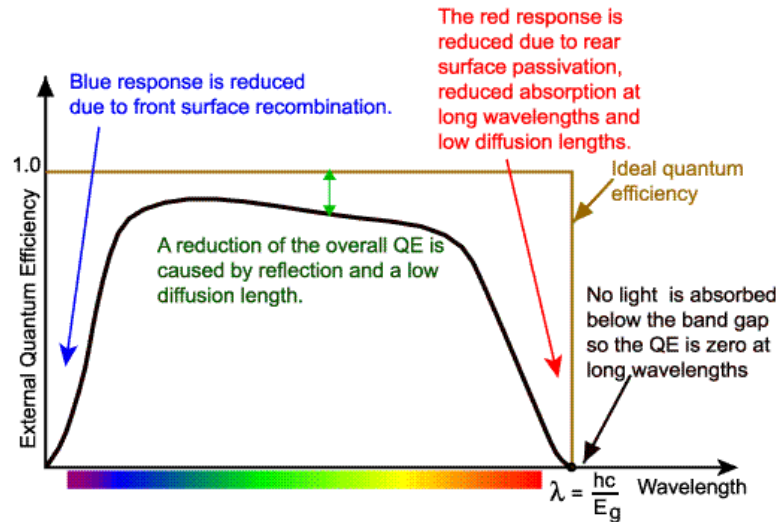
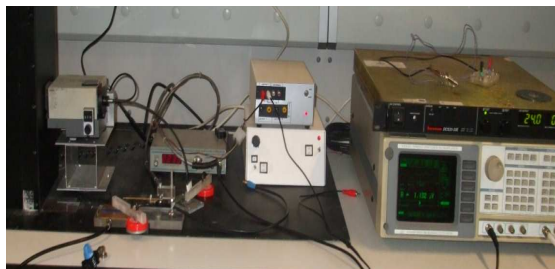


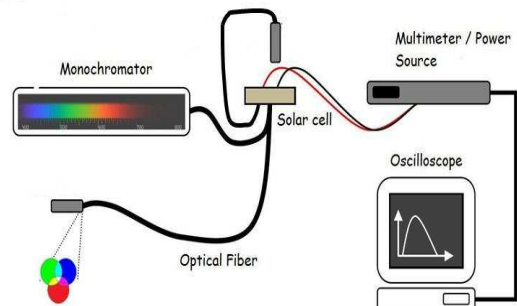
Figure 69 - Quantum Efficiency of a silicon solar cell. The QE of an ideal solar cell is marked in brown, while the QE of a real solar cell is marked in black
 Source: See reference [39]

5.4.2. Experimental procedure

The spectral response measurements of Solartec and KVAZAR solar cells were obtained by an experimental setup, shown in Fig. 5.30, consisting by a Xenon lamp, a monochromator, a frequency controller, a power source, an oscilloscope and an optical fiber with two branches that is used to converge the light beam of the monochromator. To avoid the contamination of the signal it was used a modulation system of the light beam, using a synchronized chopper with a lock-in, making in this way measurements in the frequency modulation and filtering the possible existing noise added to the signal. It was also used a vacuum system to ensure as the light hits the solar cell always in the same point, fixing it and preventing possible displacements.



a)



b)

Figure 70 - System for measuring the spectral response and quantum efficiency: a) Apparatus used for measurements placed in the FCUL Laboratory, b) Schematic diagram of the installation used for the measurements

Assuming that the solar cells from the same classification group presents equal behave, the SR was carried out only in some selected cells which are representative of each group of solar cells tested in the present thesis. In the case of KVAZAR cells we have picked up two solar cells: n° 6.7 and 6.8. While, in the case of Solartec cells, we have chosen one solar cell of each group: a cell of class 26, one of class 24 and a cell with two busbars.

It is important to notice that in the case of the KVAZAR solar cells, the measurement of SR was carried out in two cells because these solar cells derive from different parts of a main solar cell which may differ in bulk quality.

The measurements were performed in for a spectrum range of [400 nm - 1200 nm]. At the 800 nm it was used a filter to ensure only infrared radiation reaches the cells. During the measurements, the values used in voltage source were (Fig. 5.31):

- Voltage = 21 V
- Current = 9.4 A

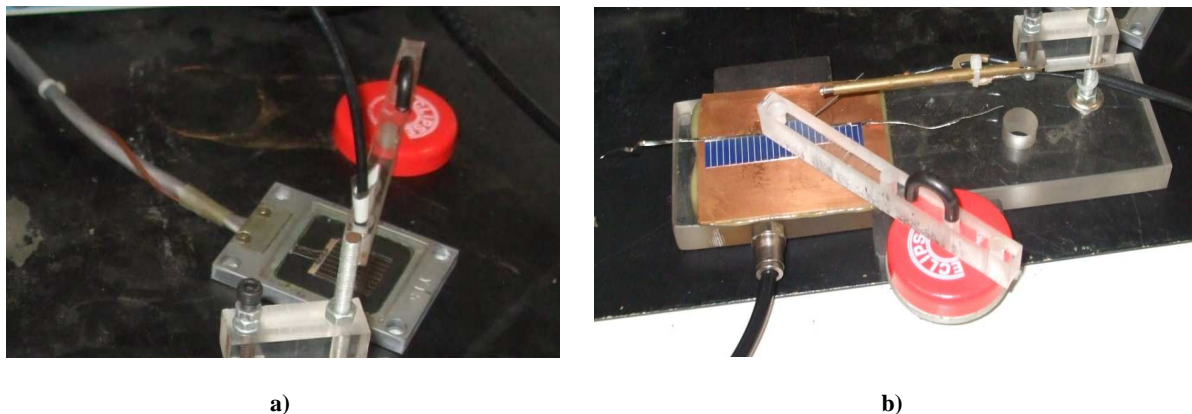


Figure 71 - Measurement of the SR in the solar cells: a) reference solar cell, b) KVAZAR or Solartec solar cell

5.4.3. Results

Figures 5.32 and 5.33 show the external quantum efficiency (QE) estimated in the KVAZAR solar cells 6.8 and 6.7, respectively. The curves reproduce the efficiency of solar cells in absorbing photons in each wavelength. As it can be seen in the Fig. 5.32 and 5.33, the SR was performed in three different positions. As can be seen, the highest quantum efficiency is achieved between the 500 nm and 900 nm, which corresponds to the visible and IV zones of the spectrum. Below 500 nm (i.e. blue light and UV zone) the QE is reduced due to the front surface recombination, while above the

1000 nm (i.e. I.V. zone), the QE is reduced due to bulk and rear surface recombination. It also can be seen that the QE obtained in the three different positions on the solar cells, is very similar.

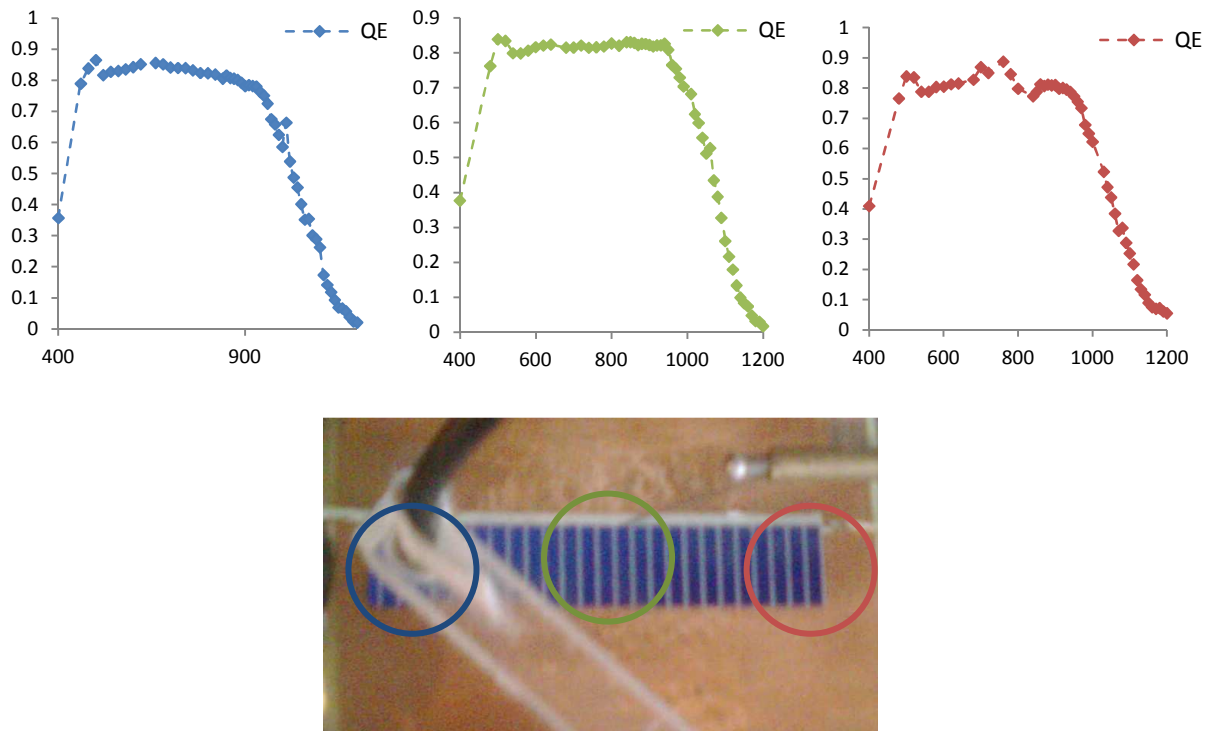


Figure 72 - External quantum efficiency of a conventional solar cell (KVZ.40 – 6.8) measured in different positions on the cell.

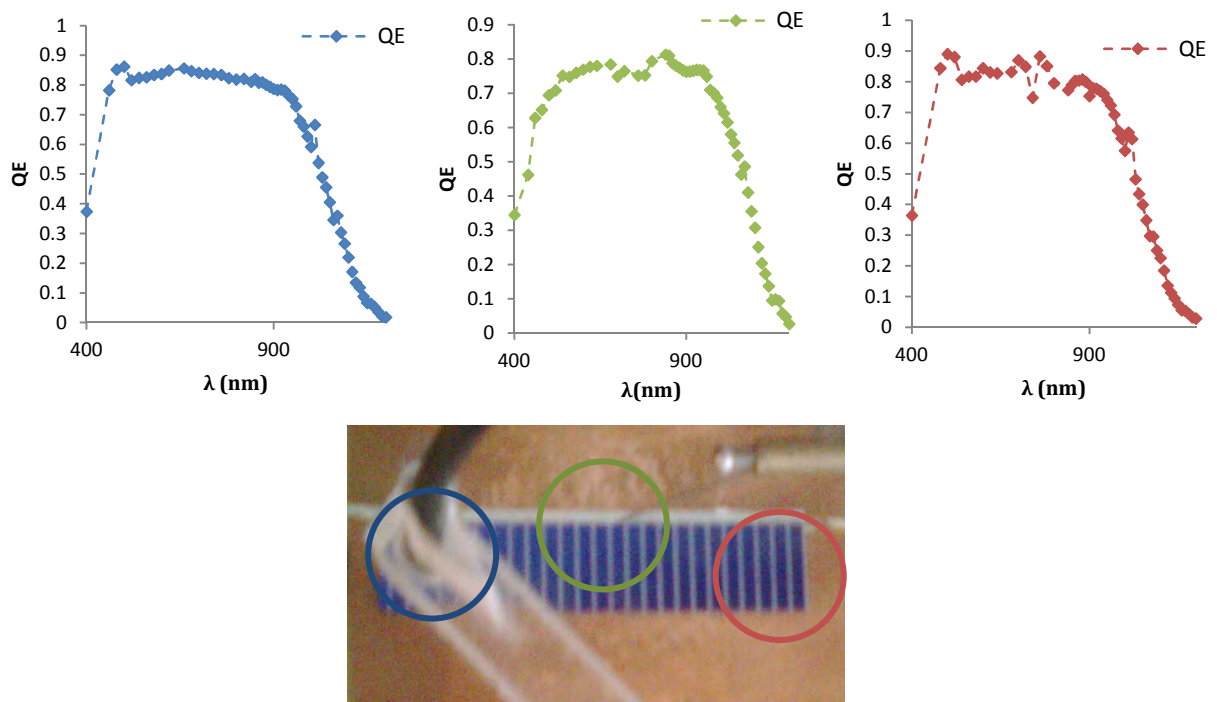


Figure 73 - External quantum efficiency of a conventional solar cell (KVZ.40 – 6.7) measured in different position

In the case of the Solartec solar cells, Fig. 5.34 shows the external quantum efficiency (QE) for the cells SLT.C24-1, SLT.C26-1 and SLT.2BB-1, respectively. As in the KVAZAR solar cells, the highest quantum efficiency is achieved between the 500 nm and 900 nm.

However, in the case of the Solartec solar cells, there are small differences in the QE curves obtained for the different classes of solar cells. While in class 24 and 2BB solar cells, between the 500 nm and 1000 nm, the quantum efficiency keeps in the highest values (values between 0.8 and 0.9), in the class 26 solar cell, although the quantum efficiency reaches its maximum values near the ideal (values between 0.9 and 0.97), the wavelength range is more reduced (only between 600 nm and 900 nm).

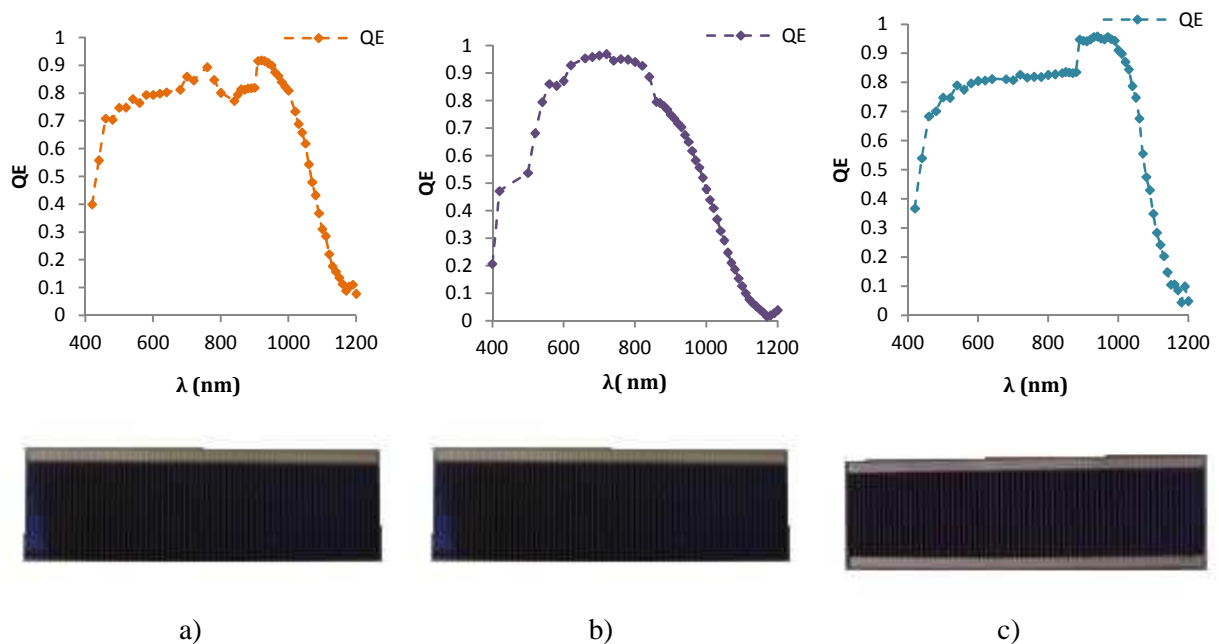


Figure 74 - External quantum efficiency of the Solartec solar cell a) class 24; b) class 26; c) with two busbar

When comparing the quantum efficiency of the KVAZAR and Solartec solar cells, it is possible to observe some differences. Figure 5.35 shows the QE curves of the KVAZAR (cell 6.8, in the center) solar cell (marked in blue) and Solartec (class 26) solar cell (marked in red).

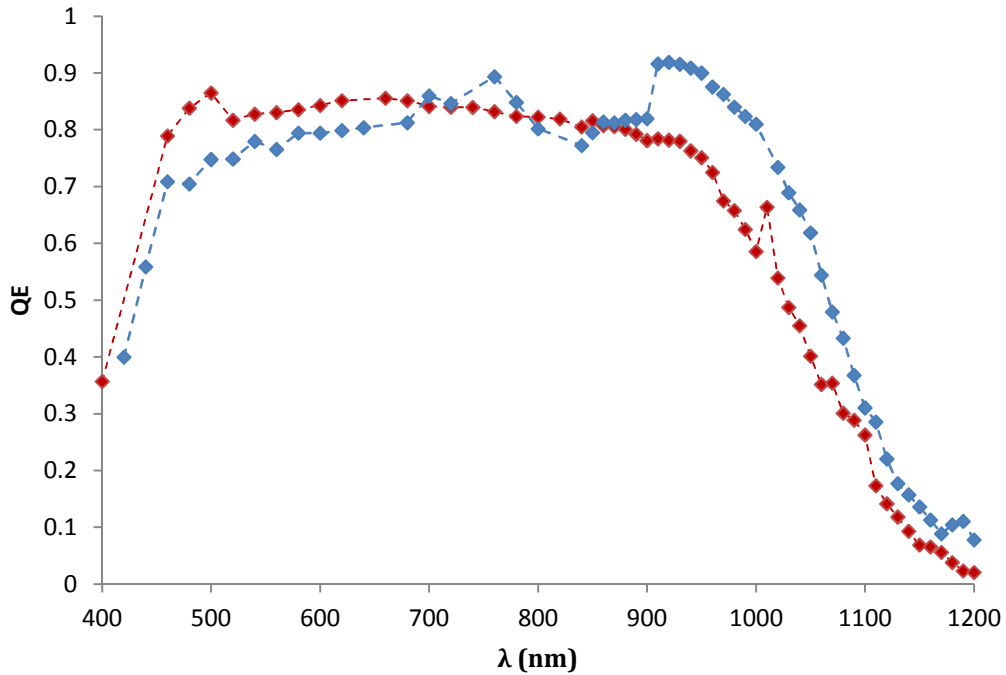


Figure 75 - QE curves obtained for the KVAZAR (red markers) and the Solartec (blue markers) solar cells.

As can be seen in the Fig. 5.35, both cells show similar behavior between 420 nm and 1200 nm. However, although the Solartec solar cells present QE values slightly lower than those reached by the KVAZAR solar cell until the 700 nm. From 820 nm onward, the QE curve of the Solartec solar cell always remains above to the QE curve of the KVAZAR solar cell.

This situation shows that the Solartec solar cells, despite showing a similar behavior to the KVAZAR solar cells along the spectrum, have a higher power of conversion the incident energy in the cell.

5.5. Thermal coefficients of solar cells

As mentioned in the previous chapters, the solar cell temperature is one of the important factors that affect how much electricity that the solar cells will produce. So, given this situation, the influence of this characteristic, should not be overlooked. In order to understand the influence of increase of the temperature in the KVAZAR and Solartec solar cells, through an experimental campaign, their thermal coefficients were calculated. In this chapter a brief description of the thermal coefficients concept is performed, passing through the description of the experimental procedure performed to measure these parameters in the KVAZAR and Solartec solar cells, ending with a description of the results obtained and the respective conclusions.

5.5.1. Thermal coefficients concept

The temperature of a solar cell is a parameter that highly influences its electrical behavior, being such variation usually described by thermal coefficients (%/°C). In the case of Voc and Isc, as the temperature increases, the first will decrease while the latter will rise. Still, it must be noticed that the Voc variation is much higher (Fig. 5.36) [45].

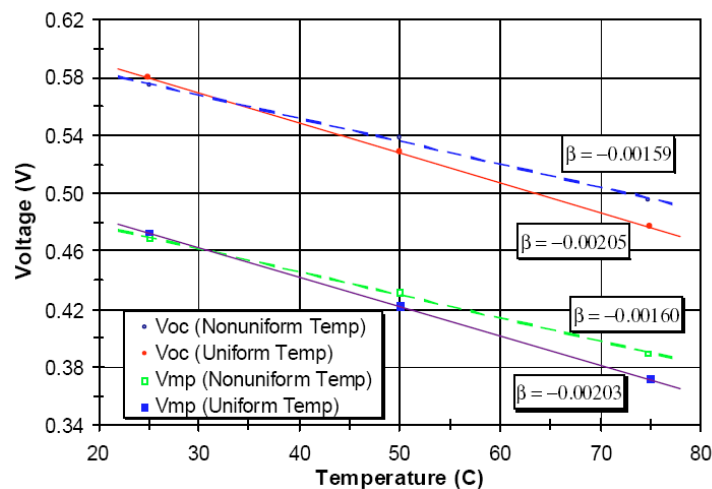


Figure 76 - Measured temperature coefficients for voltage for solar cell with uniform and nonuniform temperature during testing.
 Source: see reference [45]

According to King *et al.*[45], the procedures for measuring the thermal coefficient(s) for solar cells don't exist yet standardized, and systematic influences are common in the experimental methods performed to measure them. However, it can be stated that the most common method used to calculate the thermal coefficient is the Equivalent Cell Temperature method (ECT) [46 Germany

(2001) 156. #139]. According to I. Antón, the thermal coefficient β has a high variation with concentration level for a silicon solar cell, but when the temperature is lower than 100 °C, the thermal coefficients has very little variation, being considered constant at the usual one-sun operating conditions [45]. Usually, to estimate the thermal coefficients, the solar cell is placed in a solar simulator being illuminated with a uniform light and remains at constant temperature. The I-V curve is measured for a range of different temperatures and then the rate of change of the desired parameter with temperature (i.e. the thermal coefficients) is calculated according with equation (38)[45]:

$$CT = \frac{\Delta X}{\Delta T} = \frac{X_{(1\ sun,T)} - X_{(1\ sun,298.15\ K)}}{T - 298.15} \quad (38)$$

where $X_{(1\ sun,T)}$ is the value of the electrical parameter registered under a certain temperature and at 1 sun, $X_{(1\ sun,298.15\ K)}$ is the value of the electrical parameter at 1 sun and 25° C and T is the temperature of the solar cell and CT is the thermal coefficient in study.

5.5.2. Experimental procedure

In order to calculate the thermal coefficients of the KVAZAR and Solartec solar cells, the solar cells were exposed to a uniform light (equivalent to 1 sun), through the use of a solar simulator (Fig. 5.37). In order to exists a coherence of data, and to check if the radiation incident on cells was constant, was also carried out a control of the emitted radiation by the lamps of the solar simulator through the use of a radiation meter apparatus (Fig. 5.37).

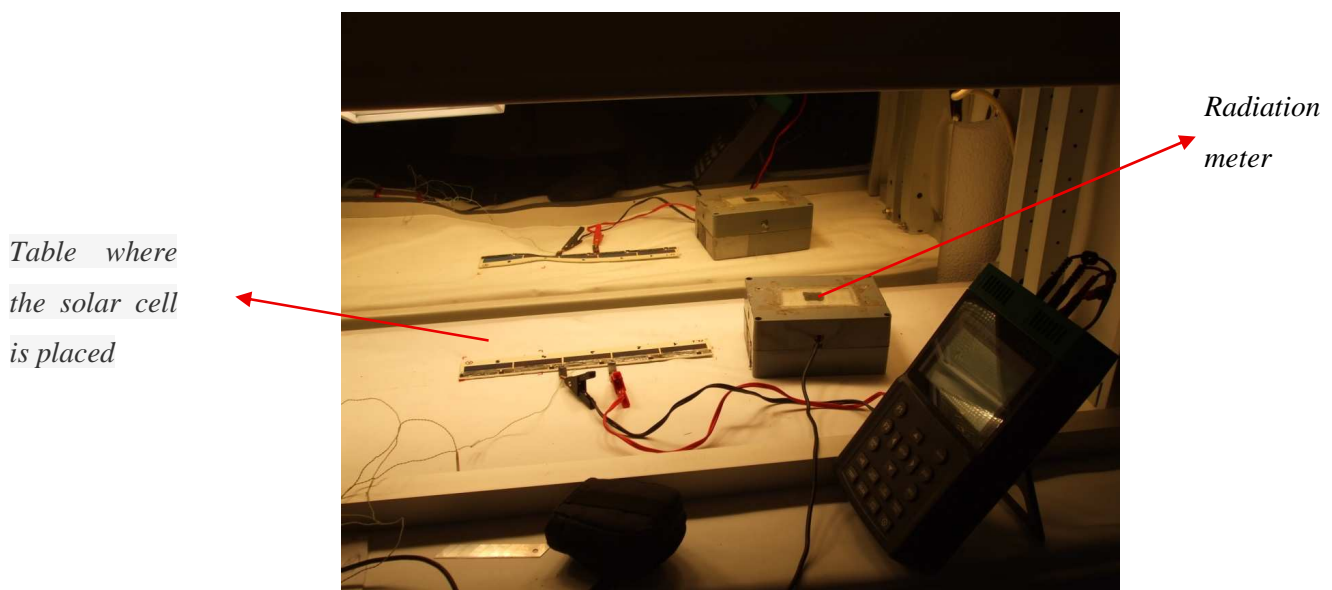


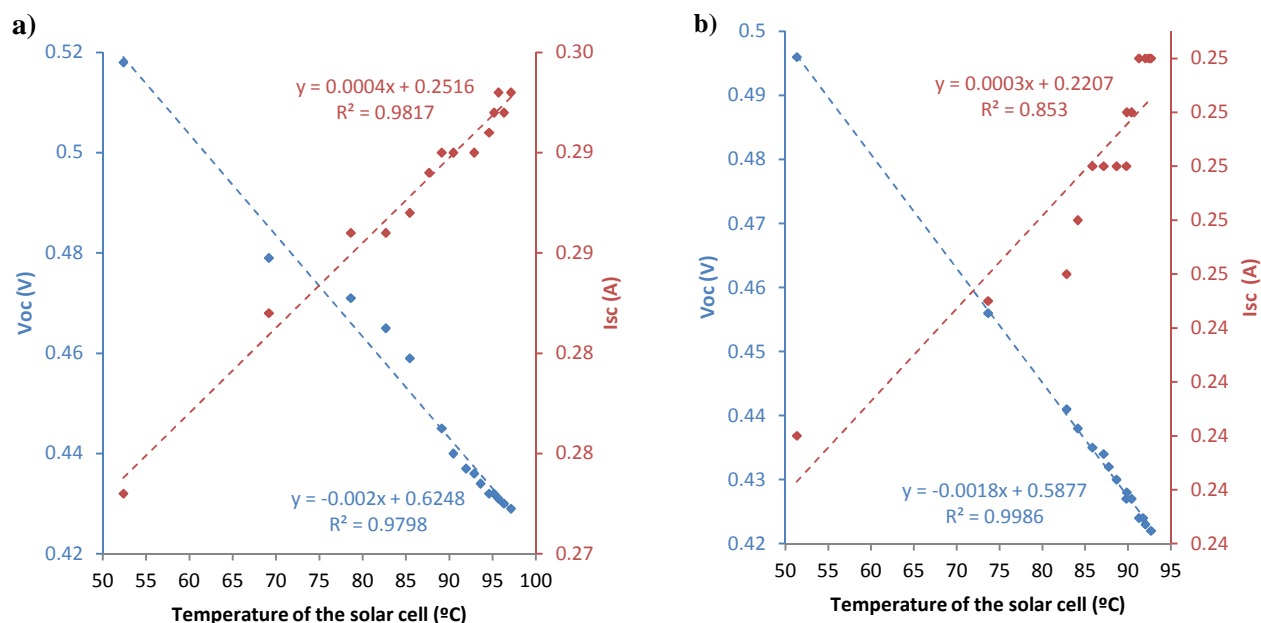
Figure 77 – Solar Simulator located in the Laboratory of the WS Energia S.A.

The I-V curves of the solar cell (one of each type of solar cell) were acquired through the I-V tracer apparatus, each 60 seconds, and solar cell temperature was measured by a thermocouple placed on the back of the solar cell.

5.5.3. Results

Through the I-V curves measured during the experiment, it was possible to visualize the behavior of the KVAZAR and Solartec solar cells as function of temperature.

Figure 5.38 presents the values registered for the Voc and Isc as a function of the temperature of the solar cells. As can be seen, when the temperature of the solar cell rises, the values of Voc decrease while the values of Isc increase. Regarding the values of Voc, Fig. 5.38 shows that in SLT.C24, SLT.2BB and KVAZAR solar cells the values of Voc decrease almost linearly, with the increase in temperature. However, the SLT.C26 solar cell shows a slightly different behavior when compared to the other studied solar cells. In this case, the decrease of Voc presents a behavior less linear, as can be seen by the value of the R^2 (value relatively less than 1). As in the case of the Voc values, the Isc increase almost linearly with the increase of temperature. This occurs to the fact of the increase of temperature of solar cells, which despite being a slight increase is enough to increase the value of Isc of solar cells.



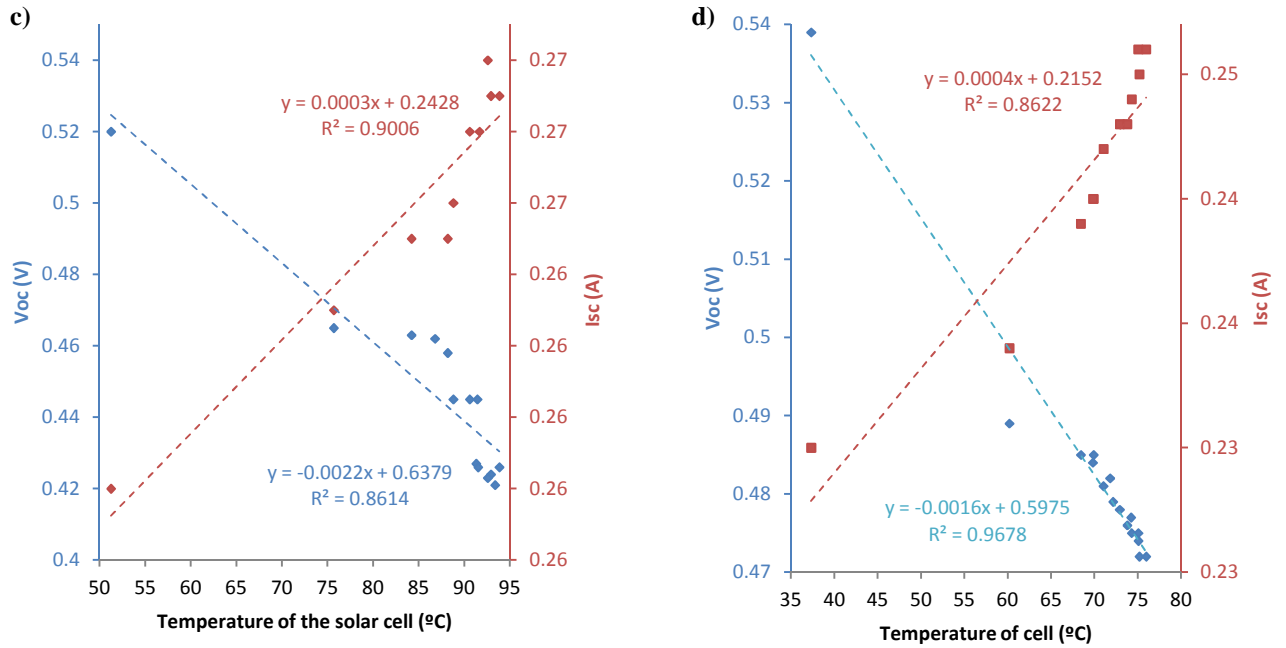


Figure 78 - Variation of the Voc and Isc as a function of the temperature of the: a) KVAZAR, b) SLT.C24, c) SLT.C26 and d) SLT.2BB solar cells.

By using equation (39) and the values obtained from the I-V curves and registered temperature, the thermal coefficients of the solar cells were calculated and are presented in Table 5.11.

Table 5.10 – Thermal coefficients estimated for the Solartec and KVAZAR solar cells

	Solartec solar cells			
	KVAZAR solar cells	SLT.C24	SLT.C26	SLT.2BB
V_{oc} (%/°C)	-0.18	-0.23	-0.23	-0.23
I_{sc} (%/degC increase)	0.05	0.03	0.03	0.04
I_{mpp} (%/degC increase)	0.03	0.02	0.02	0
V_{mpp} (%/degC increase)	-0.13	-0.23	-0.21	-0.25
FF (%/degC increase)	-0.11	-0.03	-0.07	-0.04
P_{mpp} (%/degC increase)	-0.05	-0.04	-0.06	-0.09

As can be seen in the Table 5.11, the values obtained, presents negative values in the cases of Voc, Vmpp, FF and Pmpp, and positive values in the cases of Isc and Impp, meaning that these electrical parameters decrease or increase, respectively, with temperature increase. It can also be observed that the Voc is the parameter of the solar cells that presents a higher decrease as a function of the increase of temperature.

When compared the Solartec solar cells with the KVAZAR solar cells, it can be observed that the firsts presents a lower value of decrease as a function of temperature in the FF and Pmpp.

However, in the remaining electrical parameters, the KVAZAR solar cells presents lower values of degradation as a function of the increase of temperature in the solar cell. Regarding the Solartec solar cells, the SLT.C24 presents the lowest values of thermal coefficients of V_{oc} and V_{mpp} .

5.5.4. Main conclusions

Despite all the electrical parameters of solar cell being affected by the increase in temperature, is the V_{oc} that presents a further decrease with the increase of temperature in the solar cell.

Regarding the results obtained for the Solartec solar cells, the SLT.C24 solar cells present themselves with the lowest values of thermal coefficients, when compared with the remaining Solartec solar cells.

Another conclusion that can be observed is that in comparison, the KVAZAR and Solartec solar cells show quite different thermal coefficients. While the Solartec solar cells present lower thermal coefficients in the case of FF and P_{mpp} , the KVAZAR solar cells present lower thermal coefficients in the remaining electrical parameters. So, it can be affirm that the KVAZAR solar cells seem to be the solar cells with lower decrease of electrical parameters with the increase of temperature.

The datasheets with the values measured in the experimental campaign are presented in the Annex IV.

Integration of the solar cells in the HSUN sub-receivers

In this chapter is presented the behavior of the Solartec solar cells integrated in the HSUN sub-receivers. In section 6.1 the entire HSUN system is described, while in the section 6.2 the mounting process of the sub-receivers is explained. In the section 6.3 the behavior of the solar cells integrated in the sub-receivers was analyzed.

6.1. Integration of solar cells in the HSUN technology

The HSUN technology (Fig. 6.1) is a medium concentration photovoltaic (MCPV) system that is being developed by WS Energia S.A. It has a total area of 1.68 m² and 6.3 kg/m² of weight. This technology is based on a 20X integrated parabolic trough (primary optics) that focus the light on a receiver with coupled reflective secondary optics. Each module has 7 successive primary optics (high reflective aluminum mirrors), being each receiver attached to the backside of the parabolic mirror that succeed [47]. This configuration is used as a passive cooling integrated system through which the heat dissipation of the receiver is performed.

Each HSUN receiver is composed by three sub-receivers which have five solar cells each (i.e. each HSUN receiver integrates a total of 15 solar cells).



Figure 79 – HSUN module mounted on a 2-axes tracking system

This thesis focuses on the HSUN receiver development by addressing:

- Mounting process of the receiver and preliminary tests for validation
- Optimization of the mounting process
- Evaluation of the receiver electrical performance
- Evaluation of the temperature effects on the receiver

6.2. Mounting process of the receiver and preliminary tests

The HSUN sub-receiver consists on an integrated printed circuit board (Fig. 6.2 and 6.3) that is produced and supplied by the company Globaltronic. The back surface of the five solar cells that integrate each sub-receiver is soldered to the squares showed in Fig. 6.2, and interconnected in series by soldering several Busing Ribbons to the busbar of each solar cell (Fig. 6.2 and 6.3). The mounting process will be described in detail in section 6.2.1 and the several improvements that were tested along the time until this process final was structured and tested are presented in the Annex V.

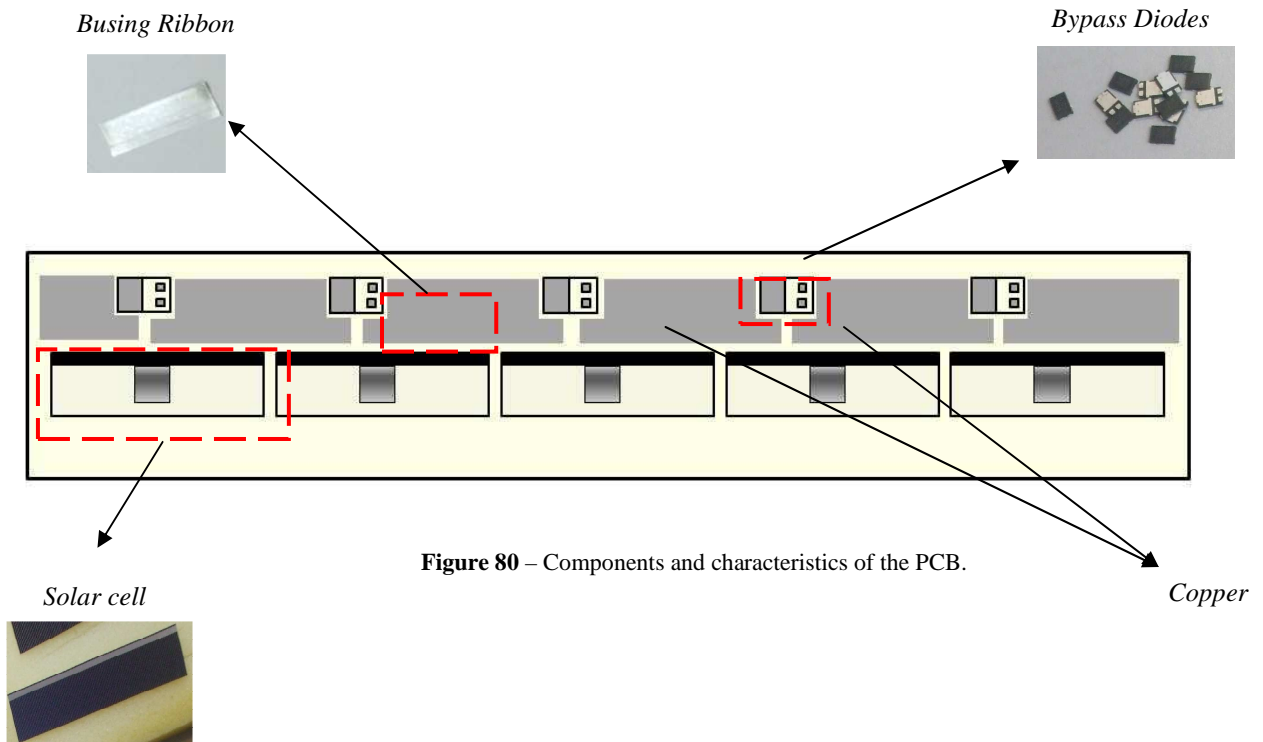


Figure 80 – Components and characteristics of the PCB.



Figure 81 – Sub-receiver. When three of these sub-receivers are connected, a receiver is obtained.

6.2.1. Process

As mentioned before, each HSUN receiver results from the attachment of three sub-receivers. The components that integrate each sub-receiver are:

- i) Printed Circuit Board (PCB)
- ii) Solar cells
- iii) Diodes
- iv) Busing ribbons

Figure 6.4 presents the specific position of each component on the PCB.

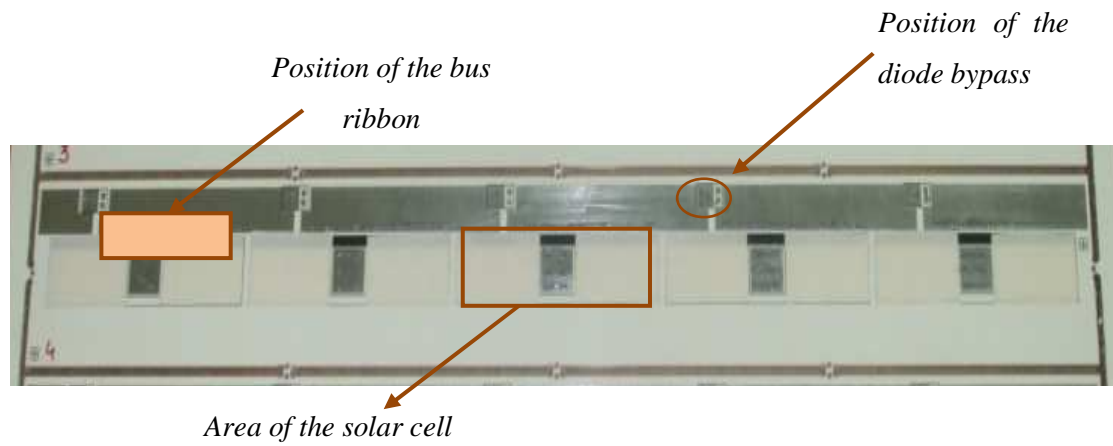


Figure 82 –Specific position of the each component on the PCB.

i) PCB

The sub-receivers PCBs are supplied as a set of six boards all integrated in a single frame as showed in Fig. 6.5. It must be noticed that the whole mounting process of each sub-receiver, i.e. placement of the components on the PCB as well as its soldering, is performed without detaching the boards from the frame.



Figure 83 – Set of six PCBs that are the base for the HSUN sub-receivers.

ii) Solar cells

The back surface of the solar cell is only soldered in the central area. Otherwise, if the whole back surface of the solar cell is soldered to the PCB, the solar cell is unable to support the thermal expansions and eventually breaks.

In order to promote a better heat dissipation from the solar cell to the PCB, the unsoldered back surface of the solar cell is filled with thermal tape. Notice that the thermal tape must be placed on the PCB before the solar cell. The thermal tape should be placed inside the delimited area for the positioning of the solar cell, as can be visualized in Fig. 6.6.

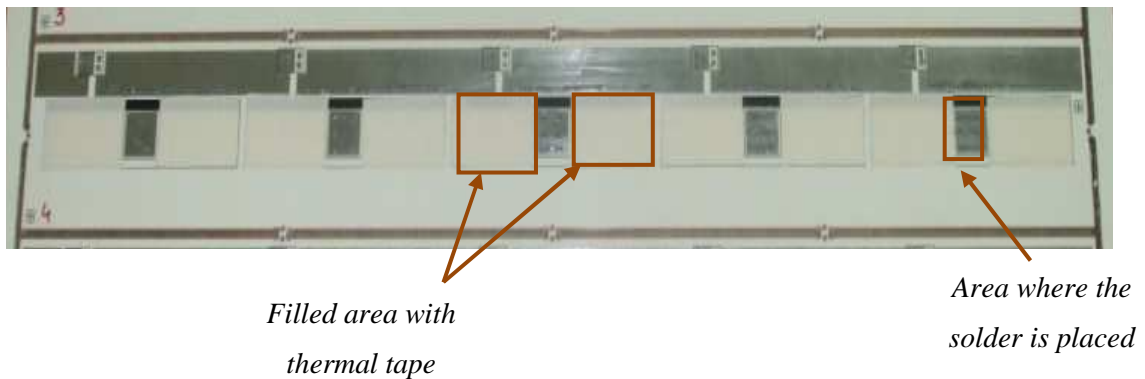


Figure 84 – Position where the thermal tape and the solder is placed on the PCB

iii) Diodes

In the printed circuit board it is also integrated a bypass diode for each solar cell. This is because, as the cells are connected in series, if one of the solar cell is damaged, the entire sub-receiver would crash, leading to high losses of efficiency in the entire system. However, through the application of these diodes, this situation may be circumvented. For a correct functioning, the bypass diode is connected in parallel, but with an opposite polarity as to the solar cell. If any of the solar cells is damaged, the diode of this cell begins to conduct current, allowing the current generated by the solar cells that stills operate flows by an external circuit [3].

iv) Bussing Ribbon

To connect the five solar cells in series, a Bussing Ribbon is soldered on the busbar of each solar cell and on the superior strip of the PCB, as can be observed in Fig. 6.5.

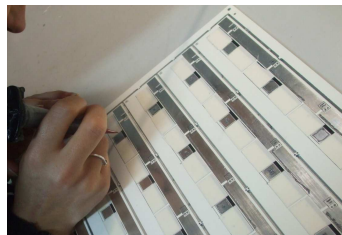
The whole mounting process of the sub-receiver is sketched in Fig. 6.7. To finalize the mounting process, the frame with six sub-receivers is placed in the furnace, where it remained around 10 minutes at a controlled temperature cycle, to accurately promote the soldering process.

STEP 1 Placement of thermal tape on the printed circuit board

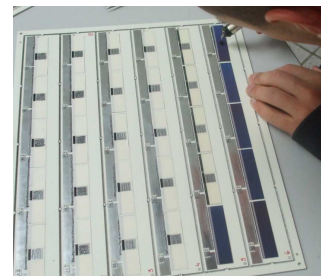
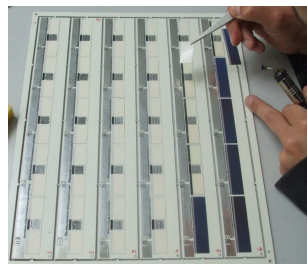


STEP 2 Placement of the soldering paste on:

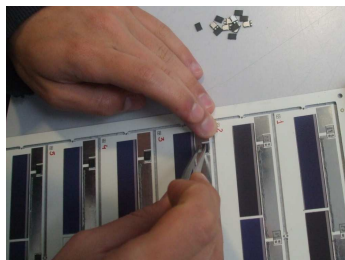
- i) the squares of PCB that are soldered to the back surface of the solar cell
- ii) the superior strip of each receiver, where the busing ribbon will be soldered



STEP 3 Removal the protective film of thermal tape and placement of the solar cells



STEP 4 Placement of the diode in the printed circuit board



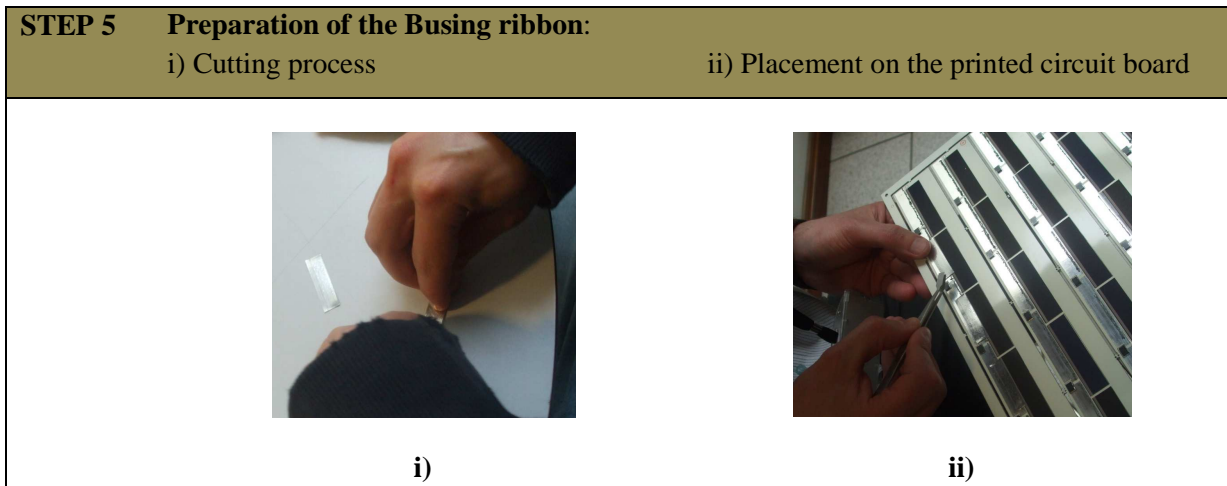


Figure 85 – Mounting process of the sub-receivers

In order to test the mounting process presented here, forty-eight sub-receivers were manufactured. These tests highlighted some failures associated to the soldering process which are described in the following lines.

6.2.2. Tests

Forty-eight sub-receivers were manufactured by using the procedure described before. The sub-receivers only differ on the amount of soldering paste that was used. It must be noticed that all the components on a sub-receiver were mounted/soldered by using the same amount of soldering paste. These sub-receivers were analyzed in two phases: i) a preliminary visual inspection of the receivers which was performed immediately after the process (i.e. soldering) carried out in the furnace, followed by ii) the evaluation of the receivers performance regarding maximum power output.

i) Visual inspection

From the 48 receivers that were mounted, 25% showed visual defects after the furnace step. Four main defects may be pointed out:

a. Arising of some spots on the front surface of the solar cells (Fig. 6.8):

Table 6.1 to 6.8 present the configurations of soldering paste and a qualitative assessment of the presence of spots on the solar cells. It must be noticed that the sub-receivers that present spots in the solar cells are also those where it was placed a larger amount of soldering paste. For example, in case of sub-receiver n° 2 the copper area, where the center of the cell is placed, was wholly filled with soldering paste and the superior strip of the sub-receiver, where the busing ribbon will be soldered, had more than three lines of soldering paste. Such soldering amount lead sub-receivers n° 2 to present the highest number of spots (Fig. 6.8).

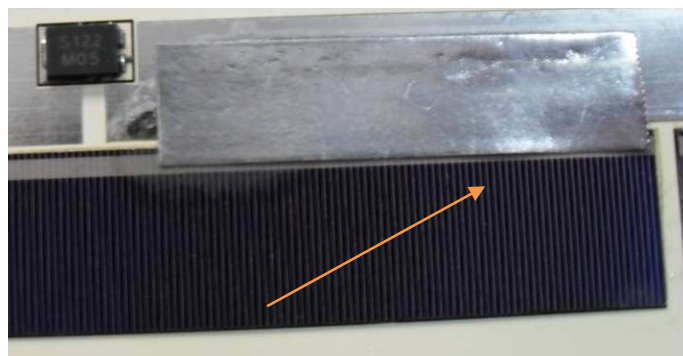


Figure 86 – Presence of spots in the solar cell of the sub-receiver n° 2.

b. Displacement of the ribbon as to its specific position.

The ribbon must be fixed on its specific position before the soldering process; otherwise some displacements from its specific position may occur during the soldering process (Fig. 6.9). For example, the solar cells are glued with thermal tape before the furnace step. This thermal tape promotes the thermal dissipation on the cells but it also warrants that they will remain on its specific position.



Figure 87 – Displacement of the ribbon from its specific position.

c. Unsoldered ribbons.

Some ribbons were not soldered to the solar cell busbar (Fig. 6.10) during the furnace step. To promote its adhesion, some flux must be applied on the busbar before the furnace step.



Figure 88 – Unsoldered ribbon

d. Displacement of the bypass diode as to its specific position.

Some diodes were displaced from its position on the PCB (Fig. 6.11) during the furnace soldering process.

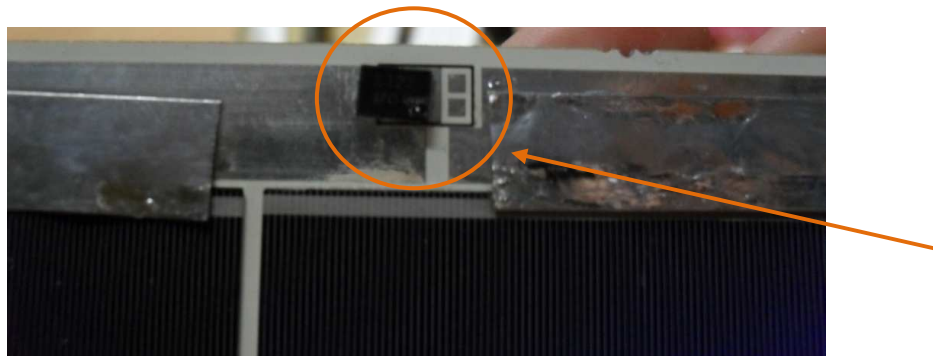


Figure 89 – Diode displaced from its position on the PCB.

Table 6.11 - Description of the soldering paste configuration used on each sub-receiver of board n° 1

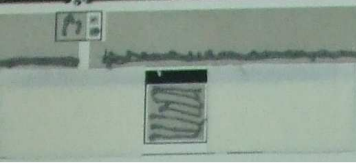

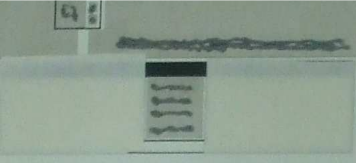
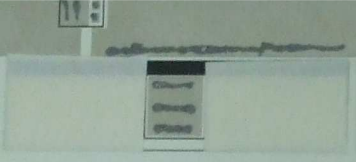
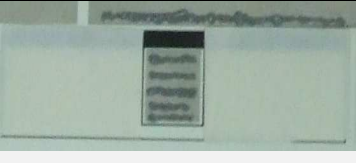

Board	Sub-receiver	Image of soldering paste configuration	VISUAL INSPECTION: Presence of spots in solar cells		ELECTRIC EVALUATION: Power (mW) registered for each sub-receiver		
			A few	None	< 400	400-500	>500
1	1		X				X
	2		X				X
	3		X				X
	4		X				X
	5		X				X
	6			X			X

Table 6.12 - Description of the soldering paste configuration used on each sub-receiver of board n° 2.



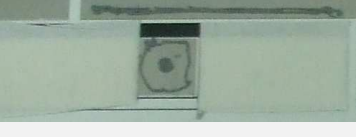
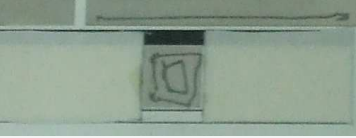


Board	Sub-receiver	Image of soldering paste configuration	VISUAL INSPECTION: Presence of spots in solar cells		ELECTRIC EVALUATION: Power (mW) registered for each sub-receiver		
			A few	None	< 400	400-500	>500
2	7			X			X
	8			X			X
	9			X			X
	10			X			X
	11				X	X	
	12			X			X

Table 6.13 - Description of the soldering paste configuration used on each sub-receiver of board n° 3.


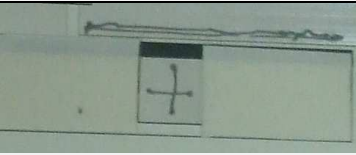
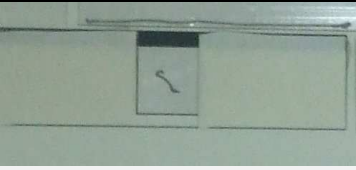
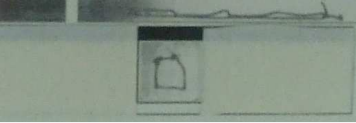

Board	Sub-receiver	Image of soldering paste configuration	VISUAL INSPECTION: Presence of spots in solar cells		ELECTRIC EVALUATION: Power (mW) registered for each sub-receiver		
			A few	None	< 400	400-500	>500
3	13			X		X	
	14		X		X		
	15			X			X
	16			X	X		
	17			X			X
	18			X		X	

Table 6.14 - Description of the soldering paste configuration used on each sub-receiver of board n° 4

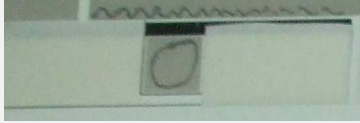

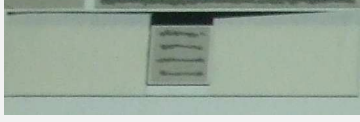



Board	Sub-receiver	Image of soldering paste configuration	VISUAL INSPECTION: Presence of spots in solar cells		ELECTRIC EVALUATION: Power (mW) registered for each sub-receiver		
			A few	None	< 400	400-500	>500
4	19		X				X
	20			X			X
	21			X			X
	22		X				X
	23			X			X
	24		X				X

Table 6.15 - Description of the soldering paste configuration used on each sub-receiver of board n° 5.

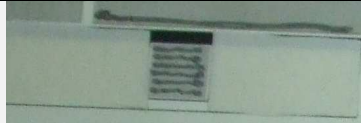

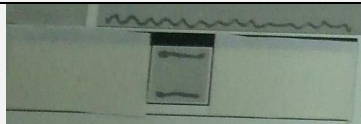
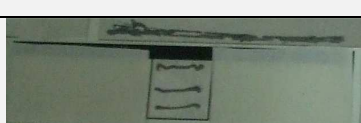
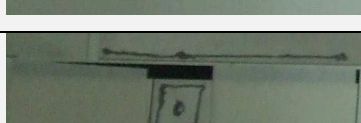

Board	Sub-receiver	Image of soldering paste configuration	VISUAL INSPECTION:		ELECTRIC EVALUATION:		
			Presence of spots in solar cells		Power (mW) registered for each sub-receiver		
			A few	None	< 400	400-500	>500
5	25			X			X
	26		X			X	
	27			X	X		
	28			X	X		
	29		X				X
	30				X		X

Table 6.16 - Description of the soldering paste configuration used on each sub-receiver of board n° 6


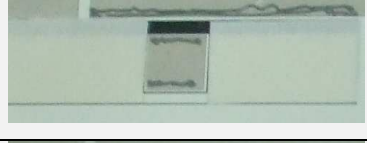
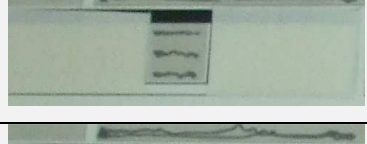
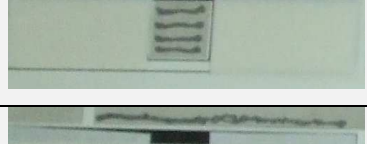
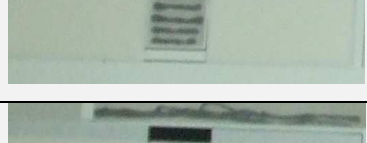
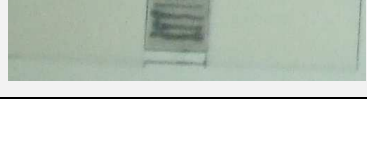
Board	Sub-receiver	Image of soldering paste configuration	VISUAL INSPECTION: Presence of spots in solar cells		ELECTRIC EVALUATION: Power (mW) registered for each sub-receiver		
			A few	None	< 400	400-500	>500
6	31						
	32			X	X		
	33			X		X	
	34			X			X
	35			X	X		
	36			X	X		

Table 6.17 - Description of the soldering paste configuration used on each sub-receiver of board n° 7.


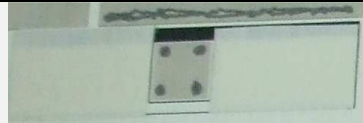

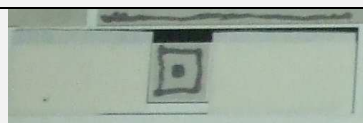

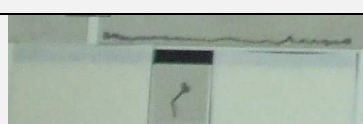
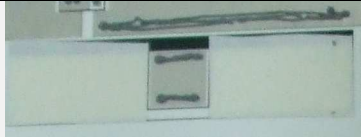
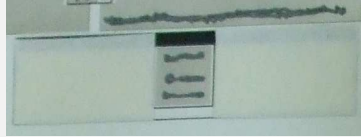
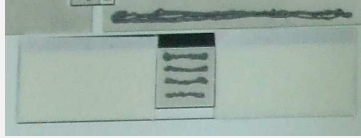
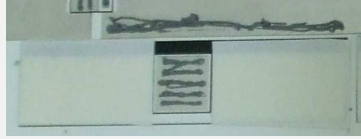
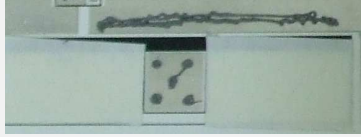

Board	Sub-receiver	Image of soldering paste configuration	VISUAL INSPECTION:		ELECTRIC EVALUATION:		
			Presence of spots in solar cells		Power (mW) registered for each sub-receiver		
			A few	None	< 400	400-500	>500
7	37			X	X		
	38			X		X	
	39			X			X
	40			X			X
	41			X			X
	42		X				X

Table 6.18 - Description of the soldering paste configuration used on each sub-receiver of board n° 8.

Board	Sub-receiver	Image of soldering paste configuration	VISUAL INSPECTION:		ELECTRIC EVALUATION:		
			Presence of spots in solar cells		Power (mW) registered for each sub-receiver		
			A few	None	< 400	400-500	>500
8	43			X			X
	44		X				X
	45		X				X
	46		X		X		
	47			X			X
	48			X			X

ii) Electrical performance of the sub-receiver

After visual inspection, the 48 sub-receivers were electrically characterized by the measurement of an I-V curve. Table 6.1 to 6.8 summarizes the Pmp measured for each sub-receiver.

The sub-receivers on which a very little amount of soldering paste was used, such as sub-receiver n° 11 and 42, presented lower power values. Since the amount of soldering paste used in these sub-receivers was minimal, the solar cell was most probably unsoldered to the PCB. Another source of the lower power values presented by the sub-receivers may be associated with an inadequate soldering of the busing ribbons to the solar cell busbar or even to the PCB, leading to a poor or inexistent electrical interconnection between the cells. Figure 6.12 shows that only 35% of the sub-receivers reached the expected power range (600-700 mW). As such the damaged sub-receivers were fixed, i.e. a manual re-soldering process was carried out by using a soldering iron with a prior application of flux on the solar cells busbar.

The re-soldering process has improved most of the sub-receivers increasing from 35% to 46% the number of sub-receivers within the expected power range. The average Pmp after the re-soldering process was about 632mW, while before it was about 455 mW. Moreover, 82% of the sub-receivers have registered a Pmp higher than 500 mW while before the re-soldering process this value was 62%.

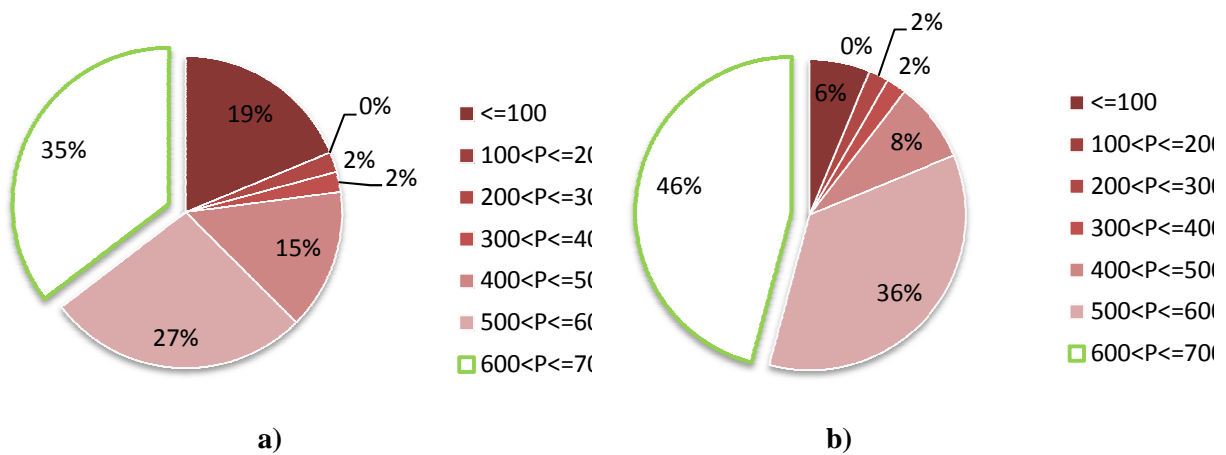


Figure 90 – Percentage of sub-receivers that are within a certain range of Pmp a) before and b) after the re-soldering process.

It can also be seen that, initially, 19% of sub-receivers had values of Pmp lower than 100mW, being this percentage diminished to 6%, after the re-soldering process.

The increase in power of some sub-receivers (n° 11,12,14,27,28,32,35,36,37,38 and 42) was due to the re-soldering process that has electrically interconnected some solar cells allowing the sub-receiver to properly work.

Figure 6.13 presents the values of Pmp before and after the re-soldering process of sub-receivers that, initially, had values of Pmp lower than 100mW.

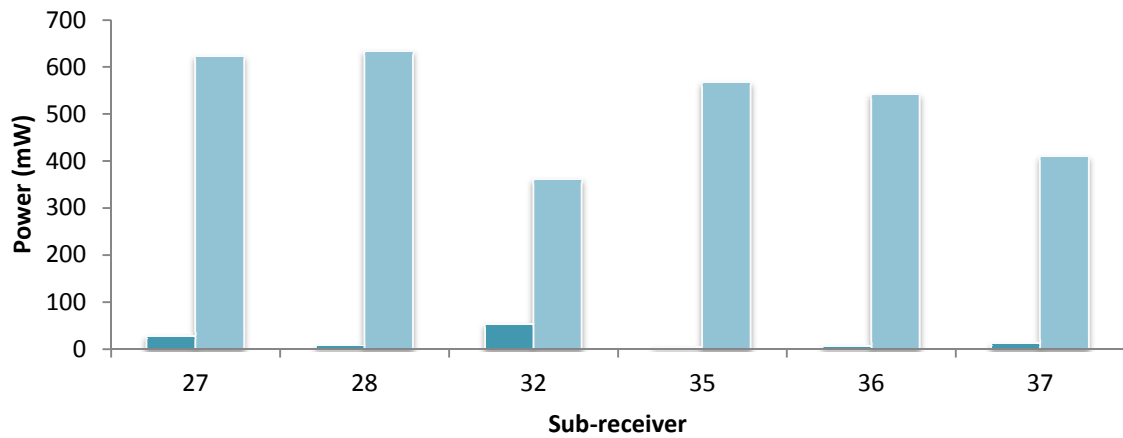


Figure 91 - Values of Pmp before (dark blue) and after (light blue) the re-soldering process of the sub-receivers that, initially, had values of Pmp lower than 100mW.

As can be seen, the re-soldering process led to an increase of the Pmp from a few 100mW up to 630mW (sub-receiver 28). Figure 6.14 highlights that after the re-soldering process the Voc of the sub-receiver may raise from less than 0.5 V up to 3 V. The increase of the Voc means that some cells weren't electrically connected to the sub-receiver before the re-soldering process. Since the cells are connected in series the voltage of the sub-receiver is strongly affected by the number of cells that are correctly soldered to it.

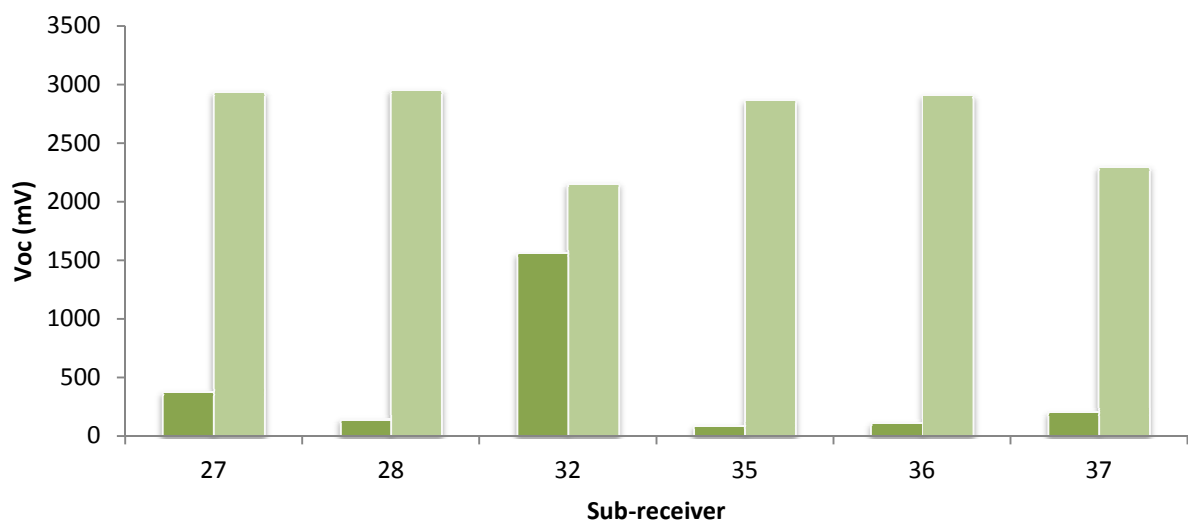


Figure 92 – Open-circuit voltage before (dark green) and after (light green) the re-soldering process of sub-receivers that, initially, had values of Pmp lower than 100mW.

Contrary to what occurred in the values of Voc, the values of Isc didn't suffer the same increase (Fig. 6.15).

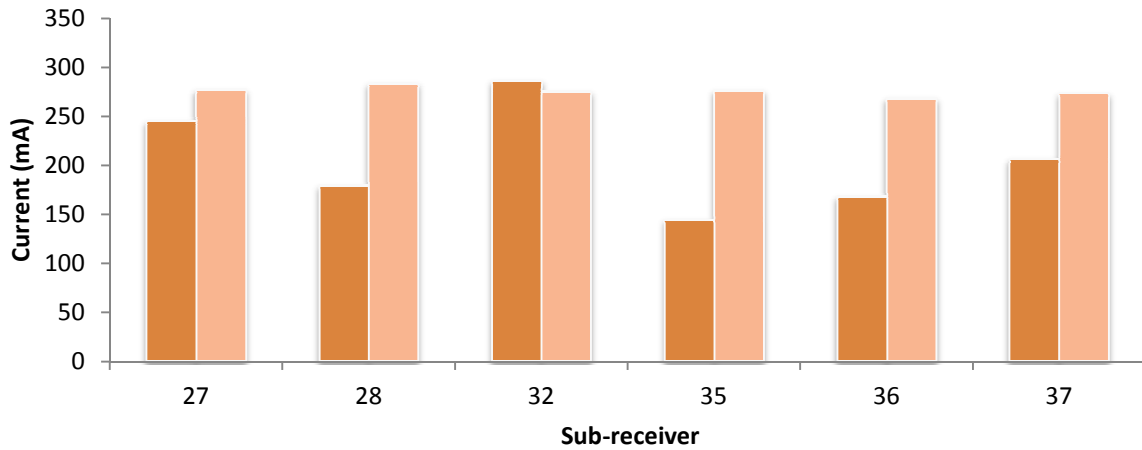


Figure 93 – Short-circuit current before (dark orange) and after (light orange) the re-soldering process of sub-receivers that, initially, had values of Pmp lower than 100mW

As can be seen in Fig. 6.15, the value of Isc has been increased only between 32 mA and 100 mA. This occurred since, when solar cells are connected in series, the current has small variations, and the current generated by a sub-receiver is close to the current generated by the cell that has the higher value of Isc due to the bypass diodes.

However, even after the re-soldering process, some sub-receivers didn't show an improvement of the Pmp and, in some of the cases, the value of Pmp had declined which means that the sub-receiver was even more damaged with the re-soldering process. In the case of sub-receivers n° 11, 12, 14, 38 and 42 the values of Isc and Pmp decreased after the re-soldering process (Fig. 6.16 and 6.17), while the values of Voc increased slightly (Fig. 6.18). However, it is noted that despite the fact that the values of Pmp decreases, the difference between values obtained before and after the re-soldering process didn't exceed the 8%.

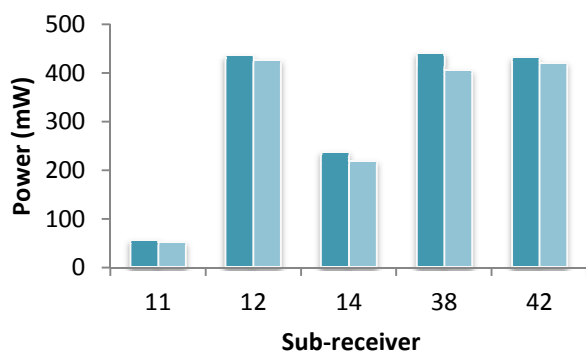


Figure 94 – Maximum power before (dark blue) and after (light blue) the re-soldering process of sub-receivers that had not presented improvements.

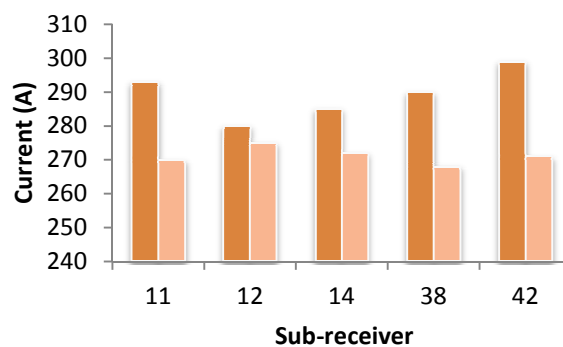


Figure 95 – Short-circuit before (dark orange) and after (light orange) the re-soldering process of sub-receivers that had not presented improvements.

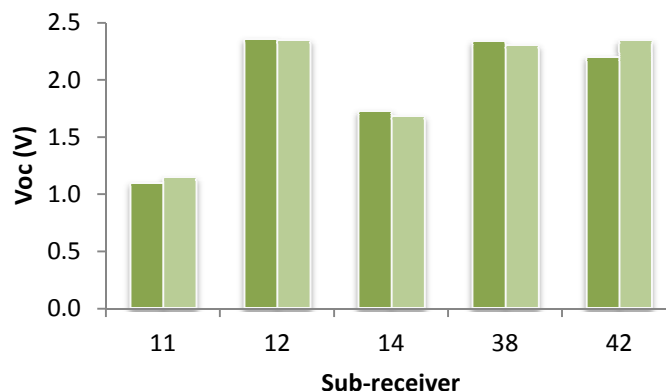


Figure 96 – Open-circuit voltage before (dark green) and after (light green) the re-soldering process of sub-receivers that had not presented improvements

As such, it can be concluded that the manual re-soldering process works, but in some it very difficult to fix them.

Another reason for the sub-receivers presents lower values of Pmp, even after the re-soldering process, is the fact that the thermal tape, that fulfills the solar cell back surface not soldered, have a certain thickness which can prevent the cell to get into contact with the soldering paste and consequently not be soldered to the PCB. However, such situation is almost impossible to rectify without damaged prematurely the solar cell.

6.2.3. Optimization of the mounting process

As described in the previous chapter, several failures were detected on the sub-receiver after the soldering process. In this section, some solutions are suggested to avoid such failures and optimize the mounting process.

a) Elimination of the spots

Regarding the spots that appeared on the solar cells, and after studying the various configurations of soldering paste, it was concluded that: i) the spots on the solar cell only appeared in the sub-receivers on which a higher quantity of soldering paste was used (see Tables 6.1-6.8, sub-receivers n° 1,2, 3,4,5,12,14,19,22,24,26,25,42,44,45,46) however, ii) in the sub-receivers on which it was used only a meager amount of soldering paste (see Table 6.1-6.8, sub-receivers n° 11,12,14,16,27,28,32 and 37), the solar cells were improperly soldered to the PCB. As such, the soldering process should be optimized by using an intermediate amount of soldering paste, which lies between 4 to 5 risks of soldering paste on the copper square that is soldered to the solar cell back surface and 3 lines of soldering paste on the superior strip of copper that is soldered to the busing ribbon. Moreover, a thinner thermal tape (with the same thickness of the copper square) should promote the contact between the solar cell back surface and the copper square.

b) Avoid displacement of the busing ribbon

To avoid the displacement of the busing ribbon, before the furnace soldering step, a plate (as showed in Fig. 6.19) should be used to exert a small pressure on the ribbons, so they remain fixed and connected to the solar cell during the passage of printed circuit board in the furnace.

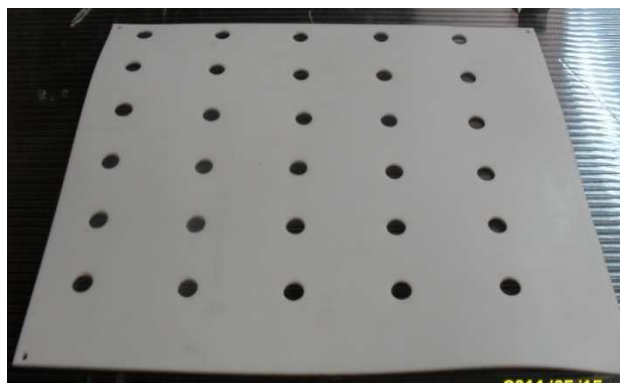


Figure 97 – Pressure Board

c) Avoid unsoldered ribbons

Regarding the unsoldered busing ribbons challenge, some procedures should be added to the mounting process of the receiver:

- a pen flux (Fig. 6.20) must be used to clean the busbar of the solar cell thus providing a higher adherence between them during the soldering process. The busbar must be cleaned before placement of the busing ribbon.
- the ribbon must be cut in a flat form, in order to achieve a completely flat area that entirely fit on the solar cell busbar to increase the contact area and promote the soldering.



Figure 98 – Pen flux

Thus, in order to understand if the solutions presented before were adequate to improve the mounting process, 6 new sub-receivers were produced by following the solutions presented in the Table 6.9.

Table 6.9 – Method used in each of the sub-receiver

Number of Sub-receiver	Configuration
1	Pen flux + Solder in the Busbar
2	Pen flux
3	Irregular Ribbons + Pen flux + Pressure
4	Pen flux
5	Pen flux + Pressure
6	Pen flux + Pressure

6.2.3.1. Tests

As in the previous chapter, to have a better analysis of the results, these are divided in two phases: i) a preliminary visual inspection of the sub-receivers and ii) evaluation of electrical performance of the sub-receivers.

iii) Visual inspection

After the process carried out in the furnace (i.e. the soldering process), only 1 of the 6 receivers showed visual defects. The resin spots on the front surface of the solar cells have only arisen at the sub-receivers in which a small amount of soldering paste was placed on the solar cell busbar (sub-receiver n° 1). Also in this sub-receiver little balls of soldering paste have risen on the solar cell busbar (Fig. 6.21). This results shows that the placement of soldering paste on the solar cell busbar will promote the soldering between the busbar and the busing ribbon but also harm the solar cells, thus invalidating the method.

The amount of soldering paste (4-5 risks of weld in the copper square and about 3 lines on superior strip) used in the soldering process was visually validated due to the inexistence of spots on the front surface of the solar cells. However, this amount of soldering will only be completely validated after the electrical performance test.

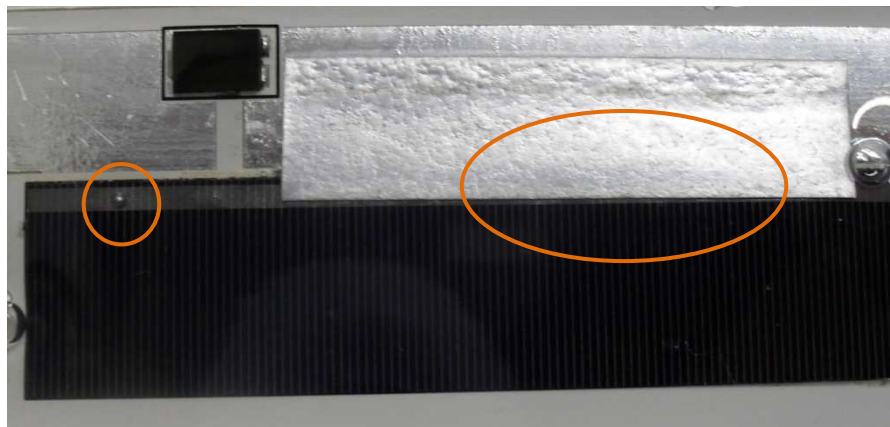


Figure 99 – Presence of spot sand balls of soldering paste on the solar cell busbar.

Regarding the displacement of the busing ribbon from its specific position during the soldering process, the use of the pressure plate was unsuccessful suggesting that other solution must be found.

The implementation of the busbar cleaning step (by using a pen flux) has showed to significantly reduce the amount of unsoldered busing ribbons.

iv) Electrical performance of the sub-receiver

As in the previous chapter, after the visual inspection, the 6 sub-receivers were electrically characterized by the I-V measurement.

It must be noticed that the sub-receiver, in which the busing ribbons were wavy, registered lower Pmp (e.g. sub-receiver n° 3). The wavy shape of the busing-ribbon led to an inefficient soldering of the ribbon to the PCB was due to a weak contact between both surfaces. Figure 6.22 show that only 50% of the sub-receivers present a Pmp between 300 - 400 mW. As such, and as in the previous chapter, a manual re-soldering was performed.

The re-soldering process has improved most of the receivers. The number of receivers within the maximum power range has risen from 50% to 83%, being the average Pmp about 500mW. Moreover, all of the sub-receivers have registered a Pmp higher than 300 mW.

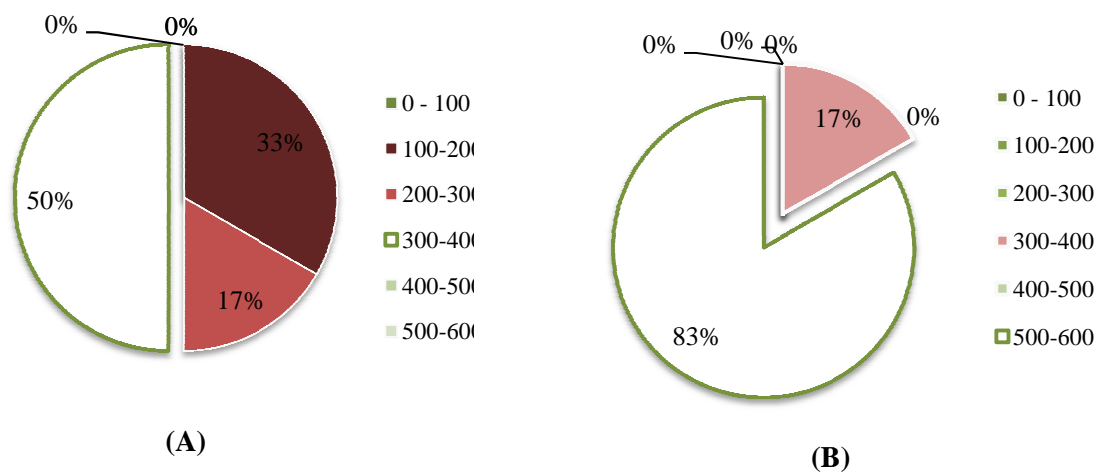


Figure 100 – Percentage of sub-receivers that are within a certain range of Pmp a) before and b) after the re-soldering process.

It can also be seen that, initially, 33% of sub-receivers had values of P_{mp} lower than 200mW, being this percentage diminished to 0%, after the re-soldering process. The sub-receivers n° 3, 5 and 6 had several disconnected solar cells that when re-soldered began to work properly. The values of P_{mp} registered for each sub-receiver before and after the soldering process are presented in Fig. 6.23.

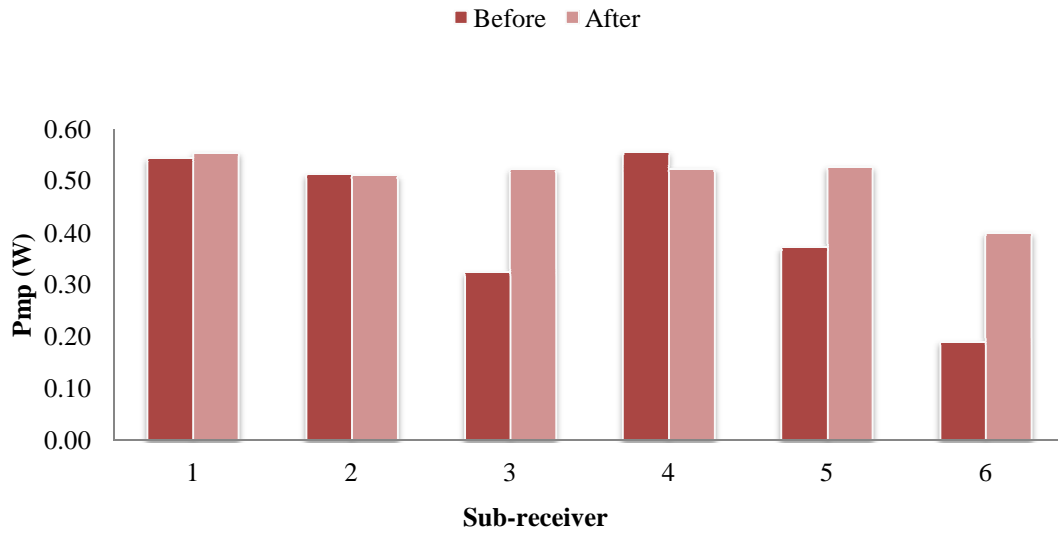


Figure 101 – Maximum power point before and after the re-soldering process of sub-receivers.

As can be seen, the re-soldering process led to an increase of the P_{mp} (increase between 10mW and 210 mW). This increase in the P_{mp} is mainly due to a significant increase in the voltage of the sub-receiver, which in turn rises due to the re-soldering of some interconnections that were not well performed before. Figure 6.25 highlights this situation since after re-soldering process the V_{oc} of the sub-receiver rose between 5 mV and 600 mV.

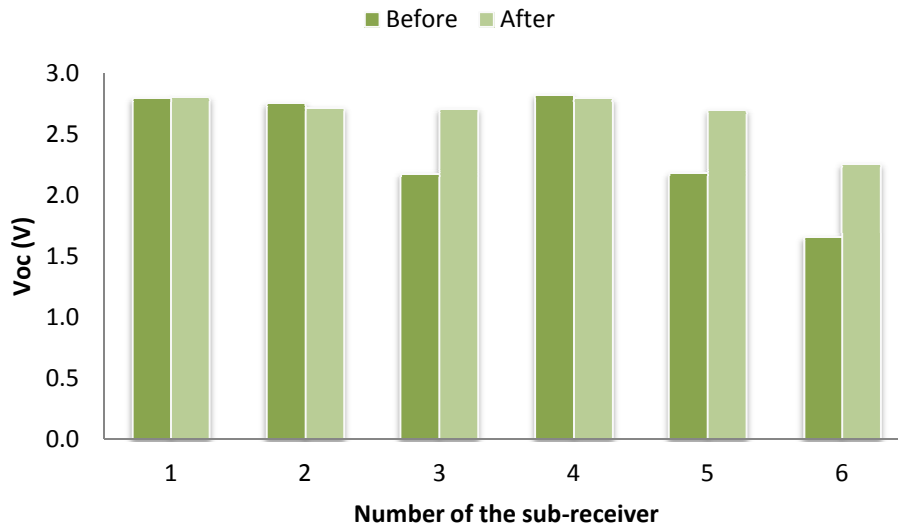


Figure 102 – Open circuit voltage before and after the re-soldering process of sub-receivers that initially, had values of Pmpp lower than 100mW

These results a significant improvement of the failures found in the mounting process of the sub-receivers. In order to solve the persistent challenges of ribbons displacement, a new configuration of busing ribbons is suggested. For example, a slight lift in the center of the ribbon would probably improve the adherence between the ribbon and the PCB.

6.3. Electrical performance

The electrical characterization of solar cells (section 4) has shown that the solar cells provided by the KVAZAR company are only suitable up to a concentration of 8 suns, while the Solartec solar cells showed to be suitable up to a concentration of 20 suns. In this section we present and discuss the tests that were carried out on sub-receivers that integrate Solartec solar cells since the HSUN system was designed to operate at a concentration of 15 suns.

Within the Solartec cell designs studied in this thesis, the SLT.2BB solar cells has presented the best electrical performance (section 4.3); however, its front grid design (two busbars instead of just one) is incompatible with the HSUN sub-receivers design that are currently being used in the HSUN system. Thus, only the cells SLT.C26 and SLT.C24 were used in the receiver tested here (the tests conducted in the NaREC solar cells (cells used actually in the HSUN system) are presented in the Annex VI).

6.3.1 Experimental procedure

Four sub-receivers (two sub-receivers integrating SLT.C26 solar cells and the remaining two integrating SLT.C24 solar cells) were mounted following the procedure presented in section 6.2. To measure the I-V curve of each cell, individually, output ribbons were soldered between each consecutive solar cell and at the ends of the sub-receiver (Fig. 6.25).



Figure 103 – Sub-receiver with the output ribbons soldered.

The I-V measurements were carried out at outdoor conditions (sunlight), i.e. the sub-receiver was placed towards the sun at optimized position without being integrated in the HSUN module (Fig. 6.26). During all the experiment, the sub-receiver temperature, the ambient temperature and the incident radiation were recorded at the same time of the I-V curve measurements:

- to measure the temperature of each sub-receiver a thermocouple was glued at the center of the back surface of the sub-receiver (Fig. 6.27 a);

- the incident radiation was measured with the radiation meter apparatus, which was placed side-by-side with the sub-receiver (Fig. 6.27 b), and the ambient temperature was measured by using a thermocouple.



Figure 104 – Experimental set to measure the I-V curves under outdoor conditions.

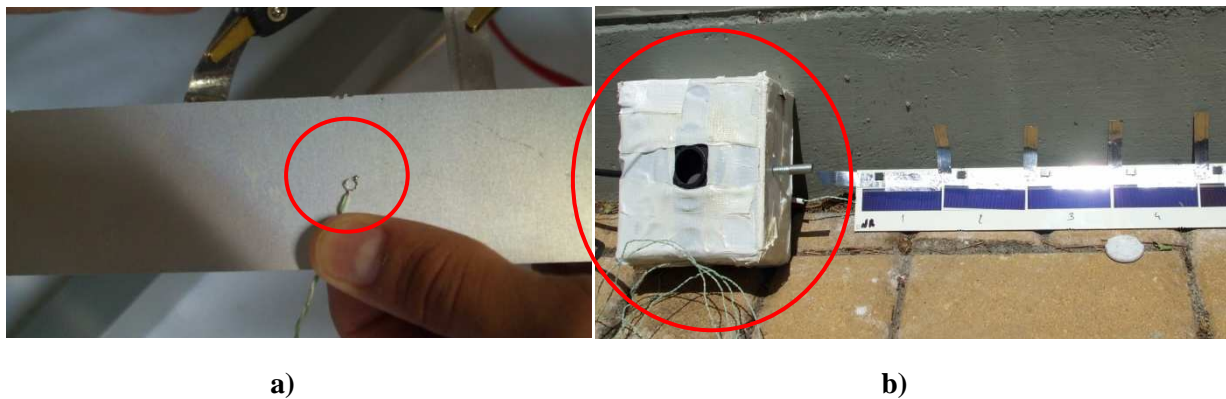


Figure 105 – Placement of the a) thermocouple at the rear surface of the sub-receiver and b) the radiation meter apparatus side-by-side with the sub-receiver.

6.3.2. Results

All the I-V curves measured for each solar cell and for corresponding sub-receiver during the experiments, previously described, may be found in Annex VII. Figure 6.28 shows the I-V curve of the sub-receivers with the corresponding irradiation and temperature of the PCB back surface at the time of the measurements. The average ambient temperature registered during all the experiment was $30.5 (\pm 0.5) ^\circ\text{C}$.

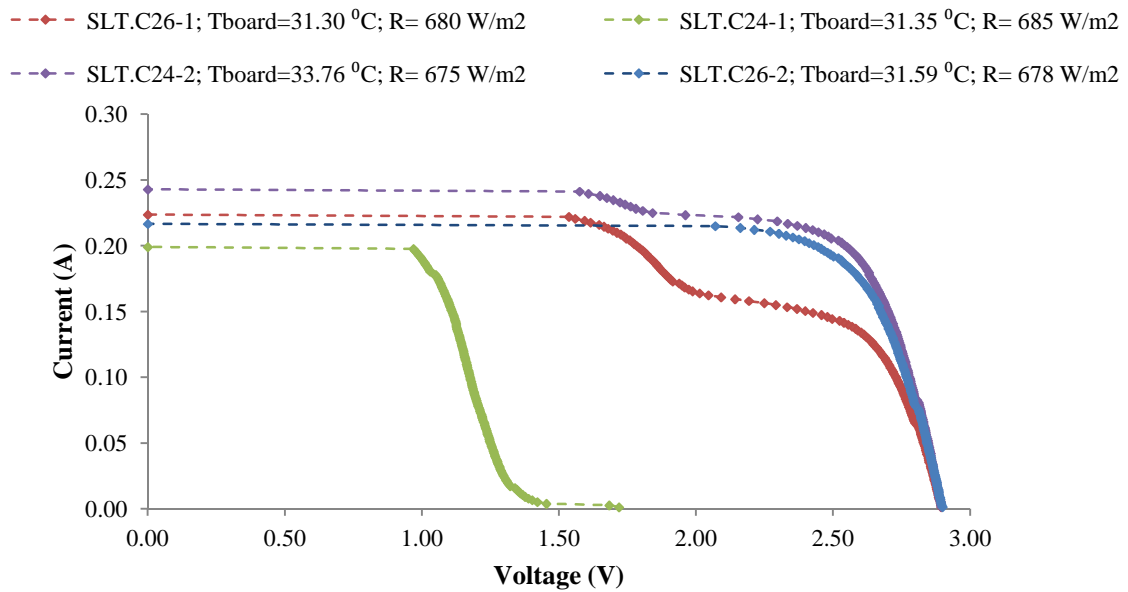


Figure 106 – I-V curves measured to SLT.26 sub-receiver n°1, SLT.24 sub-receiver n°1, SLT.24 sub-receiver n°2 and SLT.26 sub-receiver n°2 under outdoor conditions. The average ambient temperature at the time of the whole experiment was $30.5 \pm 0.5^\circ\text{C}$.

Figure 6.29 highlights a problem on the SLT.C24-1 sub-receiver since its V_{oc} is considerably lower than the expected one (2.90 V). The V_{oc} registered for this sub-receiver (1.72 V) suggests that only 3 cells were properly working since the typical V_{oc} of the solar cells under study is about 0.58V under STC conditions (see section 4.1). Also in Fig.6.29, it must be noticed that the diodes are working properly, it is important to note that the fact that solar cells aren't in the same operating mode (which will be discussed in detail in the next sections), causes adverse effects on the I-V curve of the sub-receiver (Fig. 6.29) and, consequently, in the maximum output power produced by the system. Figure 6.30 presents the P_{mp} of the sub-receiver, the average of the P_{mp} produced by each solar cell, individually. This figure highlights that higher deviations of the individual P_{mp} of each solar cell to the average P_{mp} of the solar cells, that integrate the sub-receiver, lead to lower P_{mp} of the whole sub-receivers, i.e. solar cells operating in different conditions lead to higher losses in the system.

In the following sections the behavior of each individual solar cell is analyzed in detail taking into account the incident radiation (section 6.3.2.1.) and cell temperature (6.3.2.2.).

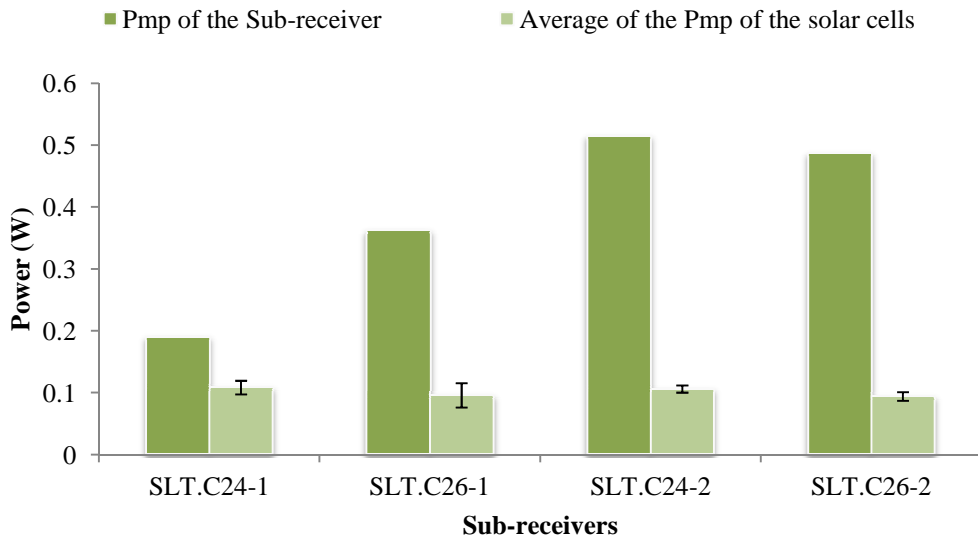


Figure 107 – Measured values of Pmp of the sub-receiver and the average of the Pmp of the solar cells.

Figure 6.30 presents the values of FF of the sub-receivers estimated through the I-V curves. When these values are compared, it is possible to say that the averages of FF of the solar cells are very similar between themselves (difference between 0.5% and 2%). However, as in the case of the values of Pmp, higher deviations of the individual FF of each solar cell to the average FF of the solar cells, that integrate the sub-receiver, lead to lower FF of the entire sub-receivers.

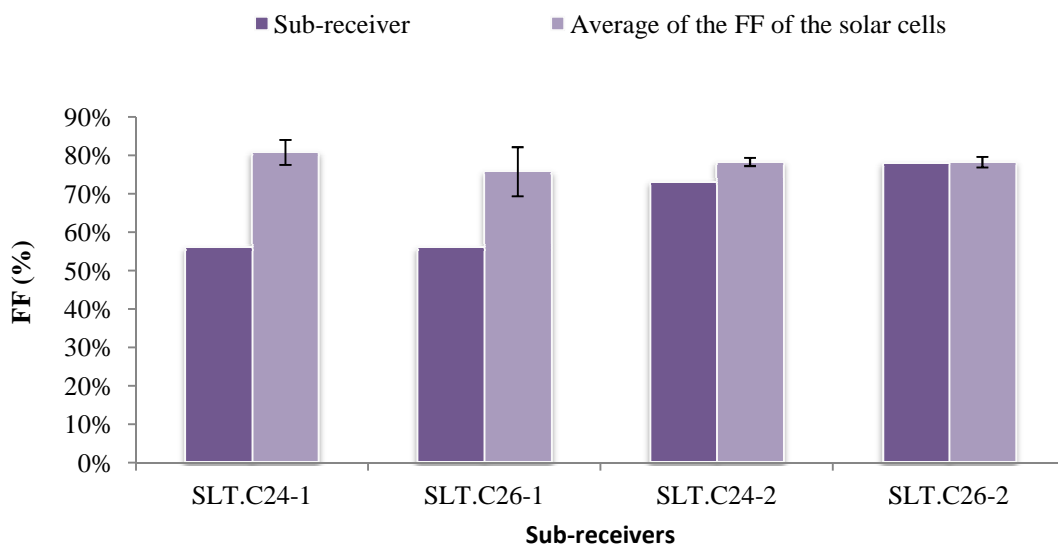


Figure 108 – Estimated values of FF of the sub-receiver and the average of the FF of the solar cells.

6.3.2.1. Analysis of the results taking into account the incident radiation

Figure 6.31 presents the values of I_{sc} and V_{oc} that were measured for each solar cell, individually, and for the sub-receiver under the conditions previously mentioned. This figure also presents the expected values for the I_{sc} and V_{oc} of Solartec cells under the irradiation registered during the measurements and considering a cell temperature of 25°C. It must be noticed that almost all the solar cells present a value of I_{sc} higher than the expected one. Such mismatch may be related with two factors:

- i) a slight deviation of the radiation meter as to the optimum position of the receiver may lead the radiation meter to register lower irradiation values than the irradiation that is indeed falling on the receiver;
- ii) higher cell temperatures lead to a slight increase of the I_{sc} (see section 6.3.2.2).

Since the I_{sc} only varies by 0.03%/°C and is extremely sensitive to the irradiation that falls on the cell, the mismatch in Fig. 6.31 is most probably due to a deviation in the radiation meter position.

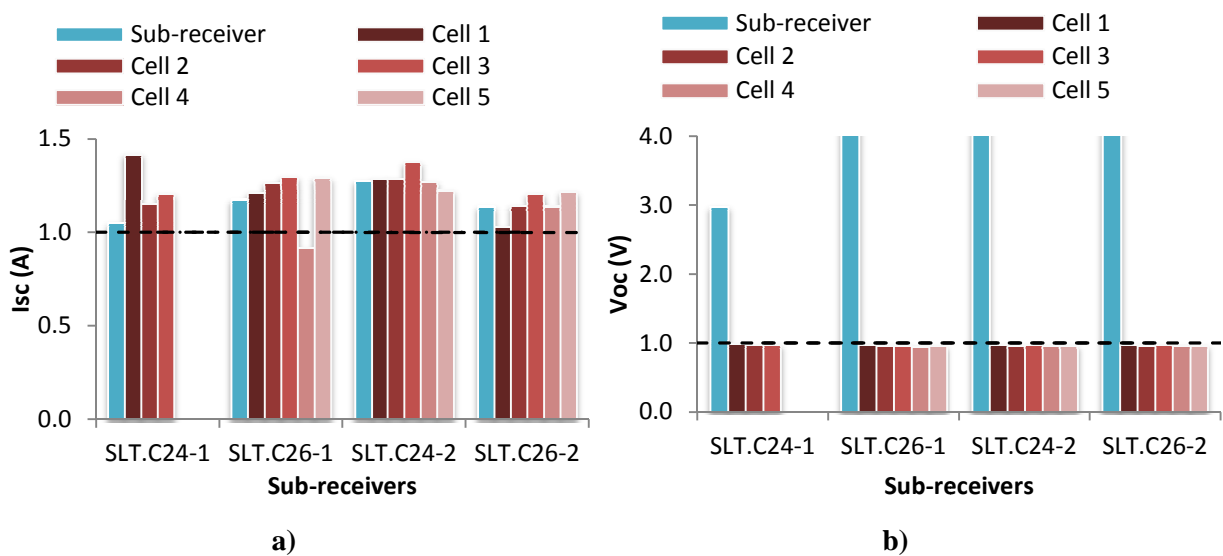


Figure 109 –Values of a) I_{sc} and b) V_{oc} of each solar cell (different red hue bars) and sub-receiver (blue bars) normalized at outdoor conditions: 680 W/m² and 30.5 (±0.5) °C of ambient temperature normalized for the I_{sc} and V_{oc} expected. The dashed black lines indicate the estimated I_{sc} and V_{oc} (see Chapter 4) for a solar cell with the same characteristics of the ones in analysis. This value was estimated for the same atmospheric conditions and considering a temperature of 25°C registered for the cell.

By performing the ratio between the average of the I_{sc} measured for each cell (notice that the inoperable cells of the SLT.C24-1 sub-receiver were disregarded for this average value) and the I_{sc} estimated for 1 sun, the expected incident radiation level that falls on the cells would be 10% higher

than the value measured by the radiation meter, i.e. 800W/m^2 instead of the 680W/m^2 measured. Taking into account the radiation level that results from the previous fit, we have estimated again the “Expected” I_{sc} and V_{oc} and the results are presented in the Fig. 6.32.

This figure shows that with 800W/m^2 , the I_{sc} measured is very similar to the value expected while the V_{oc} variation is barely visible. So, assuming that the position of radiation meter was not optimized can be concluded that the real incident radiation level at the moment of the measurements in the solar cells was about 800W/m^2 .

Looking to the behavior of each solar cell individually (Fig. 6.32 a)) in the same sub-receiver, it is noticeable that the cells present a different behavior when exposed to the same conditions. Such difference may be related with accumulated dust on the cells.

Regarding the V_{oc} , the values registered for each cell are lower than the values expected for the 800W/m^2 of irradiation. However, we must bear in mind that the theoretical V_{oc} was estimated for a temperature of 25°C . Since higher temperatures reduce the V_{oc} and the temperature of the PCB back surface was $39 (\pm 0.9)^\circ\text{C}$, it is expected a better match of the measured V_{oc} values as to the expected V_{oc} after a temperature correction, which is discussed in the next section.

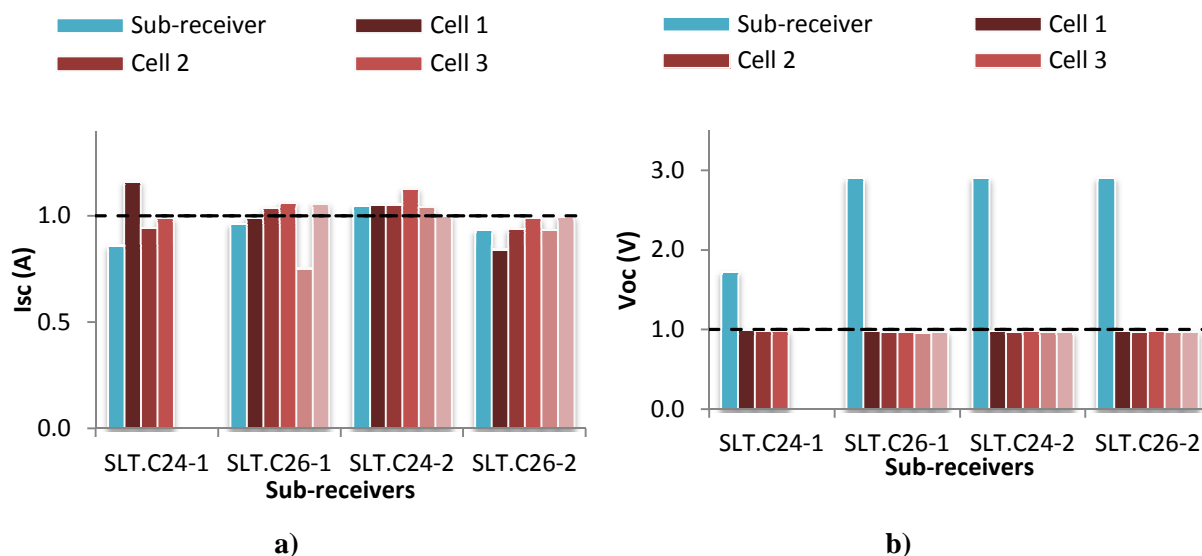


Figure 110 –Values of a) I_{sc} and b) V_{oc} of each solar cell (different red hue bars) and sub-receiver (blue bars) normalized at outdoor conditions: 800W/m^2 and $30.5 (\pm 0.5)^\circ\text{C}$ of ambient temperature normalized for the I_{sc} and V_{oc} expected. The dashed black lines indicate the estimated I_{sc} and V_{oc} (see Chapter 4) for a solar cell with the same characteristics of the ones in analysis. This value was estimated for the same atmospheric conditions and considering a temperature of 25°C registered for the cell.

6.3.2.2. Analysis of the results taking into account the radiation and cell temperature

6.3.2.2.1. Experimental procedure

In order to observe the effects of the temperature in the SLT.C26 and SLT.C24 solar cells integrated in the sub-receivers we have registered each 60 seconds the I-V curves of solar cell n°3 of each sub-receiver during 15 minutes of sunlight exposure at optimal position. As in the previous experiment, the irradiation, ambient temperature and temperature of the PCB back surface were recorded.

The I-V curves were acquired through the I-V Tracer apparatus and the solar cell temperature was measured by a thermocouple placed on the back surface of sub-receiver, right next to the rear area of the cell that is being measured cell n° 3 (Fig. 6.33), while the incident radiation was measured with the radiation meter apparatus, which was placed in the same position that the solar cell measured.



Figure 111 - Placement of the Thermocouple in the back rear surface of the solar cell n° 3 of the sub-receiver. To the acquisition of temperature by the thermocouple was made always in the same location, the thermocouple was fixed with thermal tape

6.3.2.2.2. Results

As mentioned in the chapter “Thermal Coefficients” of this thesis, from the value of V_{oc} acquired at a concentration of 1 sun and the thermal coefficient estimated for the solar cells, it is possible to calculate the temperature of the cells when the I-V curves were measured. Thus, the temperature of the solar cells can be estimated through the following equation [48],

$$T (K) = \frac{V_{oc}(C, T) - V_{oc}(1sun, 298.15) - \frac{mk}{e} \times 298.15 \times \ln (C)}{\beta (C = 1) + \frac{mk}{e} \times \ln (C)} + 298.15 \quad (40)$$

Table 1 to 3, presented in the Annex VIII, presents the electrical parameters (Pmp, Impp, Vmpp, Voc and Isc) measured for each solar cell and sub-receiver. Also in these tables we present: the concentration level (in suns) estimated by the ratio between the Isc measured and the Isc at 1 sun (which is 0.29 A for the Solartec solar cells) and the temperature of the cell estimated by using the equation (40).

Figure 6.34 shows the I-V curves measured for cell n° 3 of each sub-receiver during the 15 minutes of the experience in the sunlight. The first two curves highlight the effect of the temperature on the cells Voc and Isc. It may notice that the Voc significantly decreases during the experiment period, which is mainly related with the increase of the cells and sub-receivers temperature. It can also be notice a slight increase of the Isc, which is also caused by the temperature increase.

By these figures it also can be observe that the highest Isc achieved during this experiment was 0.26 A in the SLT.C26 solar cell and 0.28 A in the SLT.C24 solar cell. By performing the ratio between the measured Isc and the Isc at 1000W/m² (which is 0.29 A) it can be concluded that the maximum irradiation registered during the experiment was about 960 W/m².

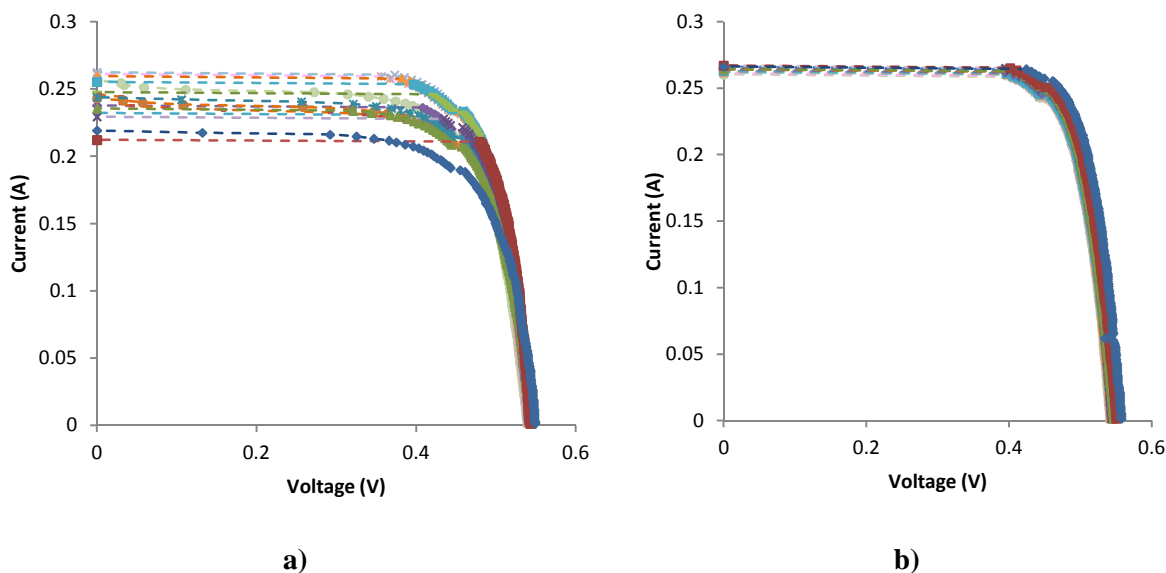


Figure 112 - I-V curves measured during 15 minutes in the sunlight exposure from the a) SLT.C26-2 and b) SLT.C24-2 sub-receivers.

Figure 6.35 presents the temperature measured on the rear surface of the PCB and the estimated temperature of the solar cell n° 3 (for both SLT.C24 and SLT.C26 sub-receivers) by using

the measured Voc. As can be observed in the figures, all solar cells tested shows an increase in the temperature measured and estimated during the experiment. This figure also highlights that the temperature measured in the rear surface of the solar cells is about $10(\pm 0.9)^\circ\text{C}$ lower than the temperature estimated to the solar cell; moreover, such difference between the two temperatures presents a constant behavior of $11(\pm 0.5)^\circ\text{C}$ and $9(\pm 0.8)^\circ\text{C}$ for the case of SLT.C26 and SLTC24, respectively. The difference between the temperatures of the cell and PCB back surface occurs due to the thermal resistances that exist on the PCB layers [49].

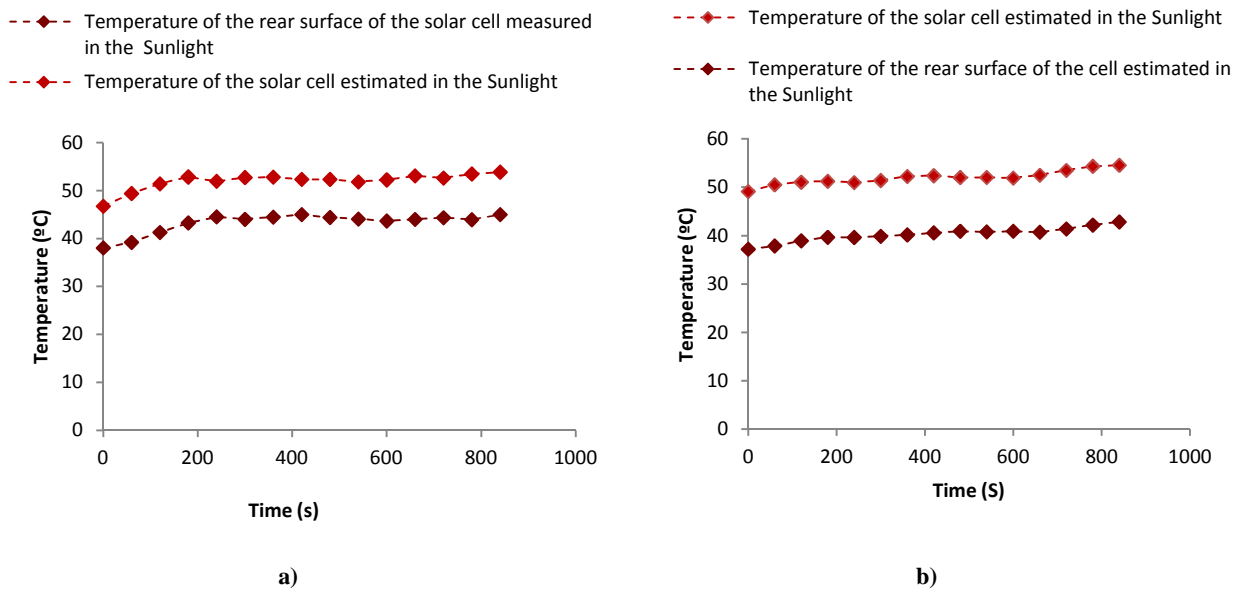


Figure 113 – Temperature of the rear surface of the cell and the temperature estimated of the a) SLT.C24 solar cell and b) SLT.C26 solar cell in the sunlight.

6.3.2.3. Adjust of the results obtained by the temperature estimated of the solar cells

In the previous section the temperature of the solar cell was calculated through the Voc produced by the solar cells when the measurement is performed. However, such temperature may be also estimated by the thermal resistances of the PCB and the irradiation falling on the cells [49] through the following equation:

$$Q = \frac{T_i - T_j}{R_{ij}} \quad (41)$$

where Q is the radiation that falls on the solar cells when the measurement is performed, $T_i - T_j$ is the difference of temperature between the two materials in analysis and R_{ij} is the thermal resistance between the materials (in this study, the thermal resistance between the back surface of the PCB and the solar cells was considered to be about $0.003^\circ\text{C}\cdot\text{W}/\text{m}^2$, according to [49]).

Figure 6.36 present the values of cell temperature estimated by the two methods, which are very similar. The temperature of the sub-receivers estimated by the thermal resistances are a little lower than the estimated from the Voc of the I-V curves measured on the sunlight, but this difference is very reduced (always lower than 4°C) and are covered by the error bars.

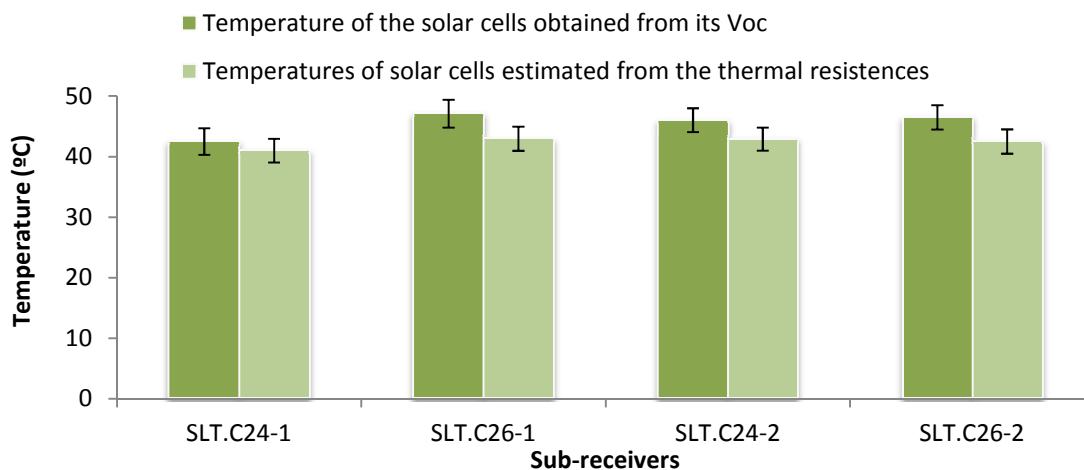


Figure 114 – Temperatures of the sub-receivers estimated by two different methods: i) from the Voc of the I-V curves measured (dark green bars) and ii) through the thermal resistances of the PCB and irradiation (light green bars).

Through the temperature estimated from these methods, it is possible to perform the adjustment of the value of Isc and Voc of the solar cells at the moment of measurement (Fig.6.37). As can be observed, the Voc measured in the sunlight are equal to the value estimated for the conditions (temperature and radiation) at the time of the measurements.

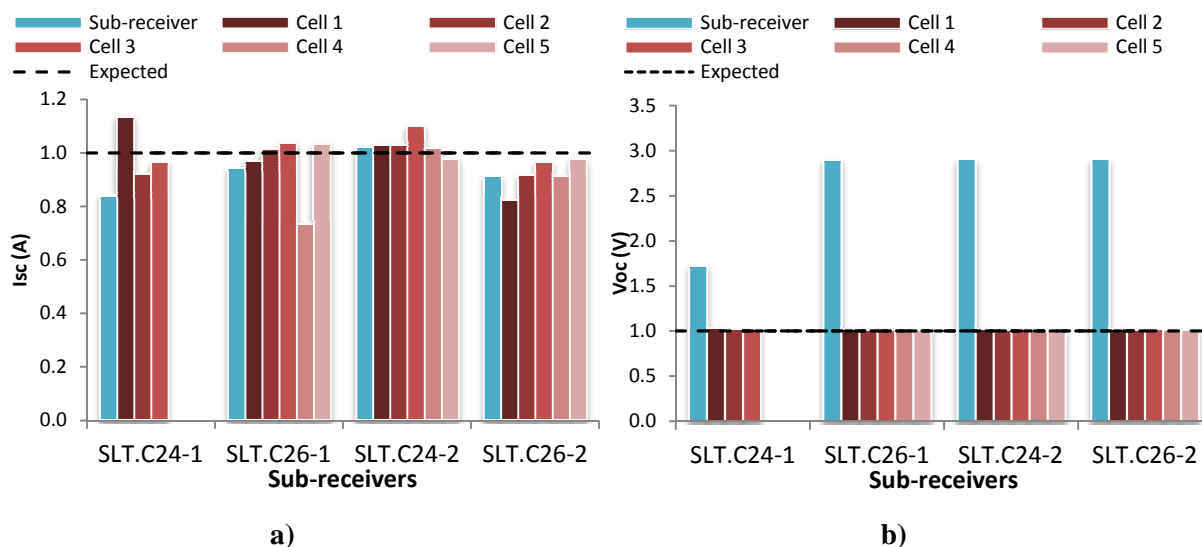


Figure 115 – Values of a) Isc and b) Voc of each solar cell (different red hue bars) and sub-receiver (blue bars) measured at outdoor conditions: 800 W/m² of irradiation and 30.5 (±0.5) °C of ambient temperature, normalized to the Isc and Voc estimated by the temperature of the solar cells (dashed black lines).

6.3.3. Main conclusions

The values of I_{sc} and V_{oc} estimated for the condition at the moment of the measurement (radiation level and temperature of the solar cells) prove to be similar to the values obtained by the measurement. So, it can be concluded that the performance of the solar cells is unaffected by their integration in the HSUN sub-receivers.

Cost-efficiency analysis of screen-printed solar cells to integrate CPV systems

Most CPV systems integrate high efficiency solar cells which are designed to operate under high levels of radiation. Such cells are more expensive than the standard screen-printed solar cell technology which is being produced at high volume by a well-standardized industry thus benefitting from economies of scale. Thus, in this thesis we have been evaluating the potential of such cells to integrate CPV systems.

The previous sections have focused on the electrical characterization and technological integration of conventional 1-sun solar cells (such as KVAZAR) and upgraded 1-sun solar cells (such as Solartec) to operate under different concentration levels. However, to really understand the potential of a specific solar cell technology, when integrated in a CPV system, we have to analyze the relation between its cost and power output, i.e. to perform a cost-efficiency analysis. As such, the cost-efficiency of a solar cell can be estimated by equation (42)[50].

$$\text{€/Watt} = \frac{\text{Price of the solar cell (€)}}{\text{Pmp of the cell (C)(W)}} \quad (42)$$

where the *Pmp of the cell (C)* is the maximum power of the cell for a concentration C.

In the following lines we perform a comparison of the cost-capacity between:

- i) Conventional 1-sun screen-printed solar cells
- ii) Upgraded screen-printed solar cells (optimized for 15 suns)

- iii) Laser Grooved Buried contact solar cells (optimized for 15 suns).

To estimate the cost-efficiency of these solar cells (NaREC, Solartec and KVAZAR solar cells) where only taking into account the unit price of the cells and not the design and the mask used in the NaREC and Solartec solar cells, since these are only paid once.

Table 7.1 presents the prices of the previously mentioned solar cell technologies being LGBC technology the most expensive ones (€ 32.44 / wafer) and KVAZAR solar cells the cheapest (5.12 € / wafer). These values were expected since the LGBC solar cells are, nowadays, mainly produced for CPV applications at a considerably lower scale than the conventional screen-printed solar cells, which present lower prices due to economies of scale.

However, when looking to the cell unitary price, we should notice that the solar cells provided by Solartec presents the lowest price/cell. This situation is due to the fact that a Solartec wafer has 14 solar cells while the KVAZAR wafer only provides 8 solar cells. So, when the price of each solar cell is calculated, the Solartec solar cells showed the cheapest unitary price.

Table 7.1 – Technology and prices of the Solartec, NaREC and KVAZAR solar cells.

	Technology	Solar cells per Wafer	Price (€)	
			Wafer	Solar cell
NaREC	LGBC optimized for 15 suns	14	32.44	2.32
Solartec	Upgraded screen-printed solar cells (optimized for 15 suns)	14	0.58	8.12
KVAZAR	Conventional silicon solar cells	8	5.12	0.64

The cost-efficiency of the solar cells was estimated through eq. 1 for a concentration level that lies between 1 and 30 suns (since the HSUN system was initially designed for a concentration of 15 suns). The Pmp values used in these calculations were provided by section 4.3. Figure 7.1 shows the expected cost-effectiveness vs. the concentration level.

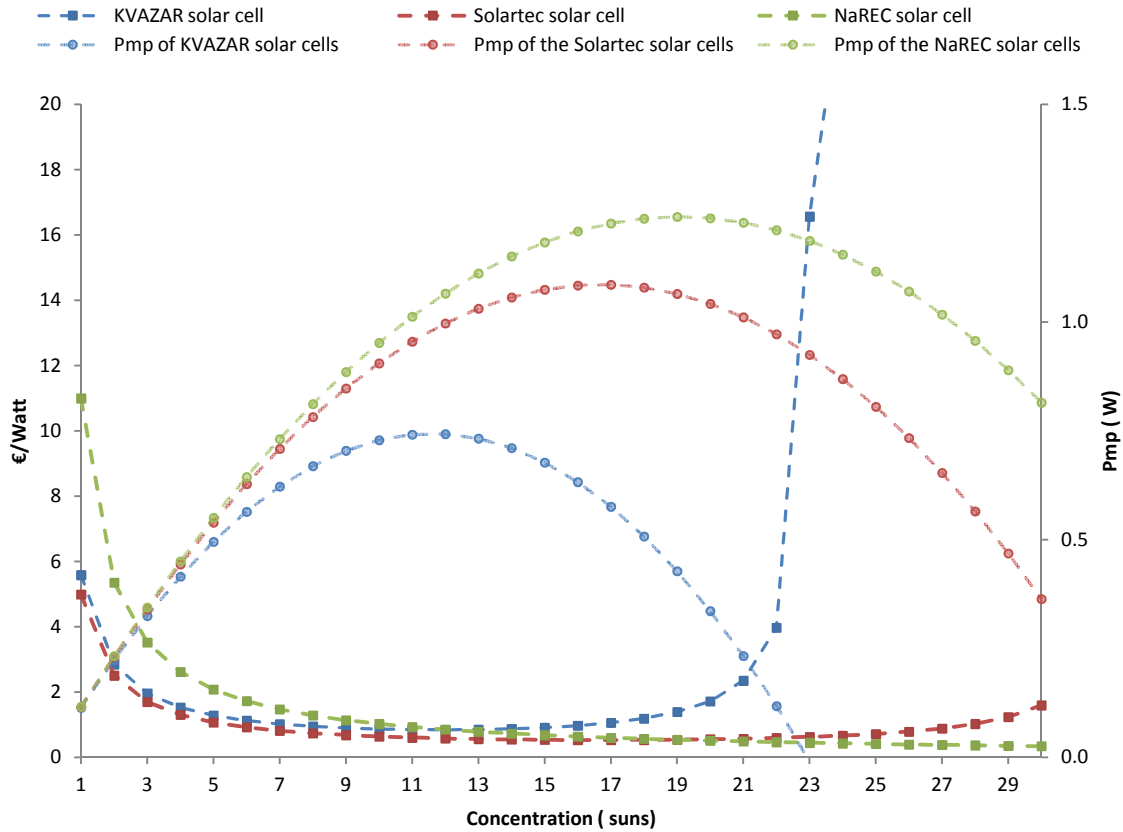


Figure 116 – Estimated cost-effectiveness and Pmp of the NaREC, Solartec and KVAZAR solar cells in function of the concentration level

Figure 7.1 highlights that the KVAZAR solar cells are not suitable to be used at least with the design/dimensions that we intend. The silicon wastage is so high that the €/Watt of KVAZAR solar cells is higher than the Solartec solar cells even at 1 sun conditions.

Regarding the Solartec solar cells, Fig. 7.1 shows that these are the solar cells that present the lowest values of €/Watt until a concentration level of 24 suns; however, after this concentration level the lowest €/Watt is achieved by the NaREC solar cells

Thus, it can be concluded that from the solar cells studied, the ones that proved to be the most cost effective to integrate the HSUN system (operating at 15 suns) are the solar cells provided by the Solartec.

CONCLUSIONS AND FUTURE WORK

8.1. Conclusions

The use of alternative and environmentally friendly energy is a crucial issue in the fight against waste and proper use of natural resources. Thus, dominate and spreading the processing technology of photovoltaic energy, as the CPV market, is the primary task for the technological areas.

The HSUN is a concentration photovoltaic (CPV) system concept under development by WS Energia S.A. It uses crystalline silicon solar cells optimized for a concentration factor of about 15 suns. However, the price of the HSUN PV receiver is strongly conditioned by the expensive high efficiency solar cells that integrate. Thus, the main purpose of this thesis regards the study of new approaches of silicon solar cells to use in the HSUN PV receiver.

In a first approach, a theoretical mathematical analysis was made in order to understand what the behavior of solar cells studied in several levels of concentration. This study, later supported by the full electrical characterization of the solar cells performed, allowed to conclude that the conventional cells provided by the KVAZAR company show to be viable only up to a concentration of 8 suns, while the modified silicon cells for concentration, provided by the Solartec company, prove to be viable up to a concentration of 20 suns. Thus, since the HSUN system operates at a concentration of 15 suns, the viability of KVAZAR solar cells proves to be insufficient to integrate this system.

Thus, for the experimental campaign performed to understand the behavior of the solar cells integrated in the HSUN sub-receivers were only tested sub-receivers.

Throughout this experimental campaign was possible to compare the results obtained experimentally with the values estimated by the theoretical model. The values appear to be similar and show that the Solartec solar cells present a good performance (according to the expectation), that is unaffected, when integrated in the sub-receivers of the HSUN system.

The best performance of solar cells when integrated into the sub-receivers, in the context of experimental campaign, was also carried out an improvement of the mounting process of the HSUN receivers. Through the preliminary tests conducted to validate this process was possible to discover some issues such unsoldered Ribbons, appearance of spots on solar cells and displacement of Ribbons. After studying the results obtained in these preliminary tests, solutions were found and implemented to optimize the process (application flux and straight cut of the ribbons). After the optimization, this process was again tested and the results showed that the solutions were feasible, eliminating the problems previously encountered. Much more experimental tests were performed and were not included in this thesis.

As the main aim of the study of these new approaches is to reduce the cost of the system, it is important not only to have a good perspective of the solar cell performance when integrated in a CPV system, but also take into account the economic viability of the solar cells. Thus, to a correct choice of the most viable solar cell to integrate the HSUN system was taken into account not only the values of output power produced by the solar cells, but also their cost-efficiency. Through this cost-efficiency, where the KVAZAR conventional solar cells, the NaREC LGBC solar cells and Solartec optimized solar cells were compared, it was concluded that the solar cells more viable up to a concentration level of 24 suns are the Solartec solar cells, being that from this concentration level the NaREC solar cells present themselves as the most viable solar cells.

Therefore, and taking into account all the work developed along this thesis, it can be concluded that the most cost-efficient solar cells to integrate the HSUN system are the mono-crystalline silicone solar cells with optimized screen-printing, such as the Solartec solar cells.

8.2. Future Work

As mentioned throughout the thesis, this work was integrated in the development of a new photovoltaic concentrator. Therefore, much work still needs to be done. One of the conclusions of the comparison of the behavior of the solar cells estimated by the mathematical model and the measurements on field is the confirmation of the values estimated. However, in this thesis, it was only possible perform measurements at 1, 2, 4 and 10 suns. So, for a complete understanding of the real behavior and validation of theoretical values of the solar cells under each concentration level, measurements under other concentration levels should be further performed.

Other development to be made is the upgrade of the design of the PCB plate, so that solar cells with new settings (as in the case of Solartec solar cells with two busbars) can be integrated and studied in the HSUN sub-receivers.

Another important issue, as evidenced in the experiments conducted in this thesis, is the effect of the inhomogeneous sunlight on the solar cells. This phenomenon shows to be harmful for the performance of the system. Thus, a study of the effect of inhomogeneous irradiation on solar cells performance seems to be a good approach to understand the real effect of this phenomenon and the solutions needed to minimize these effects on the output efficiency of the system.

As regards the soldering of the solar cells, in this thesis was conducted an improvement of the mounting the sub-receivers components and the soldering method of solar cells. However, in order to make the whole process ready for the industrialization of the HSUN system, it seems necessary to automate the entire soldering process (including the mounting of the several components on the PCB). Thus, a study in the automation of this part of the process seems to be necessary.

REFERENCES

- [1] B. ROBYNS, "Situação Actual", accessed on 29 August 2011: http://e-lee.ist.utl.pt/realisations/EnergiasRenouvelables/Enjeux/Enjeux/LesEnjeux_PO.pdf, 2008.
- [2] M. COLLARES-PEREIRA-PEREIRA, "Energias renováveis. A opção inadiável.," Lisboa, 2000
- [3] P. A. and P. J., "PHOTOVOLTAIC SOLAR ENERGY - Development and current research ", Office for Official Publications of the European Union, Bélgica, 2009.
- [4] A. Jäger-Waldau, "PV STATUS REPORT 2011," European Commission, DG Joint Research Centre, Institute for Energy, Renewable Energy Unit, Italy, 2011.
- [5] K. S., "Opportunities and Challenges for Development of a Mature Concentrating Photovoltaic Power Industry," in *Innovation for Our Energy Future*, Colorado: National Renewable Energy Laboratory, 2009.
- [6] S. H. and A. M., "Energia solar fotovoltaica: Contributo para um roadmapping do seu desenvolvimento tecnológico ", Monte da Caparica: Research Centre on Enterprise and Work Innovation, 2009.
- [7] A. M. Vallêra and M. C. Brito, "Meio Século de História Fotovoltaica," ed: Gazeta da Física, 2006.
- [8] R. F., "Development of Solar Concentrators for Large Photovoltaic Plants ", Dissertação para obtenção do Grau de Mestre em Engenharia Física Tecnológica, IST, Lisboa, 2008.
- [9] S. A. S., "Estimativa de Produção em Centrais Solares de Concentração," Dissertação realizada no âmbito do Mestrado Integrado em Engenharia Electrotécnica e de Computadores, FEUP, Porto, 2010.
- [10] A. Luque and S. H., "Handbook of Photovoltaic Science and Engineering," John Willey & Sons, England, 2003
- [11] "Concentrator Photovoltaic (CPV) Modules and Assemblies - Design Qualification and Type Approval," IEC 62108: 1bDraft, 2010
- [12] C. A. d. Nascimento, "PRINCÍPIO DE FUNCIONAMENTO DA CÉLULA FOTOVOLTAICA", Monografia apresentada ao Departamento de Engenharia da Universidade Federal de Lavras, MINAS GERAIS - BRASIL, 2004
- [13] F. M. E. Emanuel, "Módulo fotovoltaico com seguimento da posição solar", Dissertation to obtain a Master Degree in Electrical and Computer Engineering, FCT - UNL, Lisboa, 2008
- [14] D. A. D. Afonso, "Modelação e Controlo Analógico de um Sistema de Microgeração a Energia Solar", Dissertation to achieve the Master Degree in Electrical and Computer Engineering, FEUP, Porto, 2009
- [15] K. Bouzidi, M. Chegaar, and A. Bouhemadou, "Solar cells parameters evaluation considering the series and shunt resistance," *Solar Energy Materials and Solar Cells*, vol. 91, pp. 1647-1651, Nov 2007.
- [16] M. T., "Solar Electricity," s.l. :Wiley, 2000.
- [17] F. R., "Aplicação Informática para o Estudo da Viabilidade Técnico-económica de uma habitação sustentável", Dissertação apresentada na Faculdade de Ciências e Tecnologia da Universidade Nova de Lisboa, Lisboa, 2010
- [18] S. V. K., C. A., and S. G., "OUTLOOK FOR HIGH EFFICIENCY SOLAR CELLS TO BE USED WITH AND WITHOUT CONCENTRATION," vol. 36, ed. Matera: Energy Convers. Mgmt, 1995, pp. 239-255.
- [19] L. A. and A. V., "Concentrator Photovoltaics," vol. 130, ed. Athanta: Springer Series in optical sciences 2007.
- [20] D.-H. Neuhaus, A. Munzer, and E, "Review Article: Industrial Silicon Wafer Solar Cells," ed. Hindawi Publishing Corporation, *Advances in OptoElectronics: Dissertation to obtain a Master Degree in Electrical and Computer Engineering*, 2007, p. doi:10.1155/2007/24521.

-
- [21] F. Reis, "Why use NaREC solar cells on the HSUN® receiver?," WS Energia S.A.: Private communication, 2011.
- [22] V. M., M. C., A. I., and S. G., "Laser grooved buried contact cells optimised for linear concentration systems," vol. 94, ed. Madrid: Solar Energy Materials & Solar Cells, 2009, pp. 187–193.
- [23] V. A. Chaudhari and C. S. Solanki, "From 1 Sun to 10 Suns c-Si Cells by Optimizing Metal Grid, Metal Resistance, and Junction Depth," *International Journal of Photoenergy*, 2009.
- [24] J. Coello, Castro, A. M., S. G. I., and M. A. Vázquez, "Conversion of commercial si solar cells to keep their efficient performance at 15 suns," *Progress in Photovoltaics: Research and Applications*, 2004, pp. 12: 323–331. doi: 10.1002/pip.534.
- [25] K. E. V. and B. G., "Back-contact Solar Cells: A Review ", Wiley InterScience, 2005, pp. 107–123, Bélgica
- [26] A. Cheknane, H. S. Hilal, J. P. Charles, B. Benyoucef, and G. Campet, "Modelling and simulation of InGaP solar cells under solar concentration: Series resistance measurement and prediction," *Solid State Sciences*, vol. 8, pp. 556-559, 2006
- [27] T. Fuyuki and A. Kitiyanan, "Photographic diagnosis of crystalline silicon solar cells utilizing electroluminescence," *Applied Physics a-Materials Science & Processing*, vol. 96, pp. 189-196, Jul 2009
- [28] S. Unlimited, "Aplicação: Inspeção Electroluminescence de energia fotovoltaica com imagem SWIR," Goodrich Corporation, 2011
- [29] B. TRUE, "**Photoluminescence an Electroluminescence for Silicon Solar Cell Inspection**", http://www.laser2000.de/fileadmin/kataloge/INTEVAC_SolarCellWhitePaper_BruceTrue.pdf , APPLICATIONS SCIENTIST, INTEVAC, INC., consulted in 3rd July, 2011
- [30] A. Kitiyanan, A. Ogane, A. Tani, T. Hatayama, H. Yano, Y. Uraoka, and T. Fuyuki, "Comprehensive study of electroluminescence in multicrystalline silicon solar cells," *Journal of Applied Physics*, vol. 106, Aug 2009.
- [31] F. T. and K. A., "Photographic diagnosis of crystalline silicon solar cells utilizing electroluminescence ", ed: Springer-Verlag, 2008, pp. 189–196.
- [32] B. O., K. A., A. Y., B. J., W. J.-M., and I. K., "Quantitative evaluation of electroluminescence images of solar cells ", www.pss-rapid.com: WILEY-VCH Verlag GmbH & Co. KGaA, online 30 October 2009
- [33] C. L. Garrido-Alzar, "Algorithm for extraction of solar cell parameters from I-V curve using double exponential model," *Renewable Energy*, vol. 10, pp. 125-128
- [34] M. S., K. M., and S. G., "Silicon Solar Cells: Recombination and Electrical Parameters ", ed. Croácia: Solar Energy, 2010, p. 432
- [35] A. G. Aberle, S. R. Wenham, M. A. Green, and Ieee, "A NEW METHOD FOR ACCURATE MEASUREMENTS OF THE LUMPED SERIES RESISTANCE OF SOLAR-CELLS," in *Conference Record of the Twenty Third Ieee Photovoltaic Specialists Conference - 1993*, pp. 133-139
- [36] <http://pt.scribd.com/doc/56832517/projectofinal>, "consulted in 30th August, 2011,"
- [37] C. R., "Energias Renováveis e Produção Descentralizada", Universidade Técnica de Lisboa Instituto Superior Técnico: DEEC / Área Científica de Energia, 2008.
- [38] <http://www.californiascientific.com/resource/Solar%20Cell.pdf>, consulted in 15th August, 2011
- [39] D. Pysch, A. Mette, and S. W. Glunz, "A review and comparison of different methods to determine the series resistance of solar cells," *Solar Energy Materials and Solar Cells*, vol. 91, pp. 1698-1706, 2007
- [40] B. S. and R. A., "RAPID AND ACCURATE DETERMINATION OF SERIES RESISTANCE AND FILL FACTOR LOSSES IN INDUSTRIAL SILICON SOLAR CELLS ", ed. Atlanta: Georgia Institute of Technology, 2011
- [41] H. C. and B. S., "Effect of Light Intensity", PV Education, PV CDROM, 2011.
- [42] S. Response", "<http://pvcdrom.pveducation.org/CELLOPER/spectral.htm>", consulted in 20th August, 2011.
-

-
- [43] R. E. E. Fotovoltaica, "<http://pvcdrom.pveducation.org/CELLOPER/spectral.htm>", consulted in 20th August, 2011
- [44] Q. Efficiency", "<http://pvcdrom.pveducation.org/CELLOPER/spectral.htm>", consulted in 20th August, 2011
- [45] B. A. J., G. F. P., and K. A., "Análise da medida da Temperatura de módulos fotovoltaicos em ensaios de caracterização eléctrica," vol. 14, *Avances en Energías Renovables y Medio Ambiente: Laboratório de Energia Solar – Programa de Pós Graduação em Engenharia Mecânica – Universidade Federal do Rio Grande do Sul (UFRGS) Rua Sarmiento Leite*, 2010
- [46] A. I., S. G., and P. D., "Correction oh the Voc vs. Temperature dependence under Non-uniform concentrates Illumination ", *Proceedings of the 17th European Photovoltaic Solar Energy Conference*, , Munich, Germany (2001)
- [47] M.-L. J., P. L., R. F., C. S., W. J., S. G., and P. N., "On-Field Demonstration Results of Medium Concentration System HSun," *Faculty of Sciences of University of Lisbon, Lisboa*, 2011
- [48] A. I., S. G., and P. D., "Correction of the Voc vs. temperature dependence under non-uniform concentrated illumination," ed. Munich, Germany: *Proceedings of the 17th European Photovoltaic Solar Energy Conference*, 2001, p. 156
- [49] D. P. F. Reis, L. Pina, J. M. Lopes, S. Coelho, J. Wemans, G. Sorasio, M. C. Brito, "Thermal Modeling of a PV Receiver for CPV Applications," ed. Los Angeles: *CPV7 Conference*, 2011
- [50] P. R. C. a. G. A. Taylor, "THE ECONOMIC AND POLICY IMPLICATIONS OF GRID-CONNECTED RESIDENTIAL SOLAR PHOTOVOLTAIC POWER SYSTEMS," *M.I.T. ENERGY LABORATORY REPORT - MIT-EL 78-007, DEPARTMENT OF ENERGY, E.U.A.*, 1978

ANNEXES

Annex I – Poster and Article presented in the 26th European Photovoltaic Solar Energy Conference, in Hamburg

Annex II – Datasheets of the NaREC solar cells

Annex III – Datasheets of Solartec and KVAZAR solar cells provided by the respective companies

Annex IV – Datasheets of Solartec and KVAZAR solar cells with measured values

Annex V – Experiments performed to improve the soldering process of the solar cells

Annex VI– Experiments performed in the NaREC solar cells


Annex VII – I-V curves of the sub-receivers and the each solar cell individually

Annex VIII – Estimated temperatures of the solar cells integrated in the sub-receivers



ANNEX I

Poster and Article presented in the 26th
European Photovoltaic Solar Energy
Conference, in Hamburg





ANNEX II


Datasheets of the
NaREC solar cells





ANNEX III

Datasheets of Solartec and KVAZAR solar
cells
provided by the respective companies





ANNEX IV


Datasheets of Solartec and KVAZAR solar
cells with measured values





ANNEX V

Experiments performed
to improve the soldering process of the
solar cells





ANNEX VI

Experiments performed in the NaREC
solar cells





ANNEX VII

I-V curves of the sub-receivers and the
each solar cell individually





ANNEX VIII

Estimated temperatures of the solar cells
integrated in the sub-receivers

